Developing a framework for studying fine resolution impacts of climate change on forest ecosystems at regional scale using remote sensing and artificial intelligence

Pratima K C

A dissertation

submitted in partial fulfillment of the

requirements for the degree of

Doctor of Philosophy

University of Washington

2024

Reading Committee:

Van R. Kane

Hans-Erik Andersen

Maureen C. Kennedy

Program Authorized to Offer Degree:

School of Environmental and Forest Sciences

University of Washington

Abstract

Developing a framework for studying fine resolution impacts of climate change on forest ecosystems at regional scale using remote sensing and artificial intelligence

Pratima K C

Chair of the Supervisor Committee:

Van R. Kane

School of Environmental and Forest Sciences

Forests are one of the largest and most important terrestrial ecosystems that cover approximately 30% of the Earth's landmass. Globally, forests are important carbon pools and provide a variety of ecosystem services. However, they are undergoing rapid changes due to climate change. The forests in California's Sierra Nevada and Interior Alaska, for example, are under the threat of massive forest mortality, shift in species composition, and forest conversion to nonforest with corresponding changes in ecological processes. To overcome these challenges and build resistant and resilient forests under changing climate, we need relevant ecological assessment approaches and effective management practices that address the problems from tree scale to larger extents. To achieve this goal, fine-scale monitoring of forest conditions is required to detect potential type conversions and guide management interventions. One such approach is remote sensing-based methods validated with field data, which can reliably extend the field-based measurements across larger landscapes. To fully utilize the potential of the wide range of newly available

remote sensing data, cutting-edge artificial intelligence techniques are required. In my research, I built a robust framework designed to generate high-resolution prediction maps of forest conditions at regional scale by integrating remote sensing and artificial intelligence techniques. In my dissertation I 1) developed an automated method for identifying the forest conditions (type and mortality status); 2) applied the method to examine which remote sensing data modality performs best for detection of the forest conditions; 3) produced forest condition maps at regional scale; 4) used prediction maps to derive metrics that is useful to managers and answer ecological questions. This work addresses open questions about large scale, fine resolution ecosystem patterns monitoring under climate change. The developed framework enables us to perform repeat, fine scale monitoring of forest condition which can be used to detect relevant ecological changes and assists managers in developing effective management strategies to mitigate climate change induced impacts.

TABLE OF CONTENTS

LIST OF FIGURES

LIST OF TABLES

ACKNOWLEDGEMENTS

This dissertation research was possible with the support of important research collaborators along with mentors, family members and friends.

First, I could not have been able to complete this work without the crucial support, encouragement, and unlimited trust of my family members. I am so grateful for my parents Ramesh KC and Indira Devi Sharma who raised me to believe in myself and aim high. I thank my big brother Anup KC for his invaluable mentorship and constant encouragement. His advice to prioritize my health has been instrumental in helping me stay focused and dedicated to my work. Thank you to my sister, Upama KC who has always been my first listener to any of my ideas and has stood rock solid motivating me in achieving my goals. Thank you to my brother-in-law, Dinesh Adhikary for your support, friendship, and unlimited trust in my abilities. I thank my little niece Arya KC-Adhikary for her unlimited energy that inspired me to keep going.

I thank Van Kane, my PhD supervisor, for his unwavering support, guidance and insightful feedback throughout the journey of PhD. His guidance has been instrumental in shaping the direction of this research. I am grateful for his patience, encouragement, and the countless hours he has devoted to meetings and reviewing my work.

I thank Han-Erik Andersen, my committee member, for his mentorship and support. Working and discussing the big ideas about the utility of machine learning has been productive and led to major concepts of this work.

I thank Monika Moskal, my committee member, for her mentorship and leadership throughout. I am grateful for your input and insights in every confusion and conflict regarding the graduation process.

I thank Maureen Kennedy, my committee member, for encouraging me to think about a bigger picture and goals. Your critical question encourages me to develop a theme for this research. They have always encouraged me to think of both strengths and limitations of the research.

I thank Sean Hendryx, my partner in crime. I am so grateful to have you along my side on this journey. Our unlimited conversation and your critical feedback, comments, and input on my research has been so immense and without it I would not be able to complete my research. You were an invisible member of my dissertation committee!

I thank Liz van Wagtendonk, my research partner, for her support. You were an amazing person to work with. Our long conversations and discussions about how we can implement cutting edge technology in the field of ecology has always been fun. In fact, these conversations and collaborations were foundational to this work.

I thank Paul Hessburg, Susan Prichard, Lori Moreno, Nic Enstice, Keala Hagmann, Alina Cansler for encouraging me and being available to provide guidance when necessary.

I thank Steven Bethard for teaching such a difficult topic of neural networks in a very fun and systematic way where students from any background could understand it easily. Without taking this class I would not have dreamed of completing this dissertation.

I thank Astrid Sana, Iris Mire, Caden Chamberlian, Bryce Bartl-Geller, Jonathan Kane, Hannah Redford, Gina Cova, Anthony Steward for your friendship and discussion about research, graduate student life and its challenges. They helped to solve problems, reduce the stress, and look on the brighter side of the journey.

I thank Don Radcliffe, Alec Solemslie, Kaley Wypyszynski, Raj Dewangan, Charles Bugre, and Devon Woodley for your friendship, support, and encouragements.

I thank all my collaborators past and present for providing opportunities that have sparked and fueled a researcher inside me.

I thank Cindy Norton and Olya Mordkhin, my soul sisters and Patty Bedlov and Nick Hendryx for your friendship and positivity. Your support has encouraged me to continue this journey to complete my dissertation. Your presence had made United States a home away from home!

It is not an easy journey to be away from home and working on challenging projects. Therefore, I would like to thank each and everyone who have cross path and have encouraged and made me felt supported in United States. Thank you, all beautiful souls, without your presence I would not be able to achieve this degree.

Last but not least I would like to thank myself!

I dedicate my dissertation to my beloved parents, Indira Devi and Ramesh K C, and to my little niece, Arya KC-Adhikary who inspires me every day and encourages me to stay positive, which has been my guiding light throughout this journey.

PUBLISHED MATERIALS

A portion of the materials presented in this dissertation have been published through the peer-reviewed process. This article is reproduced in full here as Chapter 2.

Khatri-Chhetri, P., van Wagtendonk, L., Hendryx, S. M., & Kane, V. R. (2024). Enhancing individual tree mortality mapping: The impact of models, data modalities, and classification taxonomy. *Remote Sensing of Environment, 300*, 113914.

Chapter 1. INTRODUCTION

Forests are one of the largest and most important terrestrial ecosystems that cover approximately 30% of the Earth's landmass (Liu et al., 2018; Schmitt et al., 2009). Forests are important carbon pools globally and provide a variety of ecosystem services such as wildlife habitat, water and nutrient cycle, timber production, and recreation. However, forests across the globe are undergoing rapid changes due to changing climate. In particularly, mixed conifer forest in drylands and boreal forest in higher latitudes are at the risk of large-scale mortality and type conversion due to climate change-induced drought, forest fires, and increases in temperature (Barber et al., 2000; Coop et al., 2020; Ruess et al., 2021; Swain, 2015).

The forest in Sierra Nevada and Interior Alaska, for example, are under the threat of massive forest mortality (Millar & Stephenson, 2015; Ruess et al., 2021; Swain, 2015), forest conversion to nonforest, and shift in species composition (Barber et al., 2000; Coop et al., 2020; Douglas et al., 2014; Parks et al., 2019; Walker et al., 2015). Extensive tree mortality, changes in the species composition, and shift of forest to nonforest type will change ecological processes and services, significantly effecting on understory vegetation, wildlife habitat, timber production, and more broadly the global carbon budget. The change in a forest will in turn have feedback on climate. For example, climate change-induced change in forest cover is amplifying variation in daytime temperature and increases mean and maximum air temperatures across the globe (Alkama & Cescatti, 2016).

To overcome these challenges and build a resistant and resilient forest under changing climate, we need relevant ecological assessment approaches and effective management practices that address the problem from the tree scale to larger extents. The field survey can provide more

detailed information about ecological phenomena such as species composition, tree height, tree status (live vs dead), diameter at breast height, and basal area at the scale of the individual tree but are limited spatially and temporally and might just cover a few forest communities. In contrast, remote sensing data allows us to extend the plot-based measurement across the larger landscape. Both active and passive remote sensing data have been found to be useful for deriving forest inventories attributes such as diameter at breast height (DBH), tree height, basal area, tree canopy and tree species (Andersen et al., 2005; Bolton et al., 2018; Moskal & Zheng, 2012; White et al., 2016).

The recent increase in open-source, high-resolution aerial remote sensing imagery and lidar data affords a remarkable opportunity to research details of forest ecosystems, allowing for a comprehensive understanding of their dynamics and intricacies. In addition, advancements in computing hardware, software, and data analysis methods are providing opportunities to fully utilize the potential of the unprecedented source of information provided by remote sensing techniques (Liu et al., 2018; Olden et al., 2008). One such field is artificial intelligence that is efficient and computationally expressive and is concerned with identifying structure in complex, often nonlinear, data and generating accurate predictive models (Bzdok et al., 2018; Liu et al., 2018; Olden et al., 2008).

1.1 CURRENT STATE OF RESEARCH

The interaction between climate change-induced stressors such as increasing temperature, drought, and severe wildfires are resulting in large scale tree mortality (Millar & Stephenson, 2015) and shifts in dominant species (Barber et al., 2000; Walker et al., 2015). Among various forest inventory attributes, mortality and species are vital for estimating aboveground biomass and carbon thus, can be used to inform the impact of climate change on forest ecosystems.

Therefore, quantifying and mapping the spatial changes in forest conditions (mortality and species) are important for improving our ecological understanding of forest dynamics, improve estimates of aboveground biomass and carbon estimation, and support biodiversity monitoring (Byer & Jin, 2017a; Campbell et al., 2020; Fassnacht et al., 2016; Mäyrä et al., 2021; Tian & Fu, 2020).

Remote sensing has provided tools to measure forest conditions across various scales. Coarse (250 m) to moderate (30 m) resolution data are suitable for mapping forest conditions at global and regional level respectively (Byer & Jin, 2017; Xie et al., 2008). However, these resolutions often include mixed pixels that combine vegetation, soil, boulder, and understory vegetation, making it challenging to accurately identify tree mortality and species. High-resolution data can capture these phenomena at the finer scale of individual trees and be mapped at regional scales (Cheng et al., 2024; Hemming-Schroeder et al., 2023; Mäyrä et al., 2021; Stovall et al., 2019).

The high-resolution forest condition maps at regional scale are essential for addressing key ecological questions and providing managers with tools at relevant scales. Specifically for measuring population trends requires the capabilities to assess individual tree status, species, survivorship (Van Wagtendonk, 2023). Further, individual mortality maps can help investigate mortality related to species, height, and basal areas (Van Wagtendonk, 2023) which is not possible with moderate to coarse resolution remote sensing data. In addition, from high-resolution detailed maps, coarser resolution products can also be derived. In contrast, if coarser products are produced first, it is not possible to generate finer resolution products from them.

Furthermore, the increasing extent, frequency and severity of drought and fire makes the study of forest conditions at appropriate fine scale more urgent to develop strategies for management and restoration at an adequate pace and scale. Since the inception of climate

change-induced disturbances, the availability of multi-temporal, open-source, high-resolution remote sensing data products has been increasing in terms of temporal and spatial extent within the United States. These high-resolution remote sensing data combined with advanced artificial intelligence techniques provide opportunities to capture forest conditions at the scale at which the phenomenon occurs and can be mapped to a large extent. For example, capturing overstory tree loss at the scale which the phenomenon occurs – the individual tree – in turn improves our ability to answer key ecological questions and derive accurate management relevant products and metrics. Similarly, to estimate the shifts in species composition we need to map forest species at relevant scales. A forest stand is a community of trees with almost uniform species composition, structure and ages and are important unit for forest managers (Fournier et al., 2003). Therefore, capturing the forest species distribution at the forest stand scale (stand-level) in turn provides better understanding of forest ecological processes including species recruitment and net productivity.

Sierra Nevada forests are dying over larger extents due to the climate change-induced prolonged drought (Fettig et al., 2019; Restaino et al., 2019; Stephens et al., 2018; Swain, 2015; Young et al., 2017). Previous studies have identified and mapped tree mortality in this region using moderate (30 m) to coarse (250 m) resolution data at regional scale (Byer & Jin, 2017; Campbell et al., 2020; Hamilton et al., 2021). The coarser resolution imagery makes detection of mortality challenging particularly when there are few dead trees per acre (Byer & Jin, 2017). Recently, studies had mapped mortality at the scale of individual trees using lidar and high-resolution imagery (Bergmüller & Vanderwel, 2022; Hemming-Schroeder et al., 2023; Stovall et al., 2019). While these studies demonstrated large area mortality mapping at the scale of

individual overstory trees, these studies did not conduct field validation or compare the relative importance of open-source imagery at varying resolutions and model types.

In addition, the widespread drought-induced tree mortality in southern Sierra Nevada had accumulated dry surface and ladder fuels (Stephens et al., 2018) that contributed to recent large-scale fires. For example, 2020 Creek Fire was exacerbated due the pre-fire large-scale tree mortality pattern across the landscape (Lee et al., 2023). Previous studies have focused on understanding the impact of pre-fire forest growth, forest structures, and drought and competition with fire severity and post-fire tree mortality (Furniss et al., 2019; Kane et al., 2019; Van Mantgem et al., 2018, 2020). The impact of pre-fire tree mortality in fire severity and post-fire mortality was limited (Stephens et al., 2018) due to lack of automated models that can map individual overstory tree mortality over larger scales. However, the development of mortality model allows us to explore the effects of patterns of pre-fire tree mortality on subsequent fire behavior, which would aid in investigating the drivers of fire severity and post-fire mortality.

Further, the boreal forest of Interior Alaska are undergoing rapid shifts in dominant forest (spruce to broadleaf) at regional scale, due to climate change-induced increase in temperature, drought, wildfire (Barber et al., 2000; Walker et al., 2015). Previous studies have mapped boreal forest at a coarse (250 m) (Ruefenacht et al., 2008) to moderate (30 m) resolution (University of Alaska, 2017). In recent years, studies have used high-resolution remote sensing data combined with Forest Inventory and Analysis (FIA) plots (a national forest inventory program) to classify forest type (Shoot et al., 2021), estimate forest inventory attributes such as biomass and carbon (Alonzo et al., 2018). Alonzo et al. (2018) used high-resolution UAV imagery with FIA plot data to model forest type at individual crown scale and achieved 85% accuracy for identifying tree species in the Bonanza Creek experimental forest, Alaska. Shoot et al. (2021) did a case study by

combining FIA field plots with lidar and vegetation indices derived from hyperspectral data to classify forest types. The study found that the combination of lidar-derived topography, vegetation indices, and canopy height metrics produced higher accuracy. Previous studies have shown the effectiveness of lidar and high-resolution imagery in classifying forest types. However, there has been limited research using a systematic sample of field data with high-resolution airborne data (~1 m) collected under variable sky conditions (clear to overcast) during a 1-month period of the growing-season with deep learning models, which provides a means for upscaling forest type from field plots to a larger geographical extent in Interior Alaska.

1.2 CURRENT LIMITATIONS

High-resolution mapping of mortality and forest type maps aid in the continuous monitoring of forest conditions in changing climate and provide information to develop management strategies to mitigate climate change impact. Accurate and extensive mapping of forest conditions (status and species) requires both high-resolution remote sensing data and application of most suitable algorithmic approaches. The application of artificial intelligence techniques has been increasing in forest science and management since the 1990s (Jain et al., 2020; Liu et al., 2018). Previous studies have assessed the performance of a range of machine learning models for tree species (Mäyrä et al., 2021). Some of the commonly used machine learning models are random forest (RF), support vector machine (SVM), extreme gradient boosting trees (XGBoost), and deep learning models, artificial neural network (ANN), and convolutional neural network (CNN). Among these models, CNNs have emerged as a popular choice for tree species identification using high-resolution datasets (Egli & Höpke, 2020; Fricker et al., 2019; Kattenborn et al., 2019; Schiefer et al., 2020). However, it is not clear which among these

models is best for mapping individual tree mortality and mapping forest type when combining FIA field plot and remote sensing data.

Similarly, there are various multi-temporal, open-source high-resolution remote sensing imagery readily accessible across United States. For example, the National Ecological Observatory Network (NEON) high fidelity airborne lidar, NEON aerial imagery (RGB) at 0.1 m resolution, NEON hyperspectral (426 bands) at 1 m resolution, and the National Agriculture Imagery Program (NAIP) four bands (RGBNIR) imagery at 0.6 m resolution or less. Further, NASA Goddard's Lidar, Hyperspectral, Thermal (GLiHT) sensor collects data within linear swaths at 1 m or less spatial resolution over Interior Alaska and portions of the lower 48 states. However, it is not clear which of these datasets and associated spatial and spectral resolutions is best for producing accurate forest condition maps.

Our current ability to classify and map ecological phenomena such as tree mortality status (live or dead) and species composition at a large scale (over 214 thousand acres and 34 million acres) using high-resolution data has the following limitations: 1. field based studies are conducted at a limited number of sites and corresponding conditions (Barbour et al., 2002; Dial et al., 2021; Fettig et al., 2019), 2. manual interpretation of aerial imagery (ADS) (USDA, 2016), 3. lack of benchmark datasets, and 4. Lack of understanding of best high-resolution remote sensing data and models. The field observation and manual interpretation of aerial imagery are not feasible for studying forest conditions at the relevant scale (individual tree or plot level) across a large region. To address the problem, leveraging high spatial and spectral resolution remote sensing data in combination with field observations using computationally expressive models, such as deep neural networks, are necessary.

1.3 GOAL OF DOCTORAL RESEARCH

The study of impacts of climate change on forest ecosystems at a fine scale over large areas using high spatial and spectral remote sensing data necessitates the application of state-of-the-art machine learning methods. These methods have high predictive and computation power, produce highly accurate models (Bzdok et al., 2018; Olden et al., 2008), and are time-efficient. The application of machine learning models is well suited for ecological problems with large datasets (Jain et al., 2020; Liu et al., 2018; Olden et al., 2008).

The increasing frequency, extent and intensity of climate change-induced disturbances constitute an undeniable reality. The perpetuation of these events emphasizes the imperative for action, and climate change will only compound these challenges. Failure to understand the urgency of the situation will have devastating impacts on the ecosystem and economy (Conservancy, 2014). In this situation, we need a path forward with advanced computational models that allow us to detect these changes more quickly, efficiently, and accurately over large areas.

In my research, I address critical knowledge and assessment gaps discussed above by developing high-resolution forest condition maps. These maps serve as invaluable tools for detecting changes in forest conditions and aid in developing effective strategies for forest management and restoration in context of climate change. To accomplish this, I built a robust framework designed to generate high-resolution prediction maps, which include forest type and mortality at the regional scale (Figure 1). This framework integrates state-of-the-art advanced high-resolution remote sensing data with cutting-edge artificial intelligence techniques, thoroughly validated with field data.

Furthermore, I applied the developed mortality model, to analyze the mortality of the largest fire in California in recent decades. This investigation provides insights to the derived mortality metrics that can be used by managers to develop strategic plans to address impacts of compound disturbances. Further these metrics can be used to model future regeneration failure and success. By doing so, my research introduces a robust framework that not only predicts forest conditions but also enables the investigation and resolution of key ecological questions.

For instance, the tree mortality maps generated through this framework offer valuable insights into the drivers of mortality, the dynamic interplay between disturbances such as drought and fire, and the assessment of post-fire mortality to identify areas with regeneration failure. Additionally, the forest type predictions produced by this framework can be leveraged to estimate above-ground biomass, carbon content, and the underlying drivers of forest distribution. Overall, my research provides a powerful framework for predicting forest conditions at a scale appropriate for addressing complex ecological questions and facilitating informed decision-making in forest management and restoration efforts.

To assist managers and the US Forest Service in mitigating both present and future climate change-related challenges in the forests of Sierra Nevada and Interior Alaska, my work endeavored to:

1. Developed Framework
    a. Create a labeled benchmark dataset for detecting forest condition (mortality) at the scale of the individual tree,
    b. Develop a custom convolution neural network model for classification and mapping of forest conditions,

c. Determine which remote sensing data modality among airborne lidar, aerial imagery and hyperspectral performs best for detecting forest conditions,
d. Run models to generate a prediction map for entire study areas,

2. Ecological Analysis and Interpretation
    a. Determine the important topographical variables associated with the forest types (Interior Alaska).
    b. Apply mortality model to understand the interaction of mortality and forest fire (Sierra Nevada).

1.4 DEVELOPED FRAMEWORK

In my research, a robust framework integrating remote sensing and artificial intelligence techniques to detect various forest conditions, such as tree mortality and forest type distribution. The framework is an overarching process that explains each step including data preparation, labeling, model development, evaluation, and deployment. My developed framework (Figure 1) comprises of five main sections: creating labels (benchmark dataset), developing the model (machine learning and deep learning models), training and evaluating the model, and applying the model to generate high-resolution forest condition maps for the study area. For mortality classification, I manually created labels for tree mortality using high-resolution imagery (<1 m). Each tree label was based on the high-resolution (< 1 m) imagery, which took a significant amount of time to label over 15,000 trees. For forest type classification, I used field collected information to create labels. Therefore, the time required to create labels varied depending on the type of task. For training the model, I used the University of Washington's supercomputer, with training times ranging from 1 to 24 hours, depending on the type of remote sensing data.

Hyperspectral data required the most time for training. Detailed insights for each section of framework are provided into subsequent chapters.

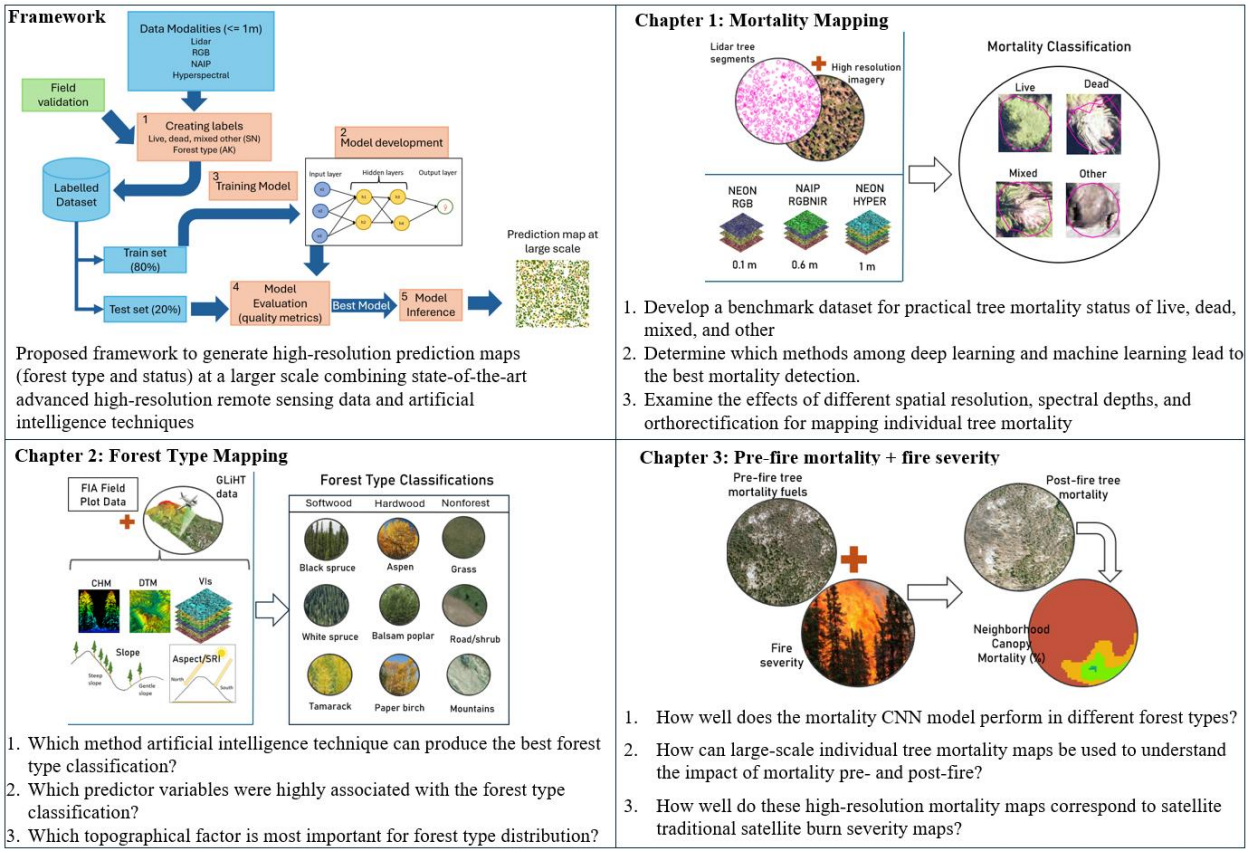

Figure 1.1: The framework used for generating high-resolution forest condition maps and each chapter with summarized research objectives.

1.5 REFERENCES

Alkama, R., & Cescatti, A. (2016). Climate change: Biophysical climate impacts of recent changes in global forest cover. *Science*, *351*(6273), 600–604. https://doi.org/10.1126/SCIENCE.AAC8083/SUPPL_FILE/AAC8083-ALKAMA-SM.PDF

Alonzo, M., Andersen, H.-E., Morton, D., & Cook, B. (2018). Quantifying Boreal Forest Structure and Composition Using UAV Structure from Motion. *Forests*, *9*(3), 119. https://doi.org/10.3390/f9030119

Andersen, H., Mcgaughey, R. J., & Reutebuch, S. E. (2005). Estimating forest canopy fuel parameters using LIDAR data. *Remote Sensing of Environment*, *94*(4), 441–449. https://doi.org/10.1016/j.rse.2004.10.013

Barber, V. A., Juday, G. P., & Finney, B. P. (2000). *Reduced growth of Alaskan white spruce in the twentieth century from temperature-induced drought stress*. *405*(June).

Barbour, M., Kelley, E., Maloney, P., Rizzo, D., Royce, E., & Fites-Kaufmann, J. (2002). Present and past old-growth forests of the Lake Tahoe Basin, Sierra Nevada, US. *Journal of Vegetation Science*, *13*(4), 461–472. https://doi.org/10.1111/J.1654-1103.2002.TB02073.X

Bergmüller, K. O., & Vanderwel, M. C. (2022). Predicting Tree Mortality Using Spectral Indices Derived from Multispectral UAV Imagery. *Remote Sensing*, *14*(9), 2195. https://doi.org/10.3390/rs14092195

Bolton, D. K., White, J. C., Wulder, M. A., & Coops, N. C. (2018). Updating stand-level forest inventories using airborne laser scanning and Landsat time series data. *Int J Appl Earth Obs Geoinformation*, *66*(December 2017), 174–183. https://doi.org/10.1016/j.jag.2017.11.016

Byer, S., & Jin, Y. (2017). Detecting Drought-Induced Tree Mortality in Sierra Nevada Forests with Time Series of Satellite Data. *Remote Sensing 2017, Vol. 9, Page 929*, *9*(9), 929. https://doi.org/10.3390/RS9090929

Bzdok, D., Altman, N., & Krzywinski, M. (2018). Points of significance: Statistics versus machine learning. *Nature Publishing Group*, 233. https://doi.org/10.1038/nmeth.4642

Campbell, M. J., Dennison, P. E., Tune, J. W., Kannenberg, S. A., Kerr, K. L., Codding, B. F., & Anderegg, W. R. L. (2020). A multi-sensor, multi-scale approach to mapping tree mortality in woodland ecosystems. *Remote Sensing of Environment*, *245*, 111853. https://doi.org/10.1016/j.rse.2020.111853

Cheng, Y., Oehmcke, S., Brandt, M., Rosenthal, L., Das, A., Vrieling, A., Saatchi, S., Wagner, F., Mugabowindekwe, M., Verbruggen, W., Beier, C., & Horion, S. (2024). Scattered tree death contributes to substantial forest loss in California. *Nature Communications*, *15*(1), 641. https://doi.org/10.1038/s41467-024-44991-z

Conservancy, S. N. (2014). *The State of the Sierra Nevada's Forests*. Sierra Nevada Conservancy 1152.

Coop, J. D., Parks, S. A., Stevens-rumann, C. S., Crausbay, S. D., Higuera, P. E., Davis, K. T., Dobrowski, S., Falk, D. A., Fornwalt, P. J., & Fulé, P. Z. (2020). Wildfire-Driven Forest Conversion in Western North American Landscapes. *BioScience*, *70*(8), 659–673. https://doi.org/10.1093/biosci/biaa061

Dial, R. J., Schulz, B., Lewis-Clark, E., Martin, K., & Andersen, H. E. (2021). Using fractal self-similarity to increase precision of shrub biomass estimates. *Ecology and Evolution*, *11*(9), 4866–4873. https://doi.org/10.1002/ECE3.7393

Douglas, T. A., Jones, M. C., Hiemstra, C. A., Arnold, J. R., & Blum, J. D. (2014). Sources and sinks of carbon in boreal ecosystems of interior Alaska: A review. *Elementa: Science of the Anthropocene*, *2*, 1–39. https://doi.org/10.12952/journal.elementa.000032

Egli, S., & Höpke, M. (2020). CNN-Based Tree Species Classification Using High Resolution RGB Image Data from Automated UAV Observations. *Remote Sensing*, *12*(23), 3892. https://doi.org/10.3390/rs12233892

Fassnacht, F. E., Latifi, H., Sterenczak, K., Modzelewska, A., Lefsky, M., Waser, L. T., Straub, C., & Ghosh, A. (2016). Review of studies on tree species classification from remotely sensed data. *Remote Sensing of Environment*, *186*, 64–87. https://doi.org/10.1016/j.rse.2016.08.013

Fettig, C. J., Mortenson, L. A., Bulaon, B. M., & Foulk, P. B. (2019). Tree mortality following drought in the central and southern Sierra Nevada, California, U.S. *Forest Ecology and Management*, *432*, 164–178. https://doi.org/10.1016/J.FORECO.2018.09.006

Fournier, R. A., Luther, J. E., Guindon, L., Lambert, M.-C., Piercey, D., Hall, R. J., & Wulder, M. A. (2003). Mapping aboveground tree biomass at the stand level from inventory information: Test cases in Newfoundland and Quebec. *Canadian Journal of Forest Research*, *33*(10), 1846–1863. https://doi.org/10.1139/x03-099

Fricker, A., Ventura, J. D., Wolf, A., North, M. P., Davis, F. W., & Franklin, J. (2019). A Convolutional Neural Network Classifier Identifies Tree Species in Mixed-Conifer Forest from Hyperspectral Imagery. *Remote Sensing*, *11*(19), 2326.

Furniss, T. J., Larson, A. J., Kane, V. R., & Lutz, J. A. (2019). Multi-scale assessment of post-fire tree mortality models. *International Journal of Wildland Fire*, *28*(1), 46. https://doi.org/10.1071/WF18031

Hamilton, D. A., Brothers, K. L., Jones, S. D., Colwell, J., & Winters, J. (2021). Wildland Fire Tree Mortality Mapping from Hyperspatial Imagery Using Machine Learning. *Remote Sensing*, *13*(2), 290. https://doi.org/10.3390/rs13020290

Hemming-Schroeder, N. M., Gutierrez, A. A., Allison, S. D., & Randerson, J. T. (2023). Estimating Individual Tree Mortality in the Sierra Nevada Using Lidar and Multispectral Reflectance Data. *Journal of Geophysical Research: Biogeosciences*, *128*(5), e2022JG007234. https://doi.org/10.1029/2022JG007234

Jain, P., Coogan, S. C. P., Subramanian, S. G., Crowley, M., Taylor, S., & Flannigan, M. D. (2020). A review of machine learning applications in wildfire science and management. *Environmental Reviews*, *28*(4), 478–505.

Kane, V. R., Bartl-Geller, B. N., North, M. P., Kane, J. T., Lydersen, J. M., Jeronimo, S. M. A., Collins, B. M., & Monika Moskal, L. (2019). First-entry wildfires can create opening and tree clump patterns characteristic of resilient forests. *Forest Ecology and Management*, *454*, 117659. https://doi.org/10.1016/j.foreco.2019.117659

Kattenborn, T., Eichel, J., & Fassnacht, F. E. (2019). Convolutional Neural Networks enable efficient, accurate and fine-grained segmentation of plant species and communities from high-resolution UAV imagery. *Scientific Reports 2019 9:1*, *9*(1), 1–9. https://doi.org/10.1038/s41598-019-53797-9

Lee, J. M., Mirocha, J. D., Lareau, N. P., Whitney, T., To, W., Kochanski, A., & Lassman, W. (2023). Sensitivity of Pyrocumulus Convection to Tree Mortality During the 2020 Creek Fire in California. *Geophysical Research Letters*, *50*(16), e2023GL104193. https://doi.org/10.1029/2023GL104193

Liu, Z., Peng, C., Work, T., Candau, J., Desrochers, A., & Kneeshaw, D. (2018). Application of machine-learning methods in forest ecology: Recent progress and future challenges. *Environmental Reviews*, *26*(4), 339–350.

Mäyrä, J., Keski-Saari, S., Kivinen, S., Tanhuanpää, T., Hurskainen, P., Kullberg, P., Poikolainen, L., Viinikka, A., Tuominen, S., & Kumpula, T. (2021). Tree species classification from airborne hyperspectral and LiDAR data using 3D convolutional neural networks. *Remote Sensing of Environment*, *256*, 112322. https://doi.org/10.1016/j.rse.2021.112322

Millar, C. I., & Stephenson, N. L. (2015). Temperate forest health in an era of emerging megadisturbance. *Science*, *349*(6250), 823–826. https://doi.org/10.1126/SCIENCE.AAA9933

Moskal, L. M., & Zheng, G. (2012). Retrieving forest inventory variables with terrestrial laser scanning (TLS) in urban heterogeneous forest. *Remote Sensing*, *4*(1), 1–20. https://doi.org/10.3390/rs4010001

Olden, J. D., Lawler, J. J., & Poff, N. L. (2008). *Machine learning methods without tears: A primer for ecologists*. *83*(2), 171–193.

Parks, S. A., Dobrowski, S. Z., Shaw, J. D., & Miller, C. (2019). Living on the edge: Trailing edge forests at risk of fire-facilitated conversion to non-forest. *Ecosphere*, *10*(3), e02651. https://doi.org/10.1002/ecs2.2651

Restaino, C., Young, D. J. N., Estes, B., Gross, S., Wuenschel, A., Meyer, M., & Safford, H. (2019). Forest structure and climate mediate drought-induced tree mortality in forests of the Sierra Nevada, USA. *Ecological Applications*, *29*(4), e01902. https://doi.org/10.1002/EAP.1902

Ruefenacht, B., Finco, M. V., Nelson, M. D., Czaplewski, R., Helmer, E. H., Blackard, J. A., Holden, G. R., Lister, A. J., Salajanu, D., Weyermann, D., & Winterberger, K. (2008). Conterminous U.S. and Alaska Forest Type Mapping Using Forest Inventory and

Analysis Data. *Photogrammetric Engineering & Remote Sensing*, *74*(11), 1379–1388. https://doi.org/10.14358/PERS.74.11.1379

Ruess, R. W., Winton, L. M., & Adams, G. C. (2021). Widespread mortality of trembling aspen (Populus tremuloides) throughout interior Alaskan boreal forests resulting from a novel canker disease. *PLOS ONE*, *16*(4), e0250078. https://doi.org/10.1371/journal.pone.0250078

Schiefer, F., Kattenborn, T., Frick, A., Frey, J., Schall, P., Koch, B., & Schmidtlein, S. (2020). Mapping forest tree species in high resolution UAV-based RGB-imagery by means of convolutional neural networks. *ISPRS Journal of Photogrammetry and Remote Sensing*, *170*, 205–215. https://doi.org/10.1016/j.isprsjprs.2020.10.015

Schmitt, C. B., Burgess, N. D., Coad, L., Belokurov, A., Besançon, C., Boisrobert, L., Campbell, A., Fish, L., Gliddon, D., Humphries, K., Kapos, V., Loucks, C., Lysenko, I., Miles, L., Mills, C., Minnemeyer, S., Pistorius, T., Ravilious, C., Steininger, M., & Winkel, G. (2009). Global analysis of the protection status of the world's forests. *Biological Conservation*, *142*(10), 2122–2130. https://doi.org/10.1016/J.BIOCON.2009.04.012

Shoot, C., Andersen, H.-E., Moskal, L. M., Babcock, C., Cook, B. D., & Morton, D. C. (2021). Classifying Forest Type in the National Forest Inventory Context with Airborne Hyperspectral and Lidar Data. *Remote Sensing*, *13*(10), 1863. https://doi.org/10.3390/rs13101863

Stephens, S. L., Collins, B. M., Fettig, C. J., Finney, M. A., Hoffman, C. M., Knapp, E. E., North, M. P., Safford, H., & Wayman, R. B. (2018). Drought, Tree Mortality, and Wildfire in Forests Adapted to Frequent Fire. *BioScience*, *68*(2), 77–88. https://doi.org/10.1093/BIOSCI/BIX146

Stovall, A. E. L., Shugart, H., & Yang, X. (2019). Tree height explains mortality risk during an intense drought. *Nature Communications*, *10*(1), 4385. https://doi.org/10.1038/s41467-019-12380-6

Swain, D. L. (2015). A tale of two California droughts: Lessons amidst record warmth and dryness in a region of complex physical and human geography. *Geophysical Research Letters*, *42*(22), 9999-10,003. https://doi.org/10.1002/2015GL066628

Tian, L., & Fu, W. (2020). Bi-Temporal Analysis of Spatial Changes of Boreal Forest Cover and Species in Siberia for the Years 1985 and 2015. *Remote Sensing*.

University of Alaska, A. (2017). *Alaska Center for Conservation Science. 2017. Alaska Vegetation and Wetland Composite*. https://accscatalog.uaa.alaska.edu/dataset/alaska-vegetation- and-wetland-composite

USDA. (2016). *New Aerial Survey Identifies More Than 100 Million Dead Trees in California*.

Van Mantgem, P. J., Falk, D. A., Williams, E. C., Das, A. J., & Stephenson, N. L. (2018). Pre-fire drought and competition mediate post-fire conifer mortality in western U.S. National Parks. *Ecological Applications*, *28*(7), 1730–1739. https://doi.org/10.1002/eap.1778

Van Mantgem, P. J., Falk, D. A., Williams, E. C., Das, A. J., & Stephenson, N. L. (2020). The influence of pre-fire growth patterns on post-fire tree mortality for common conifers in western US parks. *International Journal of Wildland Fire*, *29*(6), 513. https://doi.org/10.1071/WF19020

Van Wagtendonk, L. (2023). Comparing, matching, detecting, and predicting drought-induced tree mortality in the Sierra Nevada, California. *Doctoral Dissertation, University of Washington*.

Walker, X. J., Mack, M. C., & Johnstone, J. F. (2015). Stable carbon isotope analysis reveals widespread drought stress in boreal black spruce forests. *Global Change Biology*, *21*(8), 3102–3113. https://doi.org/10.1111/gcb.12893

White, J. C., Coops, N. C., Wulder, M. A., Vastaranta, M., Hilker, T., & Tompalski, P. (2016). Remote sensing technologies for enhancing forest inventories: A review. *Canadian Journal of Remote Sensing*, *42*(5), 619–641. https://doi.org/10.1080/07038992.2016.1207484

Xie, Y., Sha, Z., & Yu, M. (2008). Remote sensing imagery in vegetation mapping: A review. *Journal of Plant Ecology*, *1*(1), 9–23. https://doi.org/10.1093/jpe/rtm005

Young, D. J. N., Stevens, J. T., Earles, J. M., Moore, J., Ellis, A., Jirka, A. L., & Latimer, A. M. (2017). Long-term climate and competition explain forest mortality patterns under extreme drought. *Ecology Letters*, *20*(1), 78–86. https://doi.org/10.1111/ELE.12711

Chapter 2. ENHANCING INDIVIDUAL TREE MORTALITY MAPPING: THE IMPACT OF MODELS, DATA MODALITIES, AND CLASSIFICATION TAXONOMY

2.1 ABSTRACT

Tree mortality is rapidly increasing as a result of more frequent and extensive droughts and forest fires across the globe. The increasing pace and scale of disturbance and resulting mortality necessitates the study of tree mortality at the scale at which it occurs (individual trees) to develop effective management strategies. Achieving this objective requires high-resolution aerial or satellite remote sensing data supported by field validation and efficient modeling. However, the optimal remote sensing data modalities and models for mapping overstory tree mortality remain uncertain and there is a lack of benchmark datasets for reproducible research, comparison, and model improvement. In this research, we propose a framework to generate tree mortality maps at the scale of individual trees and a labeled benchmark dataset using open-source high-resolution remote sensing data. Our benchmark dataset consists of over 15,000 image crops that have been manually labeled via multi-annotator majority for live, dead, mixed, and other classes in National Ecological Observatory Network (NEON) RGB, NEON hyperspectral, and National Agriculture Imagery Program (NAIP) RGBNIR imagery. Specifically, we present a multi-class classification framework that categorizes lidar-derived tree segments as live, dead, mixed, or other. We compared the performance of different machine learning models, remote sensing data modalities and their associated spatial resolution, spectral depth, and orthorectification using our benchmark dataset. Among various models, we found Convolutional Neural Network (CNN) models outperformed all other models with the highest accuracies and F1 scores across all data modalities. Similarly, among remote sensing data modalities, NEON RGB data at 0.1 m

resolution performed best due to its high spatial resolution and high quality orthorectification. The overall accuracy of 87.27% with a macro F1 score of 0.76 was achieved using the RGB data with the CNN model. Our framework can be applied to any forest ecosystem in which lidar and raster imagery are available. We applied the framework using the best performing model and data modality to produce an individual tree mortality map over the Teakettle Experimental Forest in the southern Sierra Nevada. The framework and high-resolution mortality map can be valuable resources for forest managers and provide an invaluable basis for studying potential mortality drivers of dominant trees, forest inventory, selective logging, fire disturbance, and succession modeling.

2.2 INTRODUCTION

Globally, forest ecosystems are experiencing more frequent, warmer droughts due to increases in temperature and changes in precipitation patterns, which in turn result in increased canopy water deficit (Asner et al., 2016) and tree mortality (Allen et al., 2015; Greenwood et al., 2017; Hartmann et al., 2018; Leifsson et al., 2023; Millar & Stephenson, 2015). Resulting forest die-off events have deleterious impacts on ecosystem structure, function, services, nutrient cycle, carbon storage, and biophysical and biogeochemical land-atmosphere processes (Allen et al., 2010; Hartmann et al., 2018; Reichstein et al., 2013). As massive tree loss increases in pace and scale globally, the need to identify and map mortality grows in importance. As an example, forests in California's Sierra Nevada are suffering punctuated and chronic regional-scale tree mortality due to climate change induced increases in temperature, frequent drought, and mass fire (Adams et al., 2009; Breshears et al., 2005; Coop et al., 2020; Parks et al., 2019; Williams et al., 2013). The prolonged drought event from 2012 to 2016 alone resulted in the death of more

than 100 million trees with an estimated 35 million tree dying just in summer of 2016 (Byer & Jin, 2017; USDA, 2016).

High-resolution remote sensing data affords novel opportunities to capture overstory tree loss at the scale at which the phenomenon occurs—the individual tree—in turn improving our ecological understanding of drought-induced tree mortality impacts and the capacity to mitigate loss. Mapping mortality with high-resolution remote sensing data at the scale of overstory trees provides the most accurate assessments of tree mortality severity and pattern, which aids the development of strategies for management and restoration at a relevant pace and scale. Several previous studies focused on identifying and mapping tree mortality using moderate (30 m) to coarse (250 m) resolution at regional scale (Byer & Jin, 2017; Hamilton et al., 2021; Campbell et al., 2020). Other studies had mapped mortality at the scale of individual overstory trees using lidar and high-resolution imagery (Bergmüller & Vanderwel, 2022; Briechle et al., 2020; Fricker et al., 2019; Hemming-Schroeder et al., 2023; Kamińska et al., 2018; Stovall et al., 2019; Wing et al., 2015). Stovall et al., (2019) and Hemming-Schroeder et al., (2023) had used open-source high-resolution data for mapping individual overstory tree mortality across larger areas. While these studies demonstrateed large area mortality mapping at the scale of individual overstory trees, these studies did not compare the relative importance of open-source imagery at varying resolutions, model types, or classification taxonomy.

A critical research endeavor lies in investigating and comparing the performance of readily accessible open-source, high-resolution remote sensing imagery for individual tree mortality mapping. Further, in the United States, multi-temporal, high-resolution open-source remote sensing data are available. However, it is not clear which dataset and associated spatial resolution, spectral resolution and orthorectification is best for producing accurate mortality

maps. Examples of these products include the National Ecological Observatory Network (NEON) high fidelity airborne lidar, NEON aerial imagery (RGB) at 0.1 m resolution, NEON hyperspectral (426 bands) at 1 m resolution, and the National Agriculture Imagery Program (NAIP) four bands (RGBNIR) imagery at 0.6 m resolution or less. We synonymously refer to these different remote sensing data types as data modalities.

Accurate and extensive mapping of overstory tree mortality requires not only high-resolution data but also the application of the most suitable algorithmic approach to automate the process. Even though previous studies have assessed the performance of a range of machine learning models for tree level species classification (Mäyrä et al., 2021), it is not clear which model is best for individual tree mortality mapping. Some of the commonly used machine learning models are random forest (RF), support vector machine (SVM), extreme gradient boosting trees (XGBoost), and deep learning models, artificial neural network (ANN), and convolutional neural network (CNN). Among these models, CNNs have emerged as a popular choice for tree species identification using high-resolution datasets (Egli & Höpke, 2020; Fricker et al., 2019; Mäyrä et al., 2021; Schiefer et al., 2020).

For the comparison of models and data modalities to map mortality at the scale of individual overstory tree, there is no benchmark data available for classifying and validating individual tree mortality algorithms (Hartmann et al., 2018). Benchmark datasets have promoted progress over the past 20 years in the field of machine learning, computer vision, and natural language processing (Deng et al., 2010; Geiger et al., 2013; Lin et al., 2014) at they promote easy model comparison between studies.

Further in forested landscapes with numerous non-tree objects, such as boulders or human infrastructures, and various tree in different states of decay, binary classification of tree mortality

may not be sufficient to capture the full range of variability and thus ecological conditions. Past studies of individual tree mortality have only tested binary, live and dead classes (Bergmüller & Vanderwel, 2022; Briechle et al., 2020; Fricker et al., 2019; Hemming-Schroeder et al., 2023; Kamińska et al., 2018; Stovall et al., 2019; Wing et al., 2015). As the wildland urban interface (WUI) expands (Godoy et al., 2022; Radeloff et al., 2018), the need for a model that identifies standing dead or dying trees and non-tree objects is increasingly importance. In this study, we test the effects of a multi-class classification taxonomy that captures tree statuses of live, dead, mixed (e.g., yellowing/dying, partially dead canopies or a live and dead tree within a lidar-derived tree segment), or other (e.g., boulder, shadow, or non-tree objects).

The primary aim of this research is to understand the impact of various key factors for producing accurate individual tree mortality maps on mixed-conifer forest ecosystems that can be extended over large areas. In this study we examine the impact of modelling algorithms; remote sensing data modalities and associated spatial resolution, spectral depth, and orthorectification; and mortality classification taxonomy. To achieve this objective, we developed a large, manually labeled, mortality-status benchmark dataset of high-resolution open-source multispectral and hyperspectral datasets, which is critical for validating and improving mortality algorithms (Hartmann et al., 2018; Weinstein et al., 2021). Using benchmark data, we then compared the performance of deep learning models with other machine learning models for mapping individual overstory tree mortality. We used individual tree segments generated from high fidelity lidar data for identifying individual canopy tree crowns. The main objectives of this research are as follows:

1. Develop a benchmark dataset for practical tree mortality status of live, dead, mixed, and other that is derived from lidar delineated tree segments and open-source, high-resolution airborne imagery from multiple modalities.

2. Determine which methods among deep learning (CNN and ANN) and various machine learning (RF, SVM, and XGBoost) lead to the best mortality detection.

3. Examine the effects of different spatial resolution, spectral depths, and orthorectification for mapping individual overstory tree mortality as represented by high-resolution open-source remotely sensed data modalities RGB aerial imagery (NEON), RGBNIR aerial imagery (NAIP), and hyperspectral (NEON).

4. Using the best data modality and method identified above, produce maps of overstory tree mortality over the Teakettle experimental area for 2013, 2017, and 2018 that provides the tree status along with height and canopy area information.

2.3 MATERIALS

2.3.1 Study Area

This study uses data from the Dinkey Creek watershed and North Fork Kings River area within the Sierra National Forest located in the southern Sierra Nevada (Figure 2.1), which suffered a high level of tree mortality due to severe, warm drought (Warren, 2019). We use two areas from the region to train our mortality model, A) a site in Dinkey Creek Watershed and B) sites in Teakettle Experimental Forest within North Fork Kings River (Figure 2.1). These areas were selected because of the availability of multi-temporal aerial lidar, high-resolution aerial multispectral, and hyperspectral imagery acquired by NEON and NAIP that would be commonly collected and available over large areas.

The study areas are located in a region of the southern Sierra Nevada, which has a Mediterranean climate pattern and spans an elevation range of approximately 300 to 3000 meters (Krofcheck et al., 2017). The mean annual precipitation ranges from 50 to 100 cm based on an elevation gradient of low to high that mostly falls as snow during winter (Krofcheck et al., 2017; North et al., 2004). The temperature ranges from -3 ^{0}C to 25 ^{0}C with hot dry summer and mild moist winter (Krofcheck et al., 2017; North, 2002).

The region occupies an elevation band that is predominantly composed of Sierran Mixed-Conifer forest (Goodwin et al., 2020). The overstory vegetation in this region is dominated by white fir (*Abies concolor*), sugar pine (*Pinus lambertiana*), incense-cedar (*Calocedrus decurrnes*), Jeffrey pine (*Pinus jeffreyi*), Ponderosa Pine (*Pinus ponderosa*) and red fir (*Abies magnifica*) (Krofcheck et al., 2017; North et al., 2004). Deciduous trees are present but less common and consist of Black oak (*Quercus kellogii*), canyon live oak (*Quercus chrysolepis*), and bitter cherry (*Prunus emarginata*) (Krofcheck et al., 2017; North et al., 2004). The tree species are adapted to cool droughts; however, they are not well adapted to prolonged drought with warm and dry conditions in fire suppressed forests (Stephens et al., 2018).

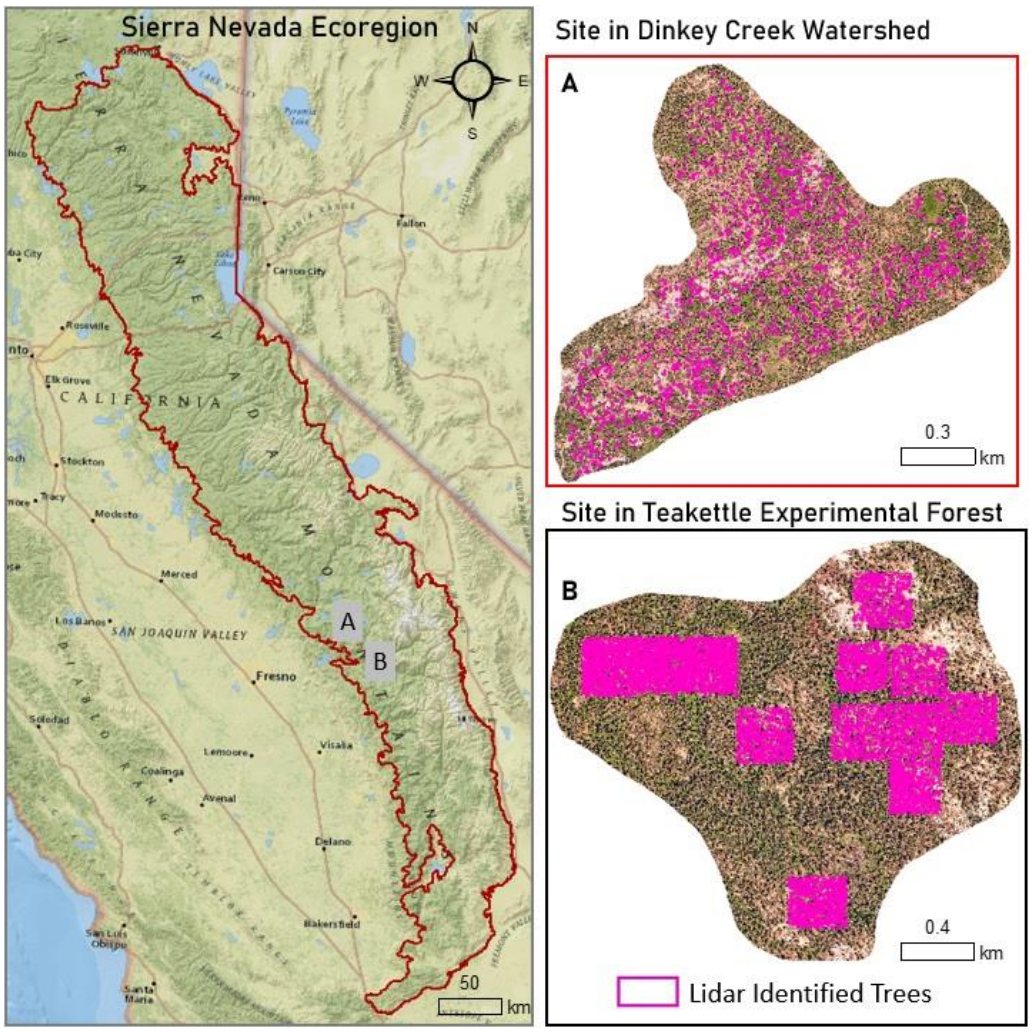

Figure 2.1: California's Sierra Nevada Ecoregion with highlighted study sites A and B that are used for training models. Site A is in Dinkey Creek Watershed and site B includes Teakettle Experimental Forest in North Fork Kings River.

2.3.2 Airborne Lidar, Ortho-imagery, Hyperspectral and Field Data

Multi-temporal high spatial and spectral resolution remote sensing aerial imaging datasets along with high pulse density airborne lidar data were available for the study area (Figure 2.1). We used multi-temporal high fidelity aerial lidar data with high spatial resolution Red-Green-Blue (RGB), four bands (RGBNIR), and hyperspectral imagery (Table 2.1) for developing the models. To create a large enough sample of dead canopy trees we used datasets from across 2013, 2017, and 2018. We highlighted a location in site A in the Dinkey Creek watershed in

Figure 2.2 to demonstrate live trees in 2013 that were mostly dead in 2018. We also used in-situ tree data collected from nine control plots in 2017 in the Teakettle Experimental Forest to validate our labels (Figure 2.1) (Goodwin et al., 2020). Field data collection included live and dead trees within the plot ≥ 5cm diameter at breast height, tree species, and agents of mortality.

2.3.3.1 National Ecological Observatory Network (NEON)

The NEON is a widespread program that oversees data collection at more than 80 sites across the United States (Weinstein et al., 2021). The annual data collection includes an aerial survey by the Airborne Observation Program (AOP) using RGB, lidar, and hyperspectral sensors and a field survey at fixed sampling plots on each site (Weinstein et al., 2021). The NEON AOP employs fixed-wing aircraft that fly at an altitude of approximately 1000m above ground to conduct surveys of sites during leaf-on-conditions mostly from May to October (Weinstein et al., 2021). NEON utilized ATCOR4r (Atmospheric and Topographic Correction) to conduct atmospheric correction on the NEON Imaging Spectrometer, followed by orthorectification, and the imagery was then output onto a fixed and uniform spatial grid using nearest neighbor resampling (Fricker et al., 2019). In this study, we used the lidar, ortho-imagery, and hyperspectral data collected by NEON's AOP at the Lower Teakettle area during the months of June 2013, 2017, and 2018. All NEON lidar and imagery data used for this analysis were downloaded from the NEON online data portal (https://data.neonscience.org/data-products/explore). The following NEON datasets for 2013, 2017, and 2018 years were downloaded and examined in this study:

1. Georectified lidar data up to 6 pulses per square meter was available by flight lines in .laz format (NEON, 2021a).

2. The NEON RGB was collected using a D8900 camera and was orthorectified to create a raster image with 0.1m spatial resolution (Weinstein et al., 2021). The RGB data was collected at 0.25 m resolution during 2013 and at 0.1 m resolution during 2017 and 2018 (NEON, 2021b). All year data was resampled to 0.1 m resolution to match the spatial resolution.
3. The hyperspectral data is at 1 m spatial resolution collected using a pushbroom instrument. NEON hyperspectral sensor collected reflectance between 380 to 2500 nm with a spectral sampling interval of 5 nm for a total of 426 bands (NEON, 2021c; Wasser, 2023).

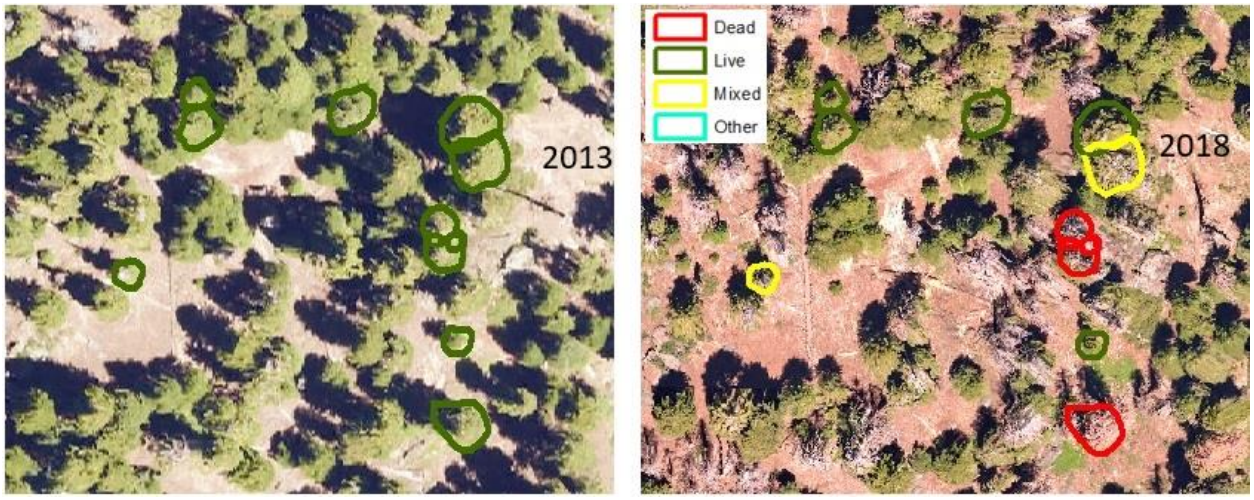

Figure 2.2: Selected imagery from NEON RGB data collected in 2013 (left) and 2018 (right) along with randomly sampled lidar derived tree segments acquired in 2013 from site A in the Dinkey Creek Watershed Many areas in the study site such as these demonstrated live trees in the early drought period (2013) which died during the prolonged drought period (2018).

2.3.3.2 National Agriculture Imagery Program (NAIP)

The NAIP is administered by the USDA Farm Service Agency and is a nation-wide effort to collect biennial imagery during the leaf-on phenology state of the agricultural growing season. The NAIP imagery consists of four bands, including Blue (420-492 nm), Green (533-587 nm), Red (604-664 nm), and Near-Infrared (683-920 nm) (USDA, 2021b) that were acquired 4877 m

above ground using Leica ADS 100 airborne digital sensor (Bhatt & Maclean, 2023). In California, the data were collected in even years and varied in spatial resolution. Although the program collects and sells commercial grade data collected at 40 cm resolution, the data are provided publicly at 1m resolution from 2010 to 2016 period. The data collected in 2018 and after are available publicly at 0.6 m resolution. All the NAIP imagery was resampled to 0.6 m resolution using the nearest neighbor method with resample tool of ArcMap (version 10.6.1). Since the NAIP program only acquires data during even years, NAIP data collected in 2012 (USDA, 2021c) and 2016 (USDA, 2021a) years were used as a supplement for the year of 2013 and 2017 NEON data (more detail provided in section 3.2). The NAIP data are available throughout the State of California.

Table 2.1: Data source, spectral and spatial resolution, and year of data used for the research.

Data type	Imagery Years	Spectral Resolution (Bands)	Spatial Resolution (m)
Lidar	2013, 2017, 2018	NIR	-
NEON RGB	2013, 2017, 2018	Blue, Green, and Red	0.1 (resampled to 0.6 and 1)
NEON Hyperspectral	2013, 2017, 2018	RGB, RGBNIR, and Visible to infrared (426 bands from 280 to 2510 nm)	1
NAIP RGBNIR	2012, 2016, 2018	Blue, Green, Red, and NIR	0.6

2.4 METHODS

The main goal of the study was to analyze the performance of various machine learning and deep learning models for identifying individual overstory tree mortality status in a mixed-conifer forest using high-resolution open-source aerial lidar, orthoimagery, and hyperspectral data. We wanted to approach this study using methods that would be appropriate for a study of mortality over large (1000s to 100,000s ha) ecosystems. We therefore identified individual overstory trees from airborne lidar data using an automated tree segmentation algorithm. We included the four mortality statuses of live, dead, mixed (partially dead), and other (boulder, shadow) for the classification. The main task was divided into five sections: 1) generating tree segments from aerial lidar data, 2) creating benchmark dataset, 3) model development, 4) model training, 5) model evaluation to finalize the best model and data modality to produce mortality map (Figure

2.3).

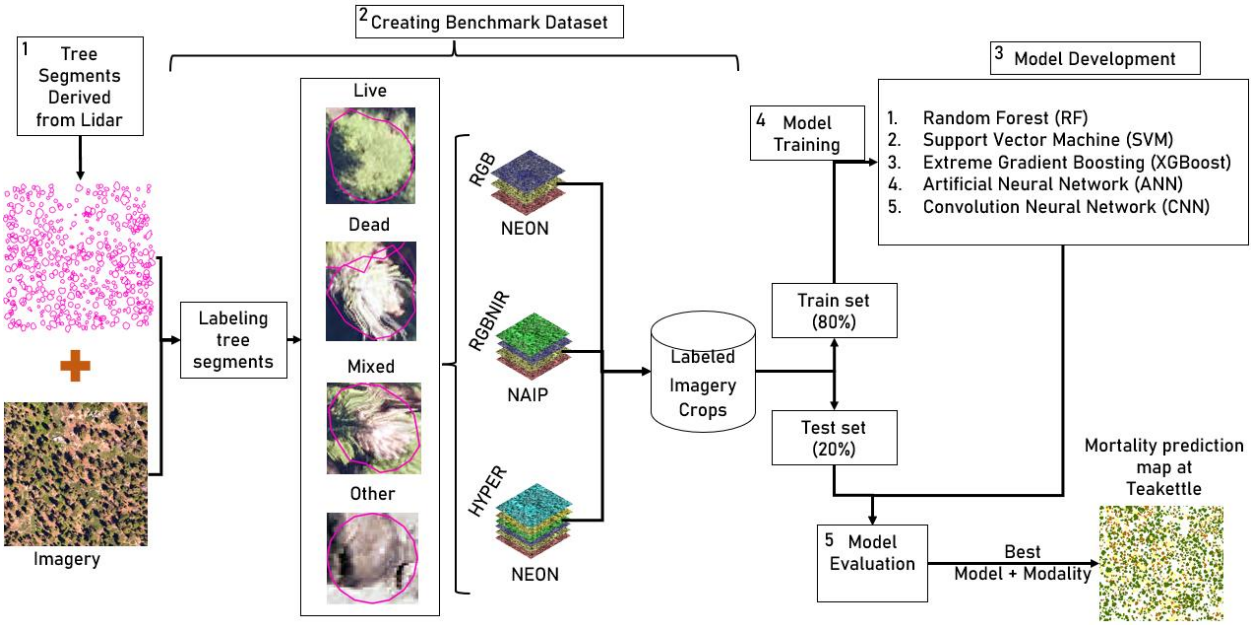

Figure 2.3: Schematic diagram of framework highlighting the five main steps with data modality and models used for the classification and mapping of overstory tree mortality status.

2.4.1 Generating Tree Segments from Airborne Lidar

We used the TreeSeg tool within the FUSION lidar processing toolset (McGaughey, 2018), to identify individual trees from lidar data. TreeSeg implements the watershed transform algorithm (McGaughey, 2018). We used watershed segmentation as it is a well-established algorithm that is commonly used in forestry workflows in this region (Jeronimo et al., 2019; Kane et al., 2019; M. P. North et al., 2017) and has been evaluated for both error of commission and omission (Jeronimo et al., 2018) and considered suitable for mapping mortality in Sierra Nevada forests (Stovall et al., 2019). The watershed transform algorithm works by utilizing a single input: the canopy height model (CHM), which is a raster product derived from lidar point cloud that represents the height above ground of the highest lidar return landing in each grid cell as a pixel value. The tree segment polygon derived from the lidar data captures tree height (above 2 m) and canopy area (Jeronimo et al., 2018). We refer to these segmented objects as tree approximate objects (TAOs) because they can either represent one canopy dominant tree or a tree with a

number of subordinate trees mistakenly identified as a single tree (Figure 2.4) (Jeronimo et al., 2018). The tree segments (TAOs) generated from 2013, 2017 and 2018 lidar data have been used in the analysis and paired with the aerial imagery from the same year (or neighboring year when required). We use lidar derived tree segments to represent overstory trees in this study because lidar segmentation is an automated process with freely available tools and can easily be extended to larger areas.

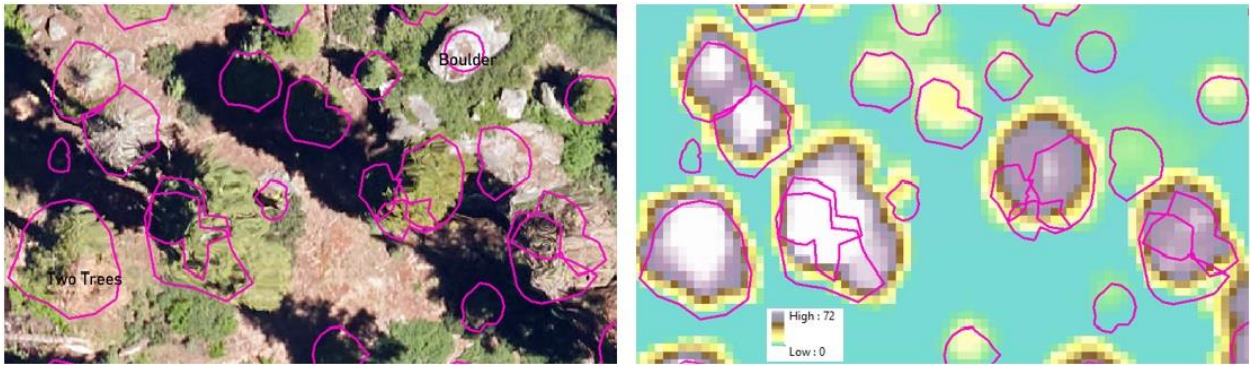

Figure 2.4: Demonstration that lidar derived tree-approximate objects (TAOs) do not always represent a single tree with NEON RGB (left) and canopy height model (CHM) (right). TAOs may represent a single tree, multiple trees or boulders, and other non-tree objects.

2.4.2 Creating Benchmark Dataset

We used two sites (Figure 2.1) to create a benchmark dataset to train and test models for mortality-status prediction. Our labeled benchmark dataset includes exclusively-human-annotated data of class labels of TAOs for live, dead, mixed, and other classes. While labeling, images containing each TAO were zoomed in using ArcMap version 10.6.1 (Esri, 2018) to be able to recognize it accurately for assigning classes.

The labeling of TAOs was based on a manual assessment of individual tree status using high-resolution NEON and NAIP imagery. To avoid inconsistency in the labeling process of TAOs, we developed the following rules for classifying TAOs. TAOs with over 80% of pixels that appeared live were classified as live. TAOs with over 80% of pixels that appeared dead were classified as

dead. Any TAO where over 20% of TAO pixels had different mortality statuses of live and dead was classified as a mixed TAO. Any TAOs that were not trees such as a boulder or shadow were classified as other (these represent the typical error of commission by tree segmentation algorithms).

To come to the final label for the TAOs, we used a multi-annotator majority. Each TAO was digitally reviewed by a minimum of 2 experts. In difficult or ambiguous cases where the first two annotators disagreed, a third expert was consulted, and the label was determined via majority. Using these labeled TAOs, we cropped each data modality using a bounding box around TAOs to create image crops (Figure 2.5). More detail about creating crops is provided in supplementary material (section S1).

To create a robust separation between training and testing data, we used intersection over union (IoU) to identify overlapping TAOs that were likely to represent the same tree across multiple years. Any TAOs with over 50% IoU were defined as multi-year TAOs and put in either the train or test set, but not both. This ensured that the same tree, even when imaged during a different year, would not end up in both the train and test set. We sampled approximately 80% of these multi-year TAOs for the train set and 20% for the test set.

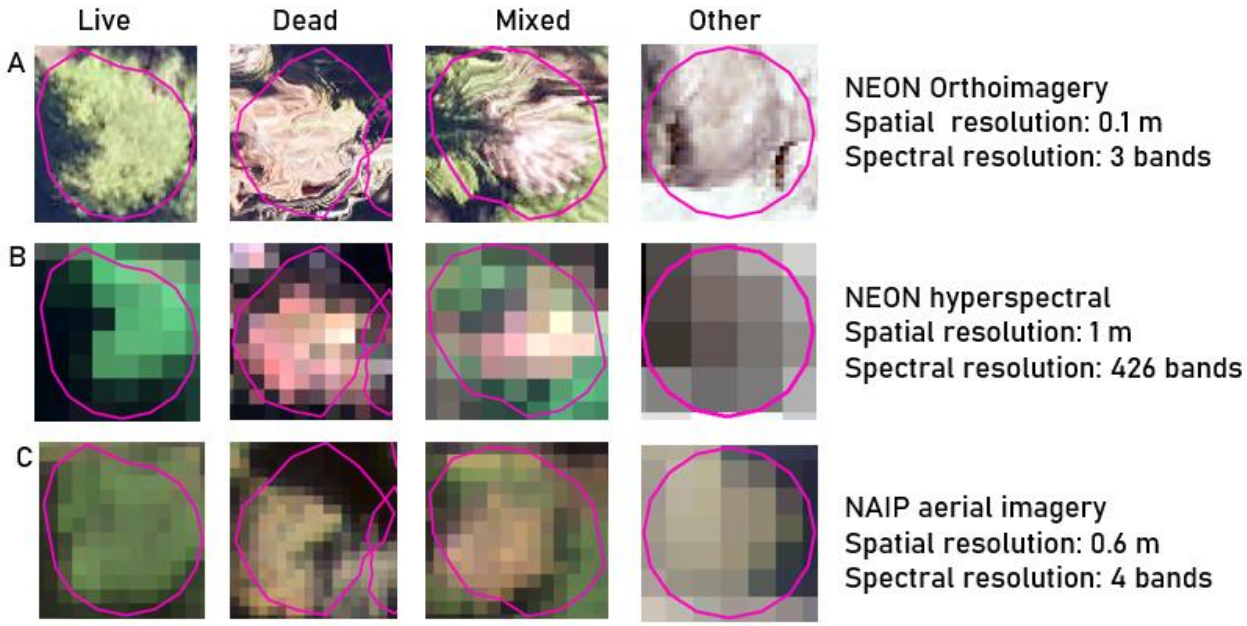

Figure 2.5: Representation of mortality classes with all data modalities used in this research, all displayed in RGB bands overlaid with TAOs. (A) represents NEON RGB data at 0.1 m spatial resolution, (B) represents NEON hyperspectral data with 426 bands at 1 m spatial resolution, and (C) represents NAIP four bands (RGBNIR) imagery at 0.6 m spatial resolution.

2.4.2.1 Labeling TAOs for NEON Products

For site A in the Dinkey Creek watershed area, we used uniform random sampling to select the training TAOs. There were around 2,700 TAOs selected for each year of 2013, 2017 and 2018. For site B, we selected TAOs that overlapped the in-situ field plot area. There were 6380 TAOs for 2017 and 1643 TAOs for 2018. Out of 15261 total TAOs, there were around 9681 unique TAOs. We used ArcMap (version 10.6.1) to overlay each year's TAOs on top of same year NEON RGB imagery to manually create labels for TAOs (Figure 2.5). For example, we overlaid 2013 lidar derived TAOs on top of 2013 NEON RGB imagery and manually assessed the tree status to assign the label for a particular TAO. We repeated the same process to create labels for site B in Teakettle experimental forest. In addition, the label created for TAOs over the field plot areas, which were in site B, were cross validated using the field measurement. For cross validating our labels, we used an automated pairwise matching of field trees to TAOs. The tree matching was conducted via a matching algorithm which minimized the 3d distance between

lidar and field measurements. We examined every matched and unmatched TAO and field tree manually and corrected errors by comparing the imagery and tree metrics. Using 3310 matched trees, we validated our labels. Our digitized labels for live agreed with field labels 97% of time, while dead agreed 94% of time.

2.4.2.2 Labeling TAOs for NAIP Products

The TAOs derived from lidar data acquired by the NEON program were not completely aligned on top of NAIP imagery (Figure 2.6) due to the difference in the orthorectification process of NAIP and NEON. This difference creates a shift of imagery when overlaid with TAOs (Figure 2.6). In addition, the NAIP program only acquires data during even years, therefore, to create labels for 2013 and 2017 lidar derived TAOs we used 2012 and 2016 NAIP imagery respectively. We used a similar process as explained in section 3.2.1 to create labels for both sites (A and B) for NAIP imagery. Even though we used the same TAOs the labels for NAIP were not always the same as NEON due to differences in projective effects and timing.

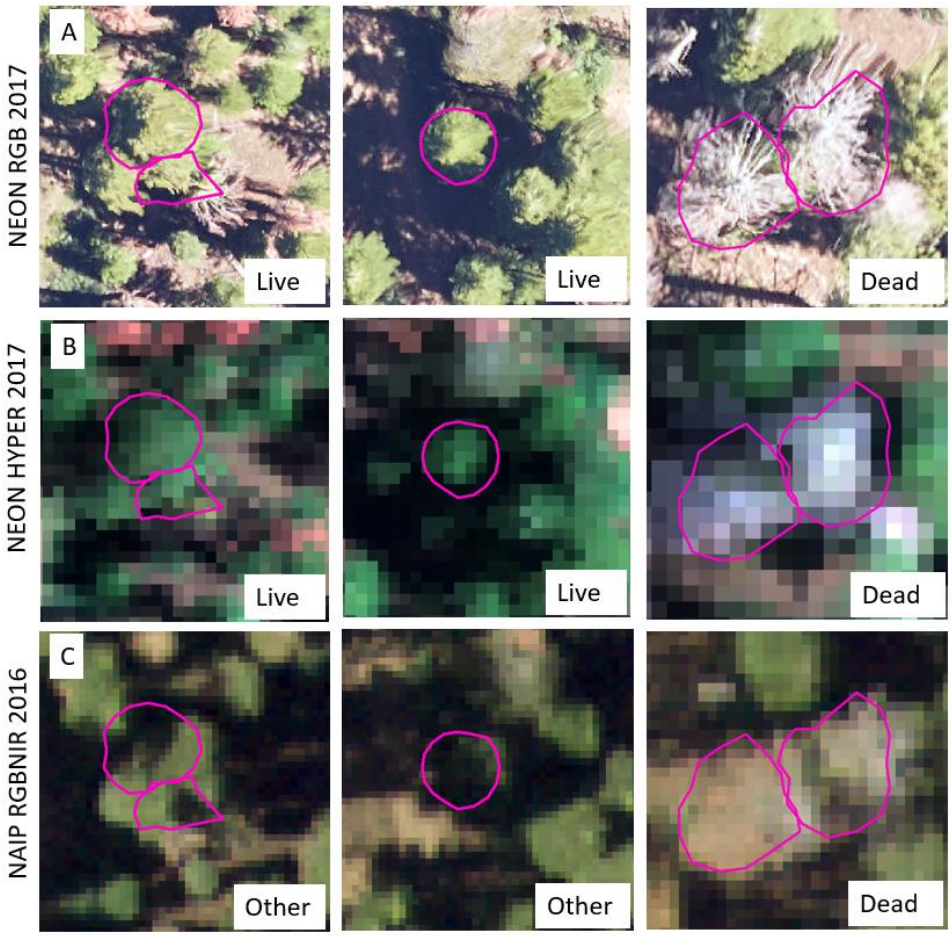

Figure 2.6: Demonstrating the effect of the difference in multi-sensor and georectification process and how lidar derived tree segment overlaps the imagery. (A) represent NEON RGB imagery collected in 2017, (B) represent NEON hyperspectral collected in 2017, (B) represent NEON hyperspectral collected in 2017, and (C) represent NAIP imagery acquired in 2016. A, B, and C are displayed in RGB with 2017 TAOs overlaid on top.

2.4.3 Model Development

We compare a range of classical machine learning models implemented in scikit-learn (Pedregosa et al., 2011) to custom deep learning CNN and ANN models. We developed a CNN architecture for the classification of individual tree mortality using the PyTorch (Paszke et al., 2019) framework in Python. Our custom CNN model is relatively simple, consisting of three convolution layers with 3x3 kernels followed by three linear layers (Figure 2.7). Each convolution layer is followed by batch normalization, rectified linear units (ReLu) as the activation function, and max pooling. Batch normalization is a technique to reduce training time

and has a regularization effect that reduces overfitting (Ioffe & Szegedy, 2015). Then, these feature maps are converted to one dimensional vector format before passing to the linear layers. Finally, we get the probabilities values of classes using the softmax in the last layer.

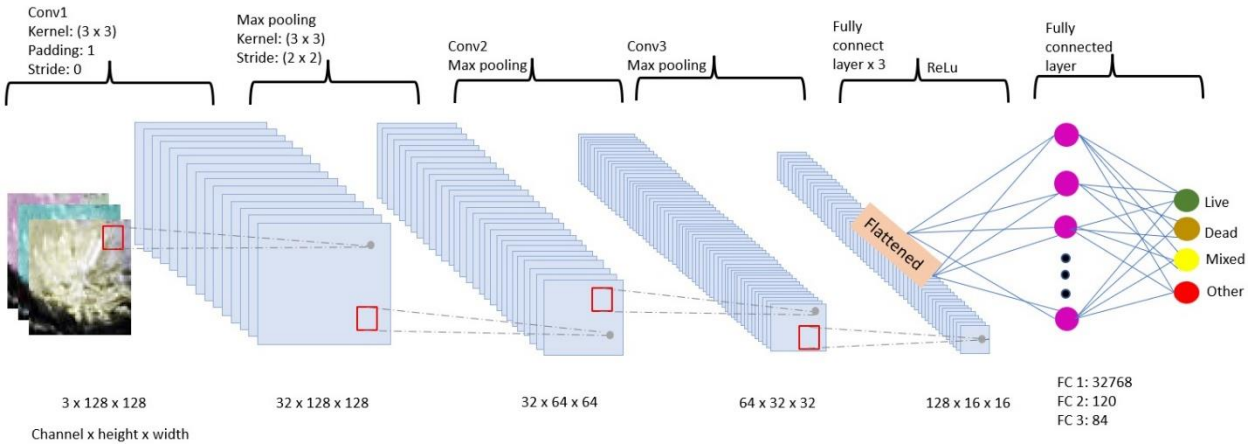

Figure 2.7: Mortality CNN model architecture for classifying mortality status of individual trees based on lidar derived tree approximate objects (TAOs). The example presented here is for NEON RGB imagery.

We compared the performance of the convolution neural network model with other widely used models such as random forest (RF), support vector machine (SVM), extreme gradient boosting (XGBoost), and artificial neural network (ANN) (Mäyrä et al., 2021). For the ANN model, we used the same model architecture as the Mortality CNN (Figure 2.7), except that we replaced all convolutional layers with linear layers. Image crops of each data modality (RGB, RGBNIR, and hyperspectral (426 bands)) were used as input for the CNN and ANN models. For the machine learning models, we extracted the seven summary statistics including minimum, first quartile, median, third quartile, standard deviation, mean, and maximum of all the spectral bands for each cropped imagery using bounding box. A total of 21 features for RGB, 28 features for NAIP, and 2982 features for hyperspectral data were used.

2.4.4 Model Training

In total, we used more than 15,000 labeled samples in this study (Table 2.2). We trained and evaluated all our models on our benchmark dataset as described in section 3.2. For all the models, we used z-score to normalize the data using the mean and standard deviation of the training set, which is a standard practice of model development. The normalization of data helps to prevent the domination of classification due to features with larger values and accelerates the convergence of deep learning methods (Mäyrä et al., 2021).

For training deep learning models, we used cross-entropy loss, Adam optimizer, and augmentation techniques to improve generalization of model on unseen data. Deep learning models were trained using NVIDIA 2080 Ti GPU on the Hyak supercomputer of the University of Washington, Seattle, United States. More in-depth detail about training models is provided in the supplementary material (Section S2). For machine learning models, we used randomized search for optimal hyperparameter selection. We used randomized search on five parameter combinations with five-fold random cross-validation on training data, then the best cross-validation score model was fitted to the complete training set.

2.4.5 Model Evaluation

To quantify model performance, we used overall accuracy (OA), precision (also known as user's accuracy (UA)) and recall (also known as producer's accuracy (PA)), and F1 score. We also used macro averages of precision, recall, and F1 score which take the average across classes for multi-class classification for determining the best data modality and model (Mäyrä et al., 2021). These metrices are derived using the following formulas with true positives (TP), true negatives (TN), false positives (FP), false negatives (FN) and total numbers of items (N).

$$(1)\mathrm{OA} = \frac{\mathrm{TP} + \mathrm{TN}}{\mathrm{N}} \qquad (2)Recall = \frac{TP}{TP+FN} \qquad (3)Precision = \frac{TP}{TP+FP}$$

$$(4)F1 = 2 * \frac{Precision * Recall}{Precision + Recall}$$

2.4.5.1 Evaluation of Different Spatial and Spectral Resolution and Orthorectification

To evaluate the performance of different spatial resolutions we resampled NEON RGB at 0.1 m resolution to 0.6 m and 1 m resolution using the resample tool in ArcMap (version 10.6.1). Similarly, to assess the impact of spectral depth, we extracted RGB and RGBNIR from NEON hyperspectral data at 1 m resolution. In addition, to evaluate the impact of the orthorectification process on model accuracy, we experimentally shifted TAOs. There are multiple factors that affect the alignment of TAOs with NAIP such as plane position, camera angle, topography, tree position, height, and lean. The cumulative effect of all these factors creates an aggregated random shift of TAO when overlaid with the NAIP imagery. We observed multiple (20) TAOs and NAIP imagery misalignment and found that they were randomly misaligned in all directions. Similarly, we also measured the gap between tree edges and TAOs in NAIP imagery. Therefore, to create an experimental shift we used uniformly random perturbations in both latitude and longitude ranging from -3 to +3 meters based on our measurements of tree shifts. We chose this simple perturbation method so as to introduce the fewest assumptions and make an unconfounded experiment investigating the importance of georectification. We then used these shifted TAOs on NEON RGB at 0.1 m resolution to measure the impact of shifted tree crowns caused by orthorectification.

2.5 RESUTLS

2.5.1 Benchmark Dataset

We created mortality status labels for over 15,000 TAOs that represent overstory individual trees. Using these labeled TAOs, we cropped NEON RGB, hyperspectral, and NAIP four bands imagery to create image crops (chips). Our benchmark dataset includes over 15,000 manually labeled image crops with mortality status of live, dead, mixed, and other for all data modalities. The total number of labeled image crops for each class for each data modality is shown in Table 2.2. The distribution of class labels for each year is presented in Table A4. This benchmark provides annotations of data for overstory tree mortality detection using multiple sensor types across the mixed-conifer forest ecosystems. The inclusion of multiple data modalities is critical because each data modality has potential strengths and limitations for model development, such as increased spatial vs increased spectral resolutions. This benchmark only measures the overstory tree mortality status and not the understory as none of the sensors detect everything that is below the top of the outermost canopy. The benchmark dataset enables reproducible results by supporting the classification, validation, and comparison of algorithms and providing the baseline for improving mortality detection algorithms in the future (Hartmann et al., 2018; Weinstein et al., 2021).

All datasets created for training and evaluating models and our train-test split will be open-sourced (see Data Availability). The published dataset consists of cropped imagery with labels for all remote sensing data modalities including RGB, hyperspectral, and NAIP.

Table 2.2: Total number of labeled TAOs across mortality classes such as live, dead, mixed, and other. Slight variation across modalities is due to temporal and orthorectification shifts in the underlying imagery as discussed in section (3.2.2).

Mortality Classes	RGB (NEON)	Hyperspectral (NEON)	Percentage (%) (NEON)	NAIP	Percentage (%) (NAIP)
Dead	2737	2737	17.93	2470	16.35
Live	9946	9946	65.17	9314	61.63
Mixed	1718	1718	11.26	2078	13.75
Other	860	860	5.64	1249	8.27
Total	15261	15261	100	15111	100

2.5.2 Classification Results

2.5.2.1 Performance of Different Models for Tree Mortality Detection

We compared the performance of CNNs with ANNs, XGBoost, RF, and SVM models for the classification of individual tree mortality using the high-resolution multi-sensor data modalities described above. The CNN model outperformed all other models with the highest macro average F1 score (0.61 to 0.76) and overall accuracy of nearly 75.26 to 87.275% across data modalities (Figure 2.8). The CNN model has the highest F1 score for all the classes across all the models (Table 2.3).

Among other models, ANN had the highest macro average F1 score and overall accuracy across all data modalities. ANN was followed by XGBoost and RF for NEON RGB and NAIP imagery (Table A1). The SVM method had significant difficulties separating mixed classes with both NEON RGB and NAIP imagery. However, SVM with NEON hyperspectral was able to separate all four classes. For NEON hyperspectral, SVM and XGBoost performed well after ANN with F1 scores of 0.64 and 0.61 respectively, and accuracy of nearly 81% (Table A1).

Table 2.3: Test set results of CNN models across remote sensing data modalities.

Mortality	RGB			Hyperspectral			NAIP		
Status	Precision	Recall	F1	Precision	Recall	F1	Precision	Recall	F1
Dead	0.85	0.90	0.87	0.84	0.87	0.85	0.72	0.68	0.70
Live	0.93	0.95	0.94	0.88	0.96	0.92	0.81	0.92	0.86
Mixed	0.60	0.54	0.57	0.65	0.37	0.47	0.50	0.36	0.42
Other	0.74	0.63	0.68	0.60	0.44	0.51	0.61	0.37	0.46
Macro avg	0.78	0.75	0.76	0.74	0.66	0.69	0.66	0.58	0.61
OA			87.27%			84.51%			75.26%

2.5.2.2 Performance of Different Data Modalities for Tree Mortality Detection

We evaluated the suite of models across all modalities in our benchmark of NEON RGB, NEON hyperspectral, and NAIP four bands imagery for the classification of individual tree mortality. Among various data modalities, NEON RGB at 0.1 m resolution had the highest macro average F1 score for the CNN model (Table 2.3) and generally the highest macro average F1 score and accuracy across all models except for SVM (Figure 2.8). This was followed by the NEON hyperspectral at 1 m resolution with 426 bands. The NAIP imagery had the overall lowest performance across all models.

NEON RGB had the highest F1 score for all classes with the best performing model, the CNN. Furthermore, NEON RGB data had the highest F1 score for live, dead, and other classes across all the models (Tables 2.3 and A1). Whereas for mixed class both NEON RGB and hyperspectral were found to have the highest F1 score depending on model (Table A1). All data modalities had above 0.9 accuracy for live class across all models (Figure A1-A4). Across all data modalities, the live and dead classes were identified with the highest accuracies whereas mixed and other classes were difficult to classify (Figure A1 to A4). The most common source of

error for mixed class was confusion with live class (Figure A1 to A4). Similarly, the main source of error for the other class was confusion with both the live and dead classes.

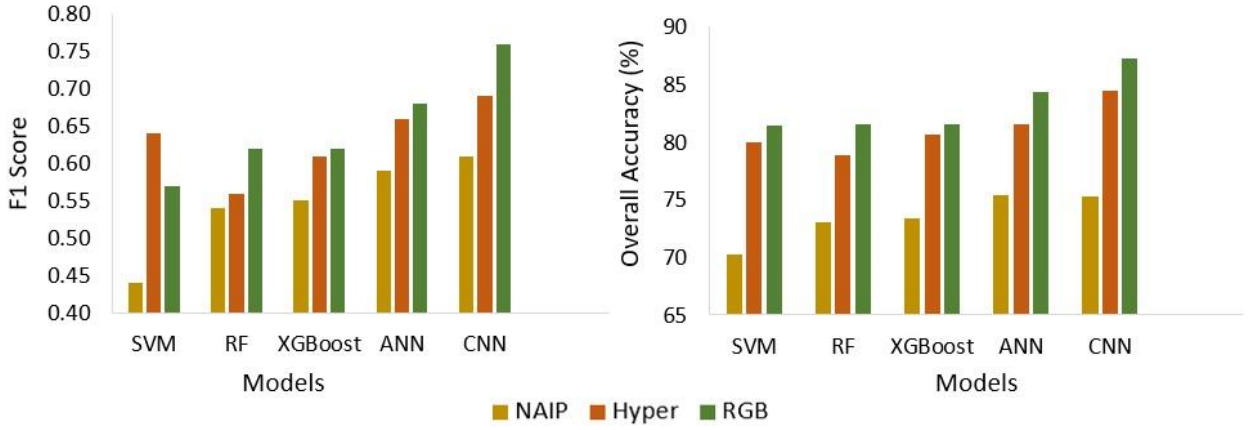

Figure 2.8: Summary of the results to show the F1 score and overall accuracy of each remote sensing data modality across models used.

2.5.2.3 Performance of Different Spatial and Spectral Resolution and Orthorectification

To understand the importance of spatial resolution, spectral depths, and orthorectification for the classification of individual overstory tree mortality, we ran CNN experiments with different spatial, spectral and orthorectified imagery. The result of NEON RGB at different spatial resolution (0.1 m, 0.6 m, and 1 m) showed there was decrease in macro average F1 score from 0.76 to 0.70 and overall accuracy from 87.27% to 84.58% with change in resolution form 0.1 m to 1 m (Figure 2. 9A). However, for spectral depth importance, the result of NEON RGB and RGBNIR derived from hyperspectral at 1 m resolution shown almost the similar overall accuracy of around 83-84% and macro average F1 score of 0.67 and 0.69 (Figure 2.9B). This showed that the extra spectral bands were not additional useful for overstory tree mortality detection. The results from experimental shifting of TAOs as described in section 3.5.1 showed that there was significant reduction in overall accuracy and macro average F1 score. There was a reduction of nearly 10% in overall accuracy and 0.19 in macro average F1 score (Figure 2.9C).

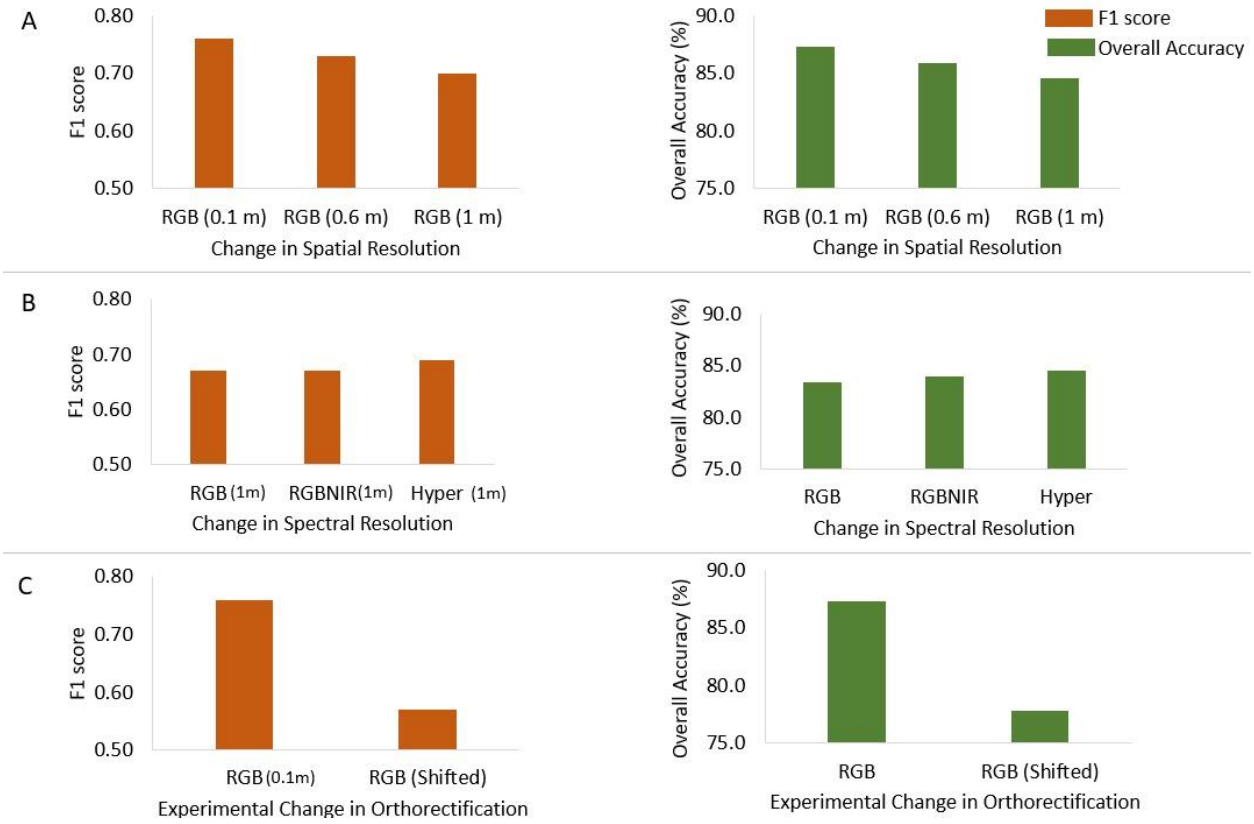

Figure 2.9: Shows the changes in macro average F1 score and overall accuracy with the change in: spatial resolution of NEON RGB from 0.1 m to 1 m (Row A); spectral depth (Row B); and change in orthorectification process as presented by experimental shift to mimic NAIP imagery orthorectification (Row C).

2.5.3 Teakettle Area Classification Map

We used the best performing model, Mortality CNN with NEON RGB, to generate the prediction of an overstory tree mortality map across Teakettle Experimental Forests for the years of 2013 (early drought), 2017, and 2018 (prolonged drought). There were around 148 to150 K unlabeled TAOs across 1000 hectares which represent overstory trees. All overstory trees were classified to be one of the mortality classes such as live, dead, mixed, and other. The distribution of the predicted mortality class is present in Table A2. For each year more than half (60-72%) of the detected trees in the area were classified as live. There were nearly 10-13% trees were classified as mixed and around 6-10% were classified as other. There was a significant increase (13%) in dead trees from 2013 (8%) to 2018 (21%). In contrast, there was a significant decrease

(12%) in live trees from 2013 (72%) to 2018 (60%) (Figure 2.10). A full tree mortality map for 2018 is presented in Figure 2.11 at the overstory tree level. The canopy mortality map not only provided the mortality status but also tree height and canopy area that can be useful for forest management. We will release the canopy mortality map for the Teakettle Experimental Forest upon acceptance.

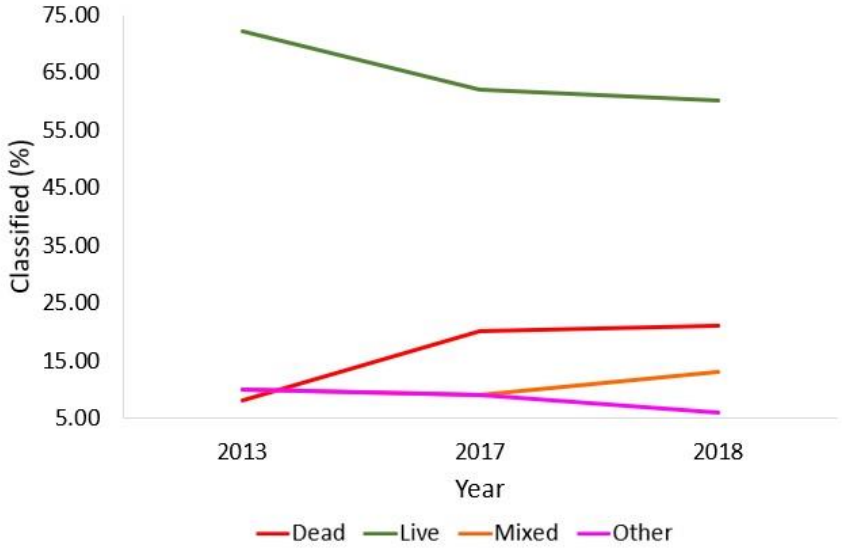

Figure 2.10: The mortality class prediction percent of TAOs for 2013, 2017, 2018.

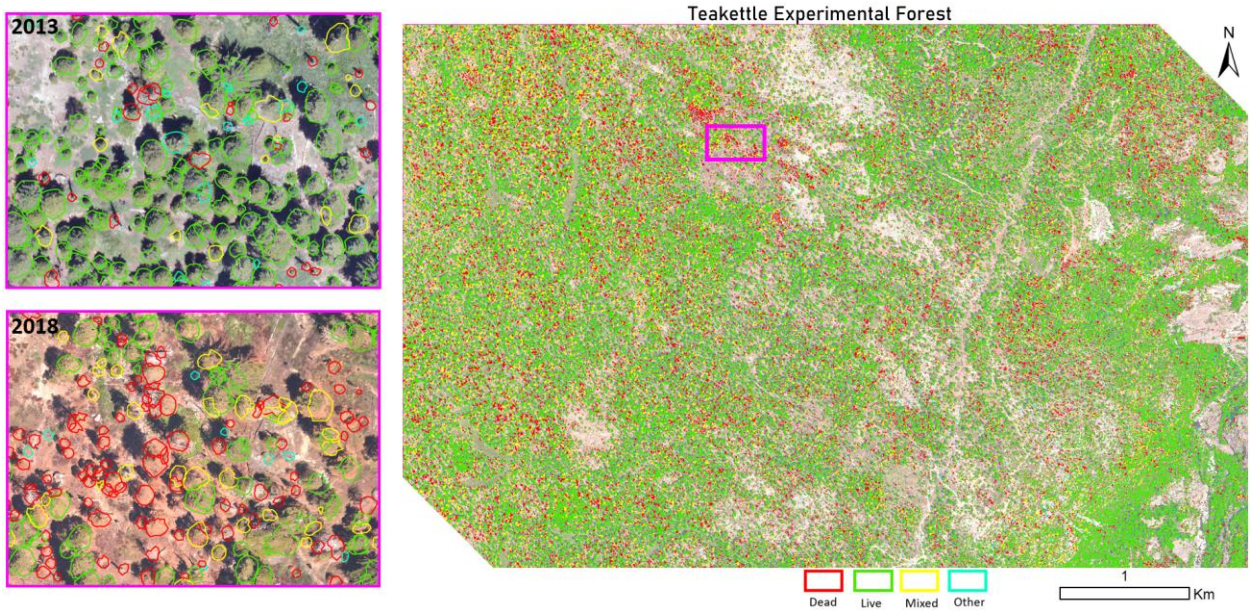

Figure 2.11: The overstory tree mortality status prediction over Teakettle Experimental Forest for the year 2018. The left side displays a zoomed-in location with mortality status for 2013 (top) and 2018 (bottom).

2.6 DISCUSSION

In this study, we provide a framework and benchmark dataset, utilizing lidar-derived tree segmentation, for mapping tree mortality over a large, mixed-conifer, temperate ecoregion using open-source and reproducible data. Further, we compared the performance of five common machine learning and deep learning models (RF, SVM, XGBoost, ANN, and CNN) and open-source high-resolution data modalities (NEON RGB, hyperspectral NAIP RGBNIR) for identifying multi-class mortality classification of live, dead, mixed, and other TAOs. Then we applied our best data and model to conduct tree mortality mapping and trend analysis for 2013, 2017, and 2018 in Teakettle Experimental Forest.

Our results showed that the CNN model and NEON RGB at 0.1 m resolution data outperformed all other models and data modalities in overall accuracy. We also found that different factors such as spatial resolution, spectral resolution and orthorectification process play key roles in the accurate detection of individual tree mortality. We showed that a multi-class approach is important for reducing the error in classification and appropriate representation of forest scenarios (reducing classification error by 8% in our study area). Developing a multi-class training and testing dataset that is supported by field validation allows the capacity to express the correct representation of forested environment.

Accurate, high-resolution overstory tree mortality maps are useful in many contexts such as to understand the potential mortality drivers of dominant trees (Campbell et al., 2020), forest inventory, selective logging, fire disturbances, and succession modeling. Mortality maps can further our understanding of overstory tree vulnerability to severe drought (Byer & Jin, 2017) and provide a strong basis for further eco-physiological, ecological, and carbon cycle studies

(Campbell et al., 2020). Our multi-class overstory mortality map can be used to derive relative canopy mortality to further study the impact of mortality in fire severity.

2.6.1 Determination of Best Models for Tree Mortality Detection

Our results demonstrated that deep learning models outperformed machine learning models for individual tree mortality classification. The CNN model, a deep learning model, outperformed all other methods in terms of overall accuracy and macro average F1 scores across all data modalities followed by ANN. The CNN model well separated all four mortality classes compared to other models.

Among machine learning models, the performance of XGBoost and RF were almost equal for NEON RGB and NAIP RGBNIR imagery. While for NEON hyperspectral the performance of SVM was best CNN and ANN. This result aligns with Mäyrä et al. (2021) who found SVM performed as well as ANN when using hyperspectral data for tree species classification. Overall, our result showed that there is a positive correlation between expressive large models (where expressivity means having a large number of input features, layers, and parameters) and classification accuracy.

Our result indicates that expressive large models are good for the multi-class classification of individual, overstory tree mortality with high-resolution imagery. This outcome aligns with the finding of Mäyrä et al. (2021) who found the CNN model performed best for the tree species classification. Further, for image classification problems, neural networks are well known as the best performing models (Krizhevsky et al., 2017; LeCun et al., 2015). The key advantage of CNN models over other models is that CNNs can automatically learn features from input data including edges, texture, patterns, and structure (Mäyrä et al., 2021). The CNN model

can utilize both spatial and spectral information while traditional machine learning models require manual feature engineering in which extracting appropriate spatial features is difficult and domain knowledge is required. Therefore, CNNs and deep learning approaches overall are a valuable method for comparing the performance of the different remote sensing data modalities for the classification of individual overstory tree mortality.

2.6.2 Determination of Best Data Modalities for Tree Mortality Detection

Our results show that there are several factors to consider when selecting high-resolution imagery for better performance. These factors include high spatial resolution, spectral resolution and orthorectification process. Our results show that NEON RGB at 0.1 m resolution performed best for the classification of overstory tree mortality using CNN model. We found that both NEON RGB at 0.1 m resolution and hyperspectral at 1 m resolution outperformed the NAIP (RGBNIR) imagery at 0.6 m resolution.

To test specifically for the effects of resolution, we resampled the NEON RGB imagery. The performance of CNN model reduced as the resolution declined slightly as resolution decreased from 0.1 m to 1 m. In contrast, the performance of RGB, RGBNIR, and hyperspectral all extracted from NEON hyperspectral at 1 m resolution had almost equal overall accuracy and F1 score. This shows that spatial resolution is more important than spectral information for overstory tree mortality classification.

To test the impact of layover effects common from orthorectification of images to the ground, we tested both NEON RGB orthorectified to the top of canopy and randomly perturbed crops to simulate the effects of overlay from orthorectification to the ground. Nearly 10% decrease in overall accuracy of shifted TAOs with NEON RGB at 0.1m resolution demonstrates the

importance of orthorectification for accurate tree mortality mapping. Similarly, the NAIP imagery had the lowest performance of all data modalities across all models. This is likely due to differences in the orthorectification process, as demonstrated by the experiment by the experiment described above. The NEON program applies an orthorectification process to balance distortion related to taller objects such as trees. The NEON program spatially resampled their imagers to reduce the discrepancy in resolution from lidar to camera, which provided a more nadir (i.e., top of the crown) view of trees. In contrast, the NAIP program orthorectifies the imagery to a digital elevation model (i.e., a ground model), which is likely at poorer spatial resolution. The differences in the balanced versus ground-based orthorectification yields a shift in the alignment of the TAO canopy and the imagery. Thus, this produces a shift in the tree crown outside the TAO canopy as illustrated in Figure 2.5. Therefore, despite the higher spectral resolution of the NAIP four bands imagery compared to the NEON RGB and finer spatial resolution than NEON hyperspectral, the performance of NAIP is lower due to the noise produced by orthorectification.

2.6.3 Importance of Multi-class Overstory Tree Mortality Maps

In our study, we implemented multi-class classification to capture the overstory tree's status such as live, dead, mixed, and other. By applying this multi-class approach, we can identify the frequency of lidar tree segmentation errors due to errors of commission in detecting non-tree objects, as well as multiple trees per lidar segments, mixed or stressed tree canopies which could be misrepresented in binary tree classification. Previous studies have predicted tree mortality as only live and dead class (Bergmüller & Vanderwel, 2022; Briechle et al., 2020; Fricker et al., 2019; Hemming-Schroeder et al., 2023; Kamińska et al., 2018; Stovall et al., 2019; Wing et al., 2015).

In many forested landscapes where there are numerous non-tree objects, such as boulders or human infrastructure, and trees in various decaying states, binary classification may not capture the full range of ecological conditions. Our labeled data presented in Table 2.2 showed that around 5.5 to 8% of our annotations were non-tree objects and 11 to 14% mixed class. This shows that a model lacking the ability to predict non-tree and mixed class would inherently have an error rate of at least 5.5 to 14% greater than its estimated error when deployed at scale in environments similar to the Teakettle Experimental Forest. Hence, in this study, we apply multi-class classification models to capture the tree's status of live, dead, mixed (partially dead), and other categories (e.g., shadow or boulder).

2.6.4 Mortality Trend Analysis

In our study, we produced a mortality map of overstory trees for the Teakettle Experimental Forest area of live, dead, mixed, and other classes for 2013, 2017, and 2018 using our best model and data modality (CNN and NEON RGB). From multi-year predictions, we found that live tree prevalence decreased by 12% and dead trees prevalence increased by 13% over the 5-year study period. By the end of the study period (2018), we found the study area trees were predicted as 21% dead with around 13% mixed, 60% live, and 5.5% other. These results showed that drought induced tree mortality increased significantly during the period of 2013 to 2018.

2.6.5 Comparison with Previous Studies

Most previous studies that have investigated tree mortality at the scale of individual tree typically used a single model type, such as random forest (Kamińska et al., 2018) ,logistic regression (Jutras-Perreault et al., 2023), maximum likelihood (Stovall et al., 2019), and CNN (Briechle et al., 2020; Fricker et al., 2019). (Bergmüller & Vanderwel, (2022) compared a limited set of methods including logistic regression and random forest.

Particularly, previous studies that were conducted in Sierra Nevada including Stovall et al. (2019) and Hemming-Schorder et al., (2023) had developed a model for binary classification (live and dead) of individual overstory trees using NAIP (RGBNIR) and vegetation indices derived from NEON hyperspectral imagery. To be able to make a comparison of our results with previous studies, we trained and evaluated our CNN model for live and dead classification across all remote sensing data modalities. The overall test-set accuracy of the CNN model for NEON RGB was 98.98%, NEON hyperspectral was 97.79% and NAIP RGBNIR was 93.02% (Table A3). Stovall et al. (2019) used NAIP imagery for the binary classification of individual trees and found overall accuracy of 88%. While using NAIP imagery we found overall accuracy of 93.02% for binary classification. Similarly, Hemming-Schroder et al., (2023) used NEON hyperspectral to derive vegetation indices for the binary classification of individual trees and found overall accuracy of 92.1%. While using all 426 bands of NEON hyperspectral with our CNN model, we found an overall accuracy of 97.79%. While we fully acknowledge that these overall accuracy results are derived from training and testing on different datasets, we present them here to give a best attempt at placing the accuracy results of our models within the context of existing work. Further, the inability to make a direct comparison on the same data of our models to prior work is a strong justification for the community's need for a fully open-source, high quality, reproducible benchmark, which we present in this work.

2.7 CONCLUSION

In this study, we presented a framework and benchmark dataset for comparative analysis of various data modalities and models for the classification of individual tree mortality in mixed-conifer forests. We compared the ability of open-sourced remote sensing data such as NEON RGB, NEON hyperspectral, and NAIP four-band imagery for the purpose of overstory tree

mortality detection. In addition, we evaluated the performance of various models such as random forest, support vector machines, eXtreme Gradient Boosting trees, a multilayer perceptron neural network, and a convolutional neural network for the task. The study found that individual, overstory tree mortality classes can be conducted with high accuracy with the given open-source remote sensing data modalities and sufficiently expressive methods such as CNNs. The NEON RGB data outperformed other data modalities due to high spatial resolution and high quality orthorectification. Similarly to previous study Mäyrä et al., (2021), we also found the CNN models outperformed the RF, SVM, XGBoost, and ANN models. Finally, we also produced an open-source, benchmark dataset to promote the research and development, validation, and improvement of tree mortality detection algorithms.

To the best of our knowledge, this is the first individual tree mortality mapping research that compared the performance of multiple open-source high-resolution datasets and different machine learning and deep learning models. This research highlights the strengths and weaknesses of these open-source data and models for mapping individual tree mortality. This study also suggests that different orthorectification methods could be applied to the NAIP imagery to perform better classification of individual overstory trees. This study demonstrates the use of lidar derived tree segments to represent individual trees, which improves the ease of mapping across larger landscapes with automated lidar tree segmentation approaches. We aim to use the mortality map produced in this study to understand the relationship between tree mortality and fire severity in future research. The development and evaluation of models and open-source data for mapping individual tree mortality will be crucial for studying future disturbance patterns such as fire severity, landscape modeling, and operationalizing high-resolution data for forest management.

APPENDIX A

Table A1: Test set results comparing methods across remote sensing data modalities.

				ANN					
Mortality	RGB			Hyperspectral			NAIP		
Status	Precision	Recall	F1	Precision	Recall	F1	Precision	Recall	F1
Dead	0.84	0.82	0.83	0.84	0.79	0.82	0.70	0.68	0.69
Live	0.88	0.98	0.93	0.86	0.94	0.90	0.79	0.94	0.86
Mixed	0.51	0.30	0.38	0.48	0.33	0.39	0.53	0.28	0.37
Other	0.74	0.50	0.59	0.57	0.48	0.52	0.72	0.33	0.45
Macro Avg	0.74	0.65	0.68	0.69	0.63	0.66	0.69	0.56	0.59
OA			84.38%			81.63%			75.42%
				XGBoost					
Dead	0.79	0.84	0.81	0.78	0.82	0.80	0.65	0.64	0.65
Live	0.85	0.96	0.90	0.84	0.95	0.89	0.76	0.95	0.85
Mixed	0.43	0.15	0.22	0.50	0.20	0.29	0.58	0.16	0.25
Other	0.71	0.45	0.55	0.62	0.36	0.46	0.67	0.34	0.45
Macro Avg	0.69	0.60	0.62	0.69	0.58	0.61	0.67	0.52	0.55
OA			81.56%			80.72%			73.36%
				RF					
Dead	0.79	0.83	0.81	0.74	0.79	0.76	0.66	0.65	0.65
Live	0.84	0.96	0.90	0.82	0.95	0.88	0.76	0.95	0.84
Mixed	0.46	0.14	0.22	0.48	0.11	0.17	0.55	0.14	0.23
Other	0.72	0.44	0.55	0.65	0.30	0.41	0.66	0.31	0.42
Macro Avg	0.70	0.60	0.62	0.67	0.54	0.56	0.66	0.51	0.54
OA			81.59%			78.91%			73.03%
				SVM					
Dead	0.77	0.86	0.81	0.76	0.82	0.79	0.64	0.64	0.64
Live	0.83	0.97	0.89	0.87	0.91	0.89	0.73	0.95	0.83
Mixed	0.00	0.00	0.00	0.42	0.30	0.35	0.00	0.00	0.00
Other	0.77	0.48	0.59	0.61	0.47	0.53	0.45	0.20	0.28
Macro Avg	0.59	0.58	0.57	0.66	0.62	0.64	0.45	0.45	0.44
OA			81.43%			80.03%			70.30%

Table A2: The distribution of predicted mortality for Teakettle Experimental Forest for year of 2013, 2017, and 2018 for all detected overstory trees.

Mortality Status	2013 (%)	2017 (%)	2018 (%)	Difference in 5 Years (%)
Dead	11,735 (7.51)	30,884 (19.85)	30,942 (20.82)	13.31 % increase dead
Live	113,066 (72.34)	97,361 (62.55)	89,568 (60.27)	12.07 % decrease live
Mixed	15,883 (10.16)	13,581 (8.73)	19,835 (13.35)	3.19 % increase in mixed
Other	15,615 (9.99)	13,797 (8.87)	8,257 (5.56)	4.43 % decrease in other
Total	156,299 (100)	155,623 (100)	148,602 (100)	

Table A3: Test set results of CNN models across remote sensing data modalities for live and dead classes.

Mortality	RGB			Hyperspectral			NAIP		
Status	Precision	Recall	F1	Precision	Recall	F1	Precision	Recall	F1
Dead	0.98	0.98	0.98	0.96	0.94	0.95	0.88	0.78	0.83
Live	0.99	0.99	0.99	0.98	0.99	0.99	0.94	0.97	0.96
Macro avg	0.99	0.99	0.99	0.97	0.97	0.97	0.91	0.88	0.89
OA			99.05%			97.91%			93.07%

Table A4: The distribution of live, dead, mixed, and other labels of the benchmark data for each year.

	NEON (RGB & Hyperspectral)			NAIP (RGBNIR)		
Mortality Status	2013	2017	2018	2013	2017	2018
Dead	156	1825	756	122	1669	679
Live	2132	5380	2434	1794	5157	2363
Mixed	349	813	556	492	985	601
Other	46	573	241	148	761	340

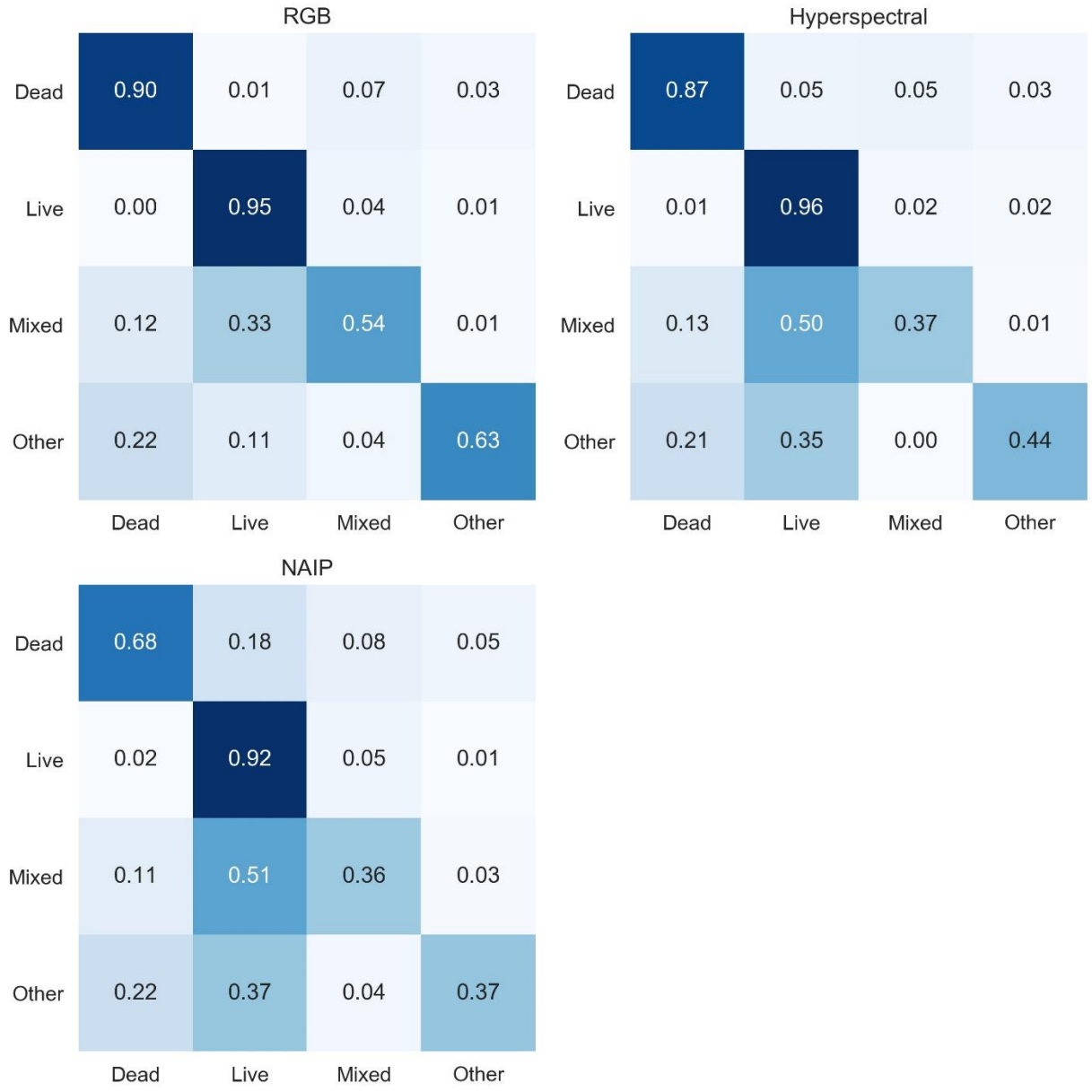

Figure A1: Confusion matrix for comparison of remote sensing data modalities with CNN model. Rows indicate correct labels and columns indicate predicted labels.

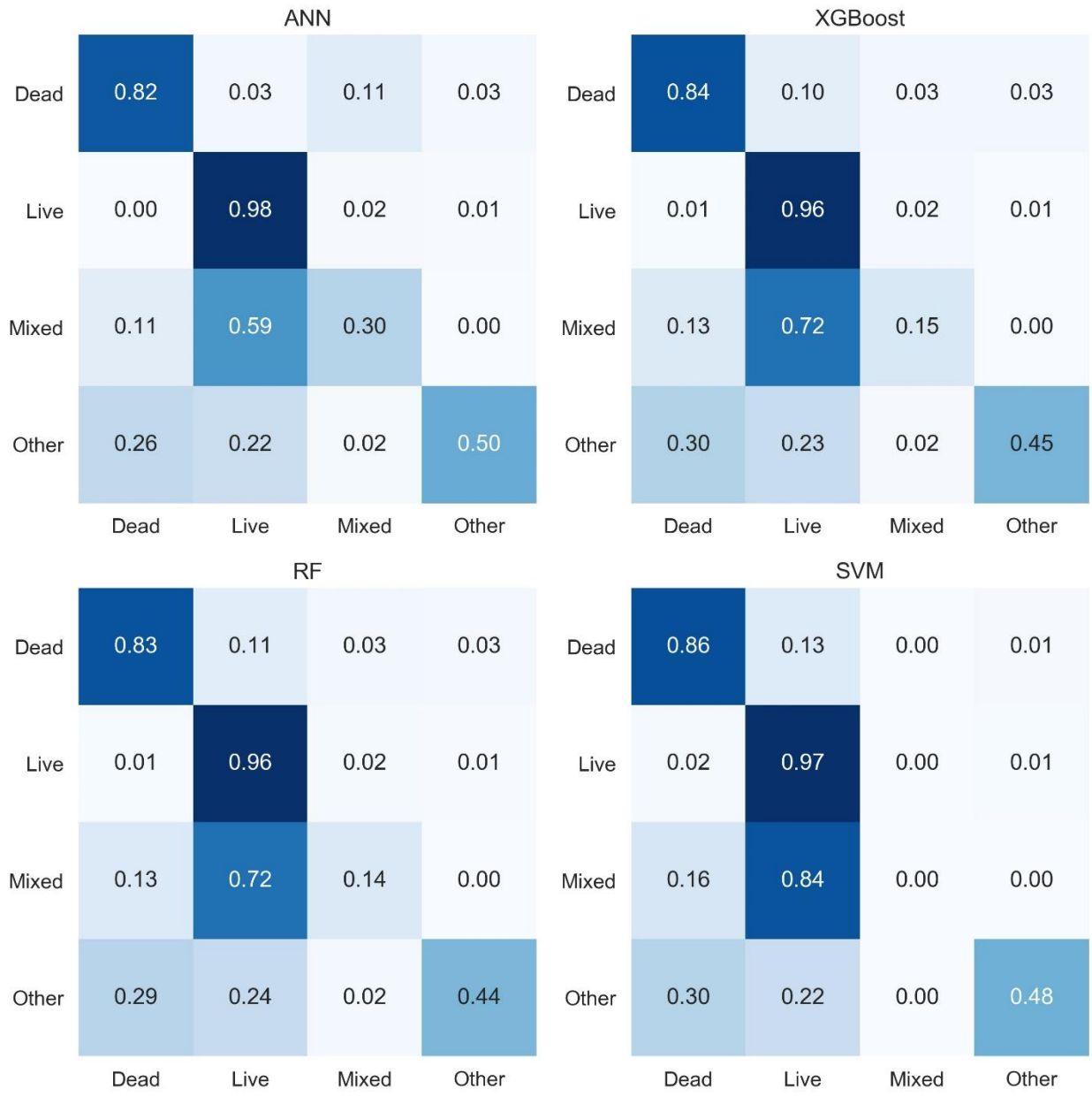

Figure A2: Confusion matrix of RGB data for comparison of other models. Rows indicate correct labels and columns indicate predicted labels.

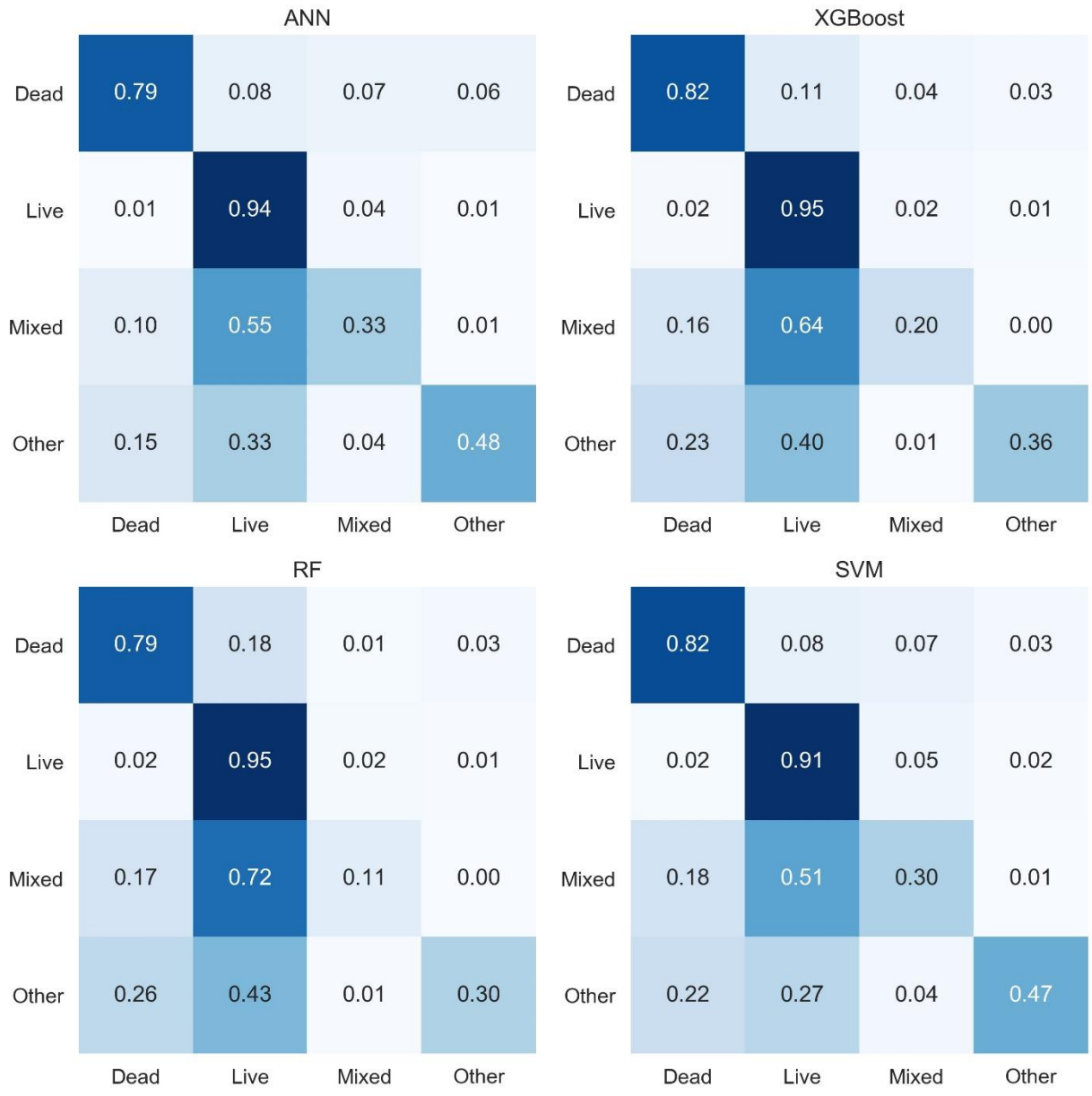

Figure A3: Confusion matrix of hyperspectral data for comparison of other models. Rows indicate correct labels and columns indicate predicted labels.

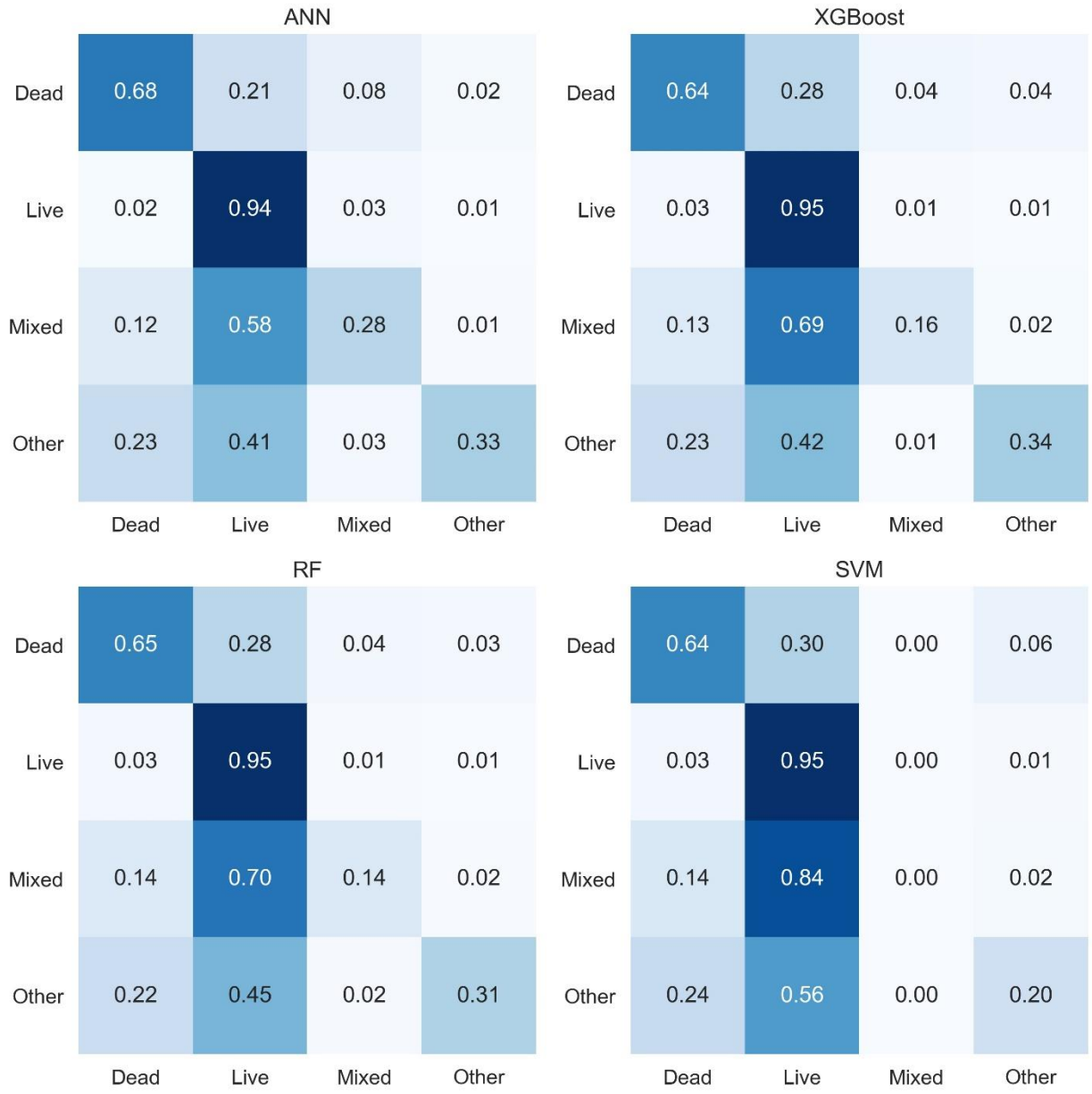

Figure A4: Confusion matrix of NAIP data for comparison of other models. Rows indicate correct labels and columns indicate predicted labels.

2.8 REFERENCES

Adams, H. D., Guardiola-Claramonte, M., Barron-Gafford, G. A., Villegas, J. C., Breshears, D. D., Zou, C. B., Troch, P. A., & Huxman, T. E. (2009). Temperature sensitivity of drought-induced tree mortality portends increased regional die-off under global-change-type drought. *Proceedings of the National Academy of Sciences*, *106*(17), 7063–7066. https://doi.org/10.1073/pnas.0901438106

Allen, C. D., Breshears, D. D., & McDowell, N. G. (2015). On underestimation of global vulnerability to tree mortality and forest die-off from hotter drought in the Anthropocene. *Ecosphere*, *6*(8), art129. https://doi.org/10.1890/ES15-00203.1

Allen, C. D., Macalady, A. K., Chenchouni, H., Bachelet, D., McDowell, N., Vennetier, M., Kitzberger, T., Rigling, A., Breshears, D. D., Hogg, E. H. (Ted), Gonzalez, P., Fensham, R., Zhang, Z., Castro, J., Demidova, N., Lim, J.-H., Allard, G., Running, S. W., Semerci, A., & Cobb, N. (2010). A global overview of drought and heat-induced tree mortality reveals emerging climate change risks for forests. *Forest Ecology and Management*, *259*(4), 660–684. https://doi.org/10.1016/j.foreco.2009.09.001

Asner, G. P., Brodrick, P. G., Anderson, C. B., Vaughn, N., Knapp, D. E., & Martin, R. E. (2016). Progressive forest canopy water loss during the 2012–2015 California drought. *Proceedings of the National Academy of Sciences*, *113*(2). https://doi.org/10.1073/pnas.1523397113

Bergmüller, K. O., & Vanderwel, M. C. (2022). Predicting Tree Mortality Using Spectral Indices Derived from Multispectral UAV Imagery. *Remote Sensing*, *14*(9), 2195. https://doi.org/10.3390/rs14092195

Bhatt, P., & Maclean, A. L. (2023). Comparison of high-resolution NAIP and unmanned aerial vehicle (UAV) imagery for natural vegetation communities classification using machine learning approaches. *GIScience & Remote Sensing*, *60*(1), 2177448. https://doi.org/10.1080/15481603.2023.2177448

Breshears, D. D., Cobb, N. S., Rich, P. M., Price, K. P., Allen, C. D., Balice, R. G., Romme, W. H., Kastens, J. H., Floyd, M. L., Belnap, J., Anderson, J. J., Myers, O. B., & Meyer, C. W. (2005). Regional vegetation die-off in response to global-change-type drought. *Proceedings of the National Academy of Sciences*, *102*(42), 15144–15148. https://doi.org/10.1073/pnas.0505734102

Briechle, S., Krzystek, P., & Vosselman, G. (2020). CLASSIFICATION OF TREE SPECIES AND STANDING DEAD TREES BY FUSING UAV-BASED LIDAR DATA AND MULTISPECTRAL IMAGERY IN THE 3D DEEP NEURAL NETWORK POINTNET++. *ISPRS Annals of the Photogrammetry, Remote Sensing and Spatial Information Sciences*, *V-2–2020*, 203–210. https://doi.org/10.5194/isprs-annals-V-2-2020-203-2020

Byer, S., & Jin, Y. (2017). Detecting Drought-Induced Tree Mortality in Sierra Nevada Forests with Time Series of Satellite Data. *Remote Sensing 2017, Vol. 9, Page 929*, *9*(9), 929. https://doi.org/10.3390/RS9090929

Campbell, M. J., Dennison, P. E., Tune, J. W., Kannenberg, S. A., Kerr, K. L., Codding, B. F., & Anderegg, W. R. L. (2020). A multi-sensor, multi-scale approach to mapping tree mortality in woodland ecosystems. *Remote Sensing of Environment*, *245*, 111853. https://doi.org/10.1016/j.rse.2020.111853

Coop, J. D., Parks, S. A., Stevens-Rumann, C. S., Crausbay, S. D., Higuera, P. E., Hurteau, M. D., Tepley, A., Whitman, E., Assal, T., Collins, B. M., Davis, K. T., Dobrowski, S., Falk, D. A., Fornwalt, P. J., Fulé, P. Z., Harvey, B. J., Kane, V. R., Littlefield, C. E., Margolis, E. Q., … Rodman, K. C. (2020). Wildfire-Driven Forest Conversion in Western North American Landscapes. *BioScience*, *70*(8), 659–673. https://doi.org/10.1093/biosci/biaa061

Deng, J., Dong, W., Socher, R., Li, L.-J., Kai Li, & Li Fei-Fei. (2010). *ImageNet: A large-scale hierarchical image database*. 248–255. https://doi.org/10.1109/CVPR.2009.5206848

Egli, S., & Höpke, M. (2020). CNN-Based Tree Species Classification Using High Resolution RGB Image Data from Automated UAV Observations. *Remote Sensing*, *12*(23), 3892. https://doi.org/10.3390/rs12233892

Esri. (2018). *ArcMap (Version 10.6.1 GIS software. Redlands, CA: Environmental Systems Research Institute* [Computer software].

Fricker, G. A., Ventura, J. D., Wolf, J. A., North, M. P., Davis, F. W., & Franklin, J. (2019). A Convolutional Neural Network Classifier Identifies Tree Species in Mixed-Conifer Forest from Hyperspectral Imagery. *Remote Sensing*, *11*(19), 2326. https://doi.org/10.3390/rs11192326

Geiger, A., Lenz, P., Stiller, C., & Urtasun, R. (2013). Vision meets robotics: The KITTI dataset: *Http://Dx.Doi.Org/10.1177/0278364913491297*, *32*(11), 1231–1237. https://doi.org/10.1177/0278364913491297

Goodwin, M. J., North, M. P., Zald, H. S. J., & Hurteau, M. D. (2020). Changing climate reallocates the carbon debt of frequent-fire forests. *Global Change Biology*, *26*(11), 6180–6189. https://doi.org/10.1111/gcb.15318

Greenwood, S., Ruiz-Benito, P., Martínez-Vilalta, J., Lloret, F., Kitzberger, T., Allen, C. D., Fensham, R., Laughlin, D. C., Kattge, J., Bönisch, G., Kraft, N. J. B., & Jump, A. S. (2017). Tree mortality across biomes is promoted by drought intensity, lower wood density and higher specific leaf area. *Ecology Letters*, *20*(4), 539–553. https://doi.org/10.1111/ele.12748

Hartmann, H., Moura, C. F., Anderegg, W. R. L., Ruehr, N. K., Salmon, Y., Allen, C. D., Arndt, S. K., Breshears, D. D., Davi, H., Galbraith, D., Ruthrof, K. X., Wunder, J., Adams, H. D., Bloemen, J., Cailleret, M., Cobb, R., Gessler, A., Grams, T. E. E., Jansen, S., … O'Brien, M. (2018). Research frontiers for improving our understanding of drought-induced tree and forest mortality. *New Phytologist*, *218*(1), 15–28. https://doi.org/10.1111/nph.15048

Hemming-Schroeder, N. M., Gutierrez, A. A., Allison, S. D., & Randerson, J. T. (2023). Estimating Individual Tree Mortality in the Sierra Nevada Using Lidar and Multispectral Reflectance Data. *Journal of Geophysical Research: Biogeosciences*, *128*(5), e2022JG007234. https://doi.org/10.1029/2022JG007234

Ioffe, S., & Szegedy, C. (2015). Batch Normalization: Accelerating Deep Network Training by Reducing Internal Covariate Shift. *International Conference on Machine Learning*, *37*, 448–456.

Jeronimo, S. M. A., Kane, V. R., Churchill, D. J., Lutz, J. A., North, M. P., Asner, G. P., & Franklin, J. F. (2019). Forest structure and pattern vary by climate and landform across active-fire landscapes in the montane Sierra Nevada. *Forest Ecology and Management*, *437*, 70–86. https://doi.org/10.1016/j.foreco.2019.01.033

Jeronimo, S. M. A., Kane, V. R., Churchill, D. J., McGaughey, R. J., & Franklin, J. F. (2018). Applying LiDAR Individual Tree Detection to Management of Structurally Diverse

Forest Landscapes. *Journal of Forestry*, *116*(4), 336–346. https://doi.org/10.1093/jofore/fvy023

Jutras-Perreault, M.-C., Næsset, E., Gobakken, T., & Ørka, H. O. (2023). Detecting the presence of standing dead trees using airborne laser scanning and optical data. *Scandinavian Journal of Forest Research*, *38*(4), 208–220. https://doi.org/10.1080/02827581.2023.2211807

Kamińska, A., Lisiewicz, M., Stereńczak, K., Kraszewski, B., & Sadkowski, R. (2018). Species-related single dead tree detection using multi-temporal ALS data and CIR imagery. *Remote Sensing of Environment*, *219*, 31–43. https://doi.org/10.1016/j.rse.2018.10.005

Kane, V. R., Bartl-Geller, B. N., North, M. P., Kane, J. T., Lydersen, J. M., Jeronimo, S. M. A., Collins, B. M., & Monika Moskal, L. (2019). First-entry wildfires can create opening and tree clump patterns characteristic of resilient forests. *Forest Ecology and Management*, *454*, 117659. https://doi.org/10.1016/j.foreco.2019.117659

Krizhevsky, A., Sutskever, I., & Hinton, G. E. (2017). ImageNet classification with deep convolutional neural networks. *Communications of the ACM*, *60*(6), 84–90. https://doi.org/10.1145/3065386

Krofcheck, D. J., Hurteau, M. D., Scheller, R. M., & Loudermilk, E. L. (2017). Restoring surface fire stabilizes forest carbon under extreme fire weather in the Sierra Nevada. *Ecosphere*, *8*(1), e01663. https://doi.org/10.1002/ecs2.1663

LeCun, Y., Bengio, Y., & Hinton, G. (2015). Deep learning. *Nature*, *521*(7553), 436–444. https://doi.org/10.1038/nature14539

Leifsson, C., Buras, A., Rammig, A., & Zang, C. (2023). Changing climate sensitivity of secondary growth following extreme drought events in forest ecosystems: A global analysis. *Environmental Research Letters*, *18*(1), 014021. https://doi.org/10.1088/1748-9326/aca9e5

Lin, T. Y., Maire, M., Belongie, S., Hays, J., Perona, P., Ramanan, D., Dollár, P., & Zitnick, C. L. (2014). Microsoft COCO: Common Objects in Context. *Lecture Notes in Computer Science (Including Subseries Lecture Notes in Artificial Intelligence and Lecture Notes in Bioinformatics)*, *8693 LNCS*(PART 5), 740–755. https://doi.org/10.1007/978-3-319-10602-1_48

Mäyrä, J., Keski-saari, S., Kivinen, S., Tanhuanpää, T., Hurskainen, P., Kullberg, P., Poikolainen, L., Viinikka, A., Tuominen, S., Kumpula, T., & Vihervaara, P. (2021). Tree species classification from airborne hyperspectral and LiDAR data using 3D convolutional neural networks. *Remote Sensing of Environment*, *256*, 112322.

McGaughey, R. J. (2018). FUSION/LDV: Software for LIDAR Data Analysis and Visualization. *USDA Forest Service Pacific Northwest Research Station, Seattle, WA*. http://forsys.cfr.washington.edu/fusion/fusionlatest.html

Millar, C. I., & Stephenson, N. L. (2015). Temperate forest health in an era of emerging megadisturbance. *Science*, *349*(6250), 823–826. https://doi.org/10.1126/science.aaa9933

NEON. (2021a). *National Ecological Observatory Network (NEON). Discrete return LiDAR point cloud (DP1.30003.001).* https://data.neonscience.org/data-products/DP1.30003.001/RELEASE-2021

NEON. (2021b). *National Ecological Observatory Network (NEON). High-resolution orthorectified camera imagery mosaic (DP3.30010.001)*. https://data.neonscience.org/data-products/DP3.30010.001

NEON. (2021c). *National Ecological Observatory Network (NEON). Spectrometer orthorectified surface directional reflectance—Flightline (DP1.30006.001)*. https://data.neonscience.org/data-products/DP1.30006.001/RELEASE-2021

North, M., Chen, J., Oakley, B., Song, B., Rudnicki, M., Gray, A., & Innes, J. (2004). Forest Stand Structure and Pattern of Old-Growth Western Hemlock/Douglas-Fir and Mixed-Conifer Forests. *Forest Science*, *50*(3), 299–311.

North, M. P. (2002). Vegetation and ecological characteristics of mixed-conifer and red fir forests at the Teakettle Experimental Forest. *US Department of Agriculture, Forest Service, Pacific Southwest Research Station*, *186*.

North, M. P., Kane, J. T., Kane, V. R., Asner, G. P., Berigan, W., Churchill, D. J., Conway, S., Gutiérrez, R. J., Jeronimo, S., Keane, J., Koltunov, A., Mark, T., Moskal, M., Munton, T., Peery, Z., Ramirez, C., Sollmann, R., White, A., & Whitmore, S. (2017). Cover of tall trees best predicts California spotted owl habitat. *Forest Ecology and Management*, *405*, 166–178. https://doi.org/10.1016/j.foreco.2017.09.019

Parks, S. A., Dobrowski, S. Z., Shaw, J. D., & Miller, C. (2019). Living on the edge: Trailing edge forests at risk of fire-facilitated conversion to non-forest. *Ecosphere*, *10*(3), e02651. https://doi.org/10.1002/ecs2.2651

Paszke, A., Gross, S., Massa, F., Lerer, A., Bradbury, J., Chanan, G., Killeen, T., Lin, Z., Gimelshein, N., Antiga, L., Desmaison, A., Köpf, A., Yang, E., DeVito, Z., Raison, M., Tejani, A., Chilamkurthy, S., Steiner, B., Fang, L., … Chintala, S. (2019). PyTorch: An Imperative Style, High-Performance Deep Learning Library. *arXiv:1912.01703 [Cs, Stat]*. http://arxiv.org/abs/1912.01703

Pedregosa, F., Varoquaux, G., Gramfort, A., Michel, V., Thirion, B., Grisel, O., Blondel, M., Prettenhofer, P., Weiss, R., Dubourg, V., Vanderplas, J., Passos, A., Cournapeau, D., Brucher, M., Perrot, M., & Duchesnay, E. (2011). *Scikit-learn: Machine Learning in Python*. *12*, 2825–2830.

Reichstein, M., Bahn, M., Ciais, P., Frank, D., Mahecha, M. D., Seneviratne, S. I., Zscheischler, J., Beer, C., Buchmann, N., Frank, D. C., Papale, D., Rammig, A., Smith, P., Thonicke, K., van der Velde, M., Vicca, S., Walz, A., & Wattenbach, M. (2013). Climate extremes and the carbon cycle. *Nature*, *500*(7462), 287–295. https://doi.org/10.1038/nature12350

Schiefer, F., Kattenborn, T., Frick, A., Frey, J., Schall, P., Koch, B., & Schmidtlein, S. (2020). Mapping forest tree species in high resolution UAV-based RGB-imagery by means of convolutional neural networks. *ISPRS Journal of Photogrammetry and Remote Sensing*, *170*, 205–215. https://doi.org/10.1016/j.isprsjprs.2020.10.015

Stephens, S. L., Collins, B. M., Fettig, C. J., Finney, M. A., Hoffman, C. M., Knapp, E. E., North, M. P., Safford, H., & Wayman, R. B. (2018). Drought, Tree Mortality, and Wildfire in Forests Adapted to Frequent Fire. *BioScience*, *68*(2), 77–88. https://doi.org/10.1093/BIOSCI/BIX146

Stovall, A. E. L., Shugart, H., & Yang, X. (2019). Tree height explains mortality risk during an intense drought. *Nature Communications*, *10*(1), 4385. https://doi.org/10.1038/s41467-019-12380-6

USDA. (2016). *New Aerial Survey Identifier More than 100 Million Dead Trees in California*.

USDA. (2021a). *2016 California Image Dates*. https://naip-image-dates-usdaonline.hub.arcgis.com/datasets/b832cbe4a874497b839471e02d60ff79_0/about

USDA. (2021b). *2018 California Image Dates*. https://naip-image-dates-usdaonline.hub.arcgis.com/datasets/6a505759625a4ae19343fd15355bdc71_0/about

USDA. (2021c). *NAIP 2012 Seamlines*. https://naip-image-dates-usdaonline.hub.arcgis.com/datasets/a9ab579647384d34a5c3b51d8e59b407_0/about

Warren, K. (2019). California Tree Mortality Numbers Released: 18 Million Trees Died In 2018. *USDA, Forest Service*. https://www.fs.usda.gov/detailfull/r5/home/?cid=FSEPRD613875&width=full

Wasser, L. A. (2023). *About Hyperspectral Remote Sensing Data*. Tutorial About Hyperspectral Remote Sensing Data. https://www.neonscience.org/resources/learning-hub/tutorials/hyper-spec-intro

Weinstein, B. G., Graves, S. J., Marconi, S., Singh, A., Zare, A., Stewart, D., Bohlman, S. A., & White, E. P. (2021). A benchmark dataset for canopy crown detection and delineation in co-registered airborne RGB, LiDAR and hyperspectral imagery from the National Ecological Observation Network. *PLOS Computational Biology*, *17*(7), e1009180. https://doi.org/10.1371/journal.pcbi.1009180

Williams, P. A., Allen, C. D., Macalady, A. K., Griffin, D., Woodhouse, C. A., Meko, D. M., Swetnam, T. W., Rauscher, S. A., Seager, R., Grissino-Mayer, H. D., Dean, J. S., Cook, E. R., Gangodagamage, C., Cai, M., & McDowell, N. G. (2013). Temperature as a potent driver of regional forest drought stress and tree mortality. *Nature Climate Change*, *3*(3), 292–297. https://doi.org/10.1038/nclimate1693

Wing, B. M., Ritchie, M. W., Boston, K., Cohen, W. B., & Olsen, M. J. (2015). Individual snag detection using neighborhood attribute filtered airborne lidar data. *Remote Sensing of Environment*, *163*, 165–179. https://doi.org/10.1016/j.rse.2015.03.013

Chapter 3. FOREST TYPE CLASSIFICATION COMBINING FIELD PLOT AND HIGH- RESOLUTION AIRBORNE REMOTE SENSING DATA USING CONVOLUTIONAL NEURAL NETWORK IN A BOREAL FOREST OF INTERIOR ALASKA

3.1 ABSTRACT

The boreal biome, the largest terrestrial biome on Earth, is increasingly vulnerable to climate change due to warming twice as rapidly as the global average. Climate change has increased the temperature, frequency, severity, and amount of area burned, which is leading to changes in the spatial extent of forest type and species range. These rapid ecological shifts necessitate fine-scale monitoring of forest type to detect potential type conversions and guide management interventions. In this study, we present a framework for forest type classification combining field plots and high-resolution remote sensing data using machine learning models in the boreal forest of Interior Alaska. For this purpose, we conducted forest type classification at three different levels, including 1. forest and nonforest, 2. hardwood, softwood, and nonforest, and 3. three dominant forest types, including paper birch, black spruce, white spruce, and nonforest. To achieve this goal, we compared the performance of two advanced modeling approaches, the convolutional neural network (CNN) and the XGBoost model. Our datasets included field and high-resolution topographic metrics including elevation, slope, aspect, and solar radiation and canopy height derived from lidar (1 m) and 44 vegetation indices derived from high-resolution (1 m) visible to near infrared (VNIR) hyperspectral data collected by NASA Goddard's Lidar, Hyperspectral and Thermal Imager (G-LiHT) sensor. The remote sensing data were collected under variable sky conditions (clear to overcast) throughout a 1-month growing-season period, and field data collected by United States Department of Agriculture (USDA) Forest Service, Forest Inventory and Analysis program (FIA). In this framework, we also studied the importance

of topographic and remote sensing variables for the classification of forest types. We found the CNN model outperformed the XGBoost model in terms of overall accuracy and a macro average F1 score for all three different forest type classifications. The CNN model achieved an overall accuracy of 93.06% for forest or nonforest, 82.59% for hardwood, softwood, and nonforest, and 74.74% for three dominant forest types including paper birch, black spruce, and white spruce along with nonforest. Among the various topographic factors, we found that elevation was the most important factor for discriminating all forest types. In addition, we found that canopy height and vegetation indices including Photochemical Reflectance Index (PRI), Pigment Specific Normalized Difference (PSND), and Gitelson and Merzlyak (GM1) were important for differentiating between hardwood and softwood while Anthocyanin Reflectance Index (ARI1) was important for differentiating between forest and nonforest. The high-resolution forest type information can improve our ecological understanding of boreal forest dynamics, estimate above ground biomass, and carbon, and support the national forest inventory and forest managers.

3.2 INTRODUCTION

The boreal forest biome is the largest terrestrial biome, covering nearly 14% (18.5 million km^2) of the entire vegetation cover of the Earth (Douglas et al., 2014; Mcguire & Chapin III, 2006), and stores nearly one-third of the terrestrial carbon (Pan et al., 2011; Walker et al., 2020). The trajectory of boreal forest ecosystems is uncertain due to increasing disturbances, thawing permafrost, changes in hydrology and warming.

This is particularly evident in boreal forest of Interior Alaska (Chapin et al., 2010; Johnstone et al., 2010), where temperatures in this region have surged nearly five times more than global mean over the past five decades, (Euskirchen et al., 2010). These dramatic changes led to an increase in fire extent, proliferation of deciduous trees following fires, and a decline in the

growth and extent of dominant conifer tree species like spruce (Beck et al., 2011; Chapin et al., 2010; Johnstone et al., 2010; Walker et al., 2023). The shift in forest type will change ecological processes and services, impact carbon uptake, and will have significant implications for the carbon and nutrient cycle, understory vegetation, and wildlife habitat (Barber et al., 2000; Johnstone et al., 2020; Kasischke et al., 2010). These rapid ecological changes require fine-scale monitoring of forests to detect potential type conversions and guide management interventions.

A combination of field data and high-resolution (~1m) remote sensing data affords the potential to produce precise and spatially extensive forest type maps for accurately monitoring shifts in this region. An earlier study mapped vegetation composition at coarse resolution (250 m) (Ruefenacht et al., 2008) and forest type at moderate (30 m) resolution (University of Alaska-Anchorage, 2017). Recently, studies have shown the effectiveness of lidar and high-resolution imagery in classifying forest types. Airborne lidar and hyperspectral data has been used to map individual tree species in boreal forests of Norway (Dalponte et al., 2014) and Finland (Mäyrä et al., 2021). Alonzo et al. (2018) used high-resolution UAV imagery with forest inventory analysis (FIA) plot data to model forest type at individual crown scale and achieved 85% accuracy for identifying tree species in the Bonanza Creek experimental forest, Alaska. Shoot et al. (2021) conducted a case study by combining FIA field plots with lidar and vegetation indices derived from hyperspectral data to classify forest types and found that the combination of lidar-derived metrics and vegetation indices produced more accurate classification. However, there has been limited research using a systematic sample of field data with high-resolution airborne data (~1 m) collected under variable sky conditions (clear to overcast) during a 1-month period of the growing-season with deep learning models, which provides a means for upscaling forest type from field plots to a larger geographical extent in Interior Alaska.

The fine-scale mapping of boreal forest type over broader extents in Interior Alaska was made possible by a new joint National Aeronautics and Space Administration (NASA) and United States Department of Agriculture (USDA) Forest Service pilot-project that was initiated in 2014 (Cahoon and Baer, 2022). The USFS, Forest Inventory and Analysis Program (FIA) was not implemented in Interior Alaska before 2014 because of the vastness and inaccessibility of the boreal forest. A joint NASA-FIA inventory pilot project was started in 2014 to leverage state-of-art remote sensing technology to support the sparse FIA inventory in Interior Alaska (Andersen et al., 2015). The high-resolution remote sensing data acquired by NASA Goddard's Lidar, Hyperspectral, and Thermal (G-LiHT) airborne imager affords an opportunity to upscale sparser field plot data to a larger area (Andersen et al., 2015; Cook et al., 2013). The high-resolution forest type information across larger areas can be used to improve our ecological understanding of boreal forest dynamics, improve estimates of aboveground biomass and carbon as well as support the FIA program and forest managers.

Even though previous studies have utilized deep learning models with high-resolution RGB (Schiefer et al., 2020) and hyperspectral (Fricker et al., 2019; Mäyrä et al., 2021) data to classify individual tree species in various forest ecosystems, the application of deep learning approaches for fine-scale mapping of dominant forest types in Interior Alaska and robustness of these approaches under different environmental conditions (e.g., solar illumination, phenological development, site quality) remains relatively unexplored. The availability of lidar, high-resolution hyperspectral data coupled with field data affords a unique opportunity to leverage deep learning models for classifying and mapping of dominant forest type at high-resolution across broader geographical extents. Moreover, the boreal forests in Interior Alaska are significantly influenced by topographical factors such as elevation, slope, aspect, and solar

radiation (Calef et al., 2005; Douglas et al., 2014; Ohse et al., 2009). Therefore, we integrated remote sensing with topographic variables to enhance the classification of forest types. Further, we investigated the key topographic factors associated with the forest type to gain deeper insights into their ecological dynamics.

The primary aim of this research was to assess the performance of state-of-the-art machine learning models for classification and mapping of forest types combining the high-resolution imagery and FIA field plot information in the boreal forest ecosystems of Interior Alaska. To achieve this objective, we compared the performance of a deep learning model, a convolutional neural network with a machine learning model, XGBoost for classifying forest type using G-LiHT remote sensing data. We used predictor variables including vegetation indices (VIs) derived from hyperspectral imagery and digital terrain model (DTM), slope, aspect, canopy height model (CHM), and solar radiation index (SRI) derived from lidar data. Our study included forest type classification at three levels, including 1. forest and nonforest, 2. hardwood and softwood and nonforest and 3. dominant forest types include paper birch, black spruce, white spruce, and nonforest.

Our overall objective was to determine how well forest types could be classified to support monitoring of changes in boreal forests. We did this by addressing the following three research questions:

1. Does a convolutional neural network or XGBoost produce the most accurate forest type classification using field and high-resolution remotely sensed data?
2. Which predictor variables were strongly associated with the forest type classification?
3. Which factors among slope, aspect, elevation, and solar radiation are most important for forest type distribution?

3.3 MATERIALS

3.3.1 Study area

We studied the Tanana unit of Interior Alaska, which covers 33.4 million acres of land, of which 20.8 million acers (62%) is covered with boreal forest (Cahoon & Baer, 2022) (Figure 3.1). The study area has six dominant tree species: black spruce (*Picea mariana*), white spruce (*Picea glauca*), tamarack (*Larix laricina*), Alaska paper birch (*Betula neoalaskana*), balsam poplar (*Populus balsamifera*), and aspen (*Populus tremuloides*) (Chapin et al., 2006). Among them, black spruce is the dominant forest type covering 52% of forested area, followed by paper birch (19%) and white spruce (16%) (Cahoon & Baer, 2022).

The Tanana unit terrain consists of rolling hills, lowlands, flat bottomlands, uplands, and floodplains (Figure 3.2). The elevation ranges from sea level to a nearly 6100 m high mountain. It has a continental climate, characterized by short, warm summers and long, very cold winters (Gallant, 1995). The mean annual air temperature is -3.3 ^{0}C with absolute extremes ranging from -51 ^{0}C to 38 ^{0}C (Jorgenson et al., 2001). The average annual precipitation is about 280 mm, half of which occurs during the summer (Douglas et al., 2014; Shulski & Wendler, 2007). However, most summer precipitation is rapidly lost due to evaporation (Hinzman et al., 2006). Snow accounts for nearly 40 to 45% of the mean annual precipitation (Douglas et al., 2014; Hinzman et al., 2006).

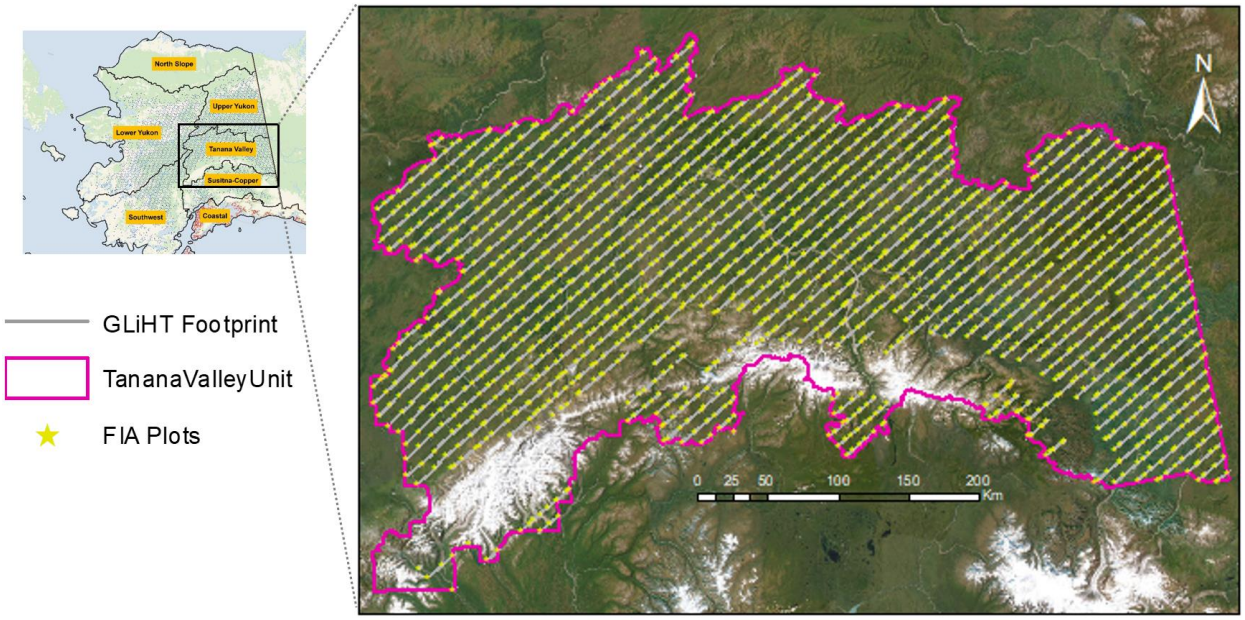

Figure 3.1: Tanana unit of Interior Alaska with GLiHT flight lines and representative FIA plot locations (actual FIA plot locations are obscured due to plot confidentiality requirements).

Figure 3.2: Landscape of Interior Alaska that is covered with mosaic of conifers and deciduous forest types with nonforest patches (Cahoon & Baer, 2022).

3.3.2 Field dataset

The USDA Forest Service, Forest Inventory and Analysis (FIA) program provides information about the forestlands of the United States with continuous monitoring. Individual FIA plots are on a hexagonal grid with one plot in the center and three subplots distributed in an inverted Y pattern (Bechtold & Patterson, 2005; Cahoon & Baer, 2022) (Figure 3.3). In 2014, a joint NASA-FIA inventory pilot project was started to leverage high-resolution remote sensing technology to support the FIA inventory in Interior Alaska (Andersen et al., 2015). In Interior Alaska, there is one FIA plot per 97.12 km^2 (30,000 acres), which is sparser than the lower 48 states because of the remoteness of the area (Andersen et al., 2015). There are total of 1,128 FIA plots in the Tanana unit, which total around 4,512 subplots (Table 3.1) with forest inventory information such as live or dead, tree height, DBH, species at tree level, and forest type information at the subplot level. The forest type is assigned to each subplot with the dominant stocking of live trees that are not overtopped (Bechtold & Patterson, 2005). If there are no trees or the plot does not meet the tree canopy cover threshold (10%) then it was classified as nonforest (USDA, 2018). Based on the FIA, the nonforest category includes shrubs, grasses, herbaceous ground cover, mountain, snow, and water. We used FIA forest type information to create our training dataset.

Table 3.1: Number of total FIA subplots with forest type information used in the analysis. Field subplots represented the field measured plots and G-LiHT subplots represented the FIA subplot that had G-LiHT data available.

Land cover	Forest Type	Tree species	Field subplots	G-LiHT subplots
Nonforest	Nonforest	Nonforest	1752	961
Forest	Softwood	White spruce	523	487
Forest	Softwood	Black spruce	1470	1381
Forest	Softwood	Tamarack	35	35
Forest	Hardwood	Aspen	200	193
Forest	Hardwood	Paper birch	505	473
Forest	Hardwood	Balsam poplar	27	27

		Total	4512	3557

3.3.3 NASA Goddard's LiDAR, Hyperspectral and Thermal (G-LiHT)

G-LiHT is an airborne imager system that has a suite of complementary instrument (lidar, VNIR imaging spectrometer, and thermal camera) that was designed to map the composition, structure and function of terrestrial ecosystems at fine spatial resolution (1 m) (Andersen et al., 2015; B. D. Cook et al., 2013). G-LiHT data was acquired at a nominal altitude of 335 m above ground level (AGL), covering a swath of ~250 m wide spaced 9200 m apart and oriented in a northeast-southwest direction. A Riegl VQ-480 airborne laser scanner (Horn, Austria) was used to acquire ~3 to 6 pulses m^{-2}, and up to 8 returns per pulse were recorded for each ~10 cm diameter pulse. Lidar data was used to derive the canopy height model and bare earth model following methods described by Cook et al. (2013). Imaging spectrometer data in the visible through infrared range (420 to 920 nm) were acquired with a Hyperspec imaging spectrometer (Headwall Photonics, Fitchburg, MA, USA). Downwelling irradiance data was acquired with an Ocean Optics (Dunedin, FL, USA) USB4000-VIS-NIR spectrometer, and used to compute at-sensor reflectance as described by Cook et al. (2013). Reflectance data were used to derive 44 different vegetation indices that represent the unique characteristics of each forest type, and data were downloaded through the G-LiHT data center (https://glihtdata.gsfc.nasa.gov/). Multi-sensor data produced by G-LiHT provides a unique opportunity for scientists to develop synergistic algorithms to monitor forest conditions using data fusion (Cook et al., 2013).

3.3.3.1 Lidar derived metrics

For this study, we used various metrics derived from lidar (Table 3.2). We resampled the lidar point clouds and processed the data to produce 1 m resolution digital terrain model (DTM)

using a classification of ground returns with a morphological filter (Cook et al., 2013). Similarly, derived a canopy height model (CHM) from the highest lidar return in every 1 m grid cell (Cook et al., 2013). The slope is a measure of the steepness of a surface and the aspect represents the direction in which the slope faces. The solar radiation aspect index referred to as SRI is a metric used to quantify the orientation of land surfaces in relation to the solar radiation. Its values range from 0 to 1. We used *trasp* function available in SpatialEco package (Evans & Murphy, 2021) to calculate SRI in R. The digital terrain model was used to derive the slope, aspect, and SRI. From here onwards, we will refer to DTM as elevation.

Table 3.2: Lidar-derived canopy height and topographical metrics at 1 m spatial resolution were used for analysis.

Lidar and Topographic Metrics	Detail
Canopy Height Model (CHM)	Highest return above ground (m AGL) in each grid cell, interpolated to pixel centroid (meter)
Digital Terrain Model (DTM)	Ground points (elevation) interpolated to pixel centroid (meter)
Slope	Steepness of surface (degrees)
Aspect	Direction in which the slope faces (degrees)
Solar Radiation Index (SRI)	Amount of solar radiation reaching the specific area (unitless)

3.3.3.2 Vegetation indices

Vegetation indices that accentuate essential plant characteristics such as greenness, light use efficiency, leaf area, stress, biochemical pigmentation, chlorophyll, anthocyanin, and carotenoid content can be highly valuable for differentiating among forest types, particularly under varying illumination conditions. Vegetation indices has been used to differentiate between vegetation cover (Tain and Fu, 2021). We derived 44 different vegetation indices from hyperspectral data (1 m) to that highlight unique spectral and physiological characteristics as mentioned above (Cook

et al., 2013). We have presented 24 commonly used and important indices selected by model (section 4.2) in Table 3.3 and other vegetation indices used are presented in Table B1.

Table 3.3: The commonly used and important vegetation indices selected by the models that were used in the analysis.

Vegetation Index	Formula	Ref
Metrics describing pigments in vegetation		
Normalize Difference Vegetation Index (NDVI)	(R_800 – R_680) / (R_800+R_680)	(Rouse et al., 1974)
Simple Ratio Pigment Index (SRPI)	R_430/ R_680	(Peñuelas et al., 1993)
Metrics describing biochemical pigments		
Pigment Specific Normalized Difference (PSND)	(R_800 – R_635) / (R_800 + R_635)	(Blackburn, 1998)
Structure Insensitive Pigment Index (SIPI)	(R_800 – R_445) / (R_800 – R_680)	(Peñuelas et al., 1995)
Plant Senescence Reflectance Index (PSRI)	(R_680 – R_500) / R_750	(Merzlyak et al., 1999)
Normalized Phaeophytinization Index (NPQI)	(R_415 – R_435) / (R_415 + R_435)	(Barnes et al., 1992)
Photochemical Reflectance Index (PRI)	(R_531-R_570)/(R_531+R_570)	(Rondeaux et al., 1996)
Renormalized Difference Vegetation Index (RDVI)	(R_800−R_670) / sqrt(R_800 + R_670)	(Roujean & Breon, 1995)
Metrics describing chlorophyll pigments		
Derivative Chlorophyll Index (DCI)	D705/D722	(Zarco-Tejada et al., 2002)
Datt Index (Daat1)	R_672*(R_550 * R_708)	(Datt, 1998)
Datt Index (Datt2)	(R_850 – R_710) / (R_850 – R_680)	(Datt, 1999)
Gitelson and Merzlyak (GM1)	R_750 / R_550	(Gitelson & Merzlyak, 1994a)
Gitelson and Merzlyak (GM2)	R_750 / R_700	(Gitelson & Merzlyak, 1994b)
Greenness Index (GI)	R_554 / R_677	(Smith et al., 1995)
Maccioni (MAC)	(R_780 – R_710) / (R_780 – R_680)	(Maccioni et al., 2001)
MERIS Terrestrial Chlorophyll Index (MTCI)	(R_754 – R_709) / (R_709 – R_681)	(Dash & Curran, 2007)

Normalized Pigment Chlorophyll Index (NPCI)	(r680-r430)/(r680+r430)	(Barnes et al., 1992)
Vogelmann (VOG)	D715/D705	(Vogelmann et al., 1993)
Metrics describing anthocyanin and carotenoid content		
Anthocyanin Reflectance Index (ARI1)	(1/R_550) - (1/R_700)	(Gitelson et al., 2007)
Anthocyanin Reflectance Index (ARI 2)	R_800*((1/R_550) - (1/R_700))	(Gitelson et al., 2007)
Red Green Ratio Index (RGRI)	R_sum(600-699)/ R_sum(500-599)	(Gamon & Surfus, 1999)
Carotenoid Reflectance Index (CRI1)	(1/R_510) - (1/R_550)	(Gitelson et al., 2007)
Metrics describing leaf area, plant stress & background noise		
Carter Stress (CS2)	R_605 / R_760	(Carter, 1994)
Elvidge and Zhikang (EZ)	R_(625-795)	(Elvidge & Chen, 1995)
Aoki (AOKI)	R_500 / R_850	(Akao et al., 1981)
Triangular Vegetation Index (TVI)	0.5*(120*(Ravg760_800-Ravg530_570)-200*(Ravg650_680-Ravg530_570))	(Broge & Leblanc, 2001)

3.4 METHODS

The main aim of the study was to analyze the performance of 1) the convolutional neural network model and 2) XGBoost models for classifying forest type in Alaska's boreal forest using high-resolution G-LiHT derived metrics. We approached this study using methods that would be appropriate for mapping forest types over large ecosystems (~34 million acres). We therefore used the forest type identified at the subplot level by the FIA field data and combined it with the high-resolution G-LiHT derived data. Our method is divided into the following five sections: 1. Creating labels, 2. Model development, 3. Training models, 4. Model evaluation, and 5. Model Interpretation (Figure 3.3).

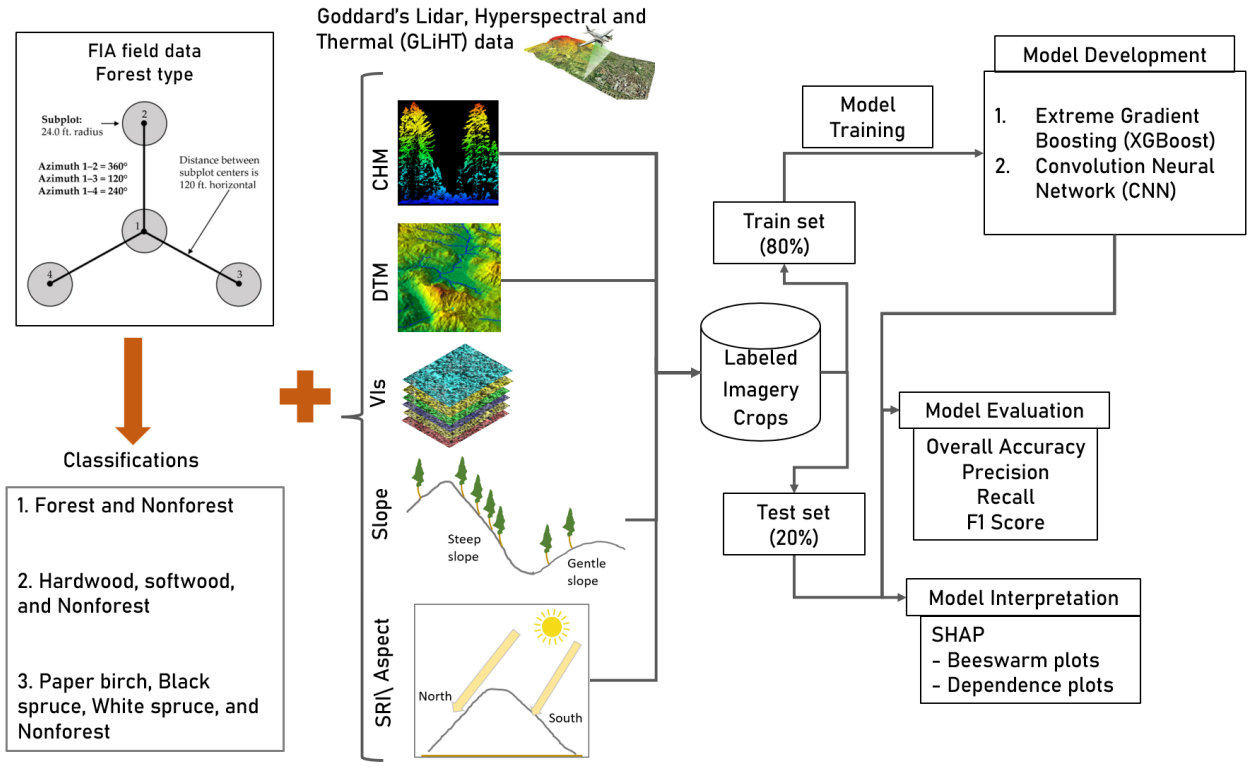

Figure 3.3: Schematic diagram of the framework, which highlights the five main steps with data modality and models used for the classification of forest types.

3.4.1 Creating labels

We used the forest type information collected at the subplot level by the FIA program to create the labeled dataset. Each subplot was around 7 m (24 ft) in radius. From the in-situ forest type labels, we derived three different taxonomies: 1. forest and nonforest, 2. softwood, hardwood, and nonforest, and 3. dominant forests paper birch, black spruce, white spruce, and nonforest. Thus, in total we had three different sets of classifications labels for each subplot. For each of these classifications, we trained and evaluated models separately.

For the CNN model, we used the location of the FIA subplot as a center to crop each predictor data using a bounding box of size 16 x 16 m. We padded the 14x14 m subplots to by 2 such that the crops were a power of two. For the machine learning model, we derived seven

summary statistics, including minimum, first quartile, median, third quartile, standard deviation, mean, and maximum of each predictor variable at the subplot level.

To create robust separation and avoid spatial autocorrelation between training and testing data, which could bias the classification results, we placed all subplots within a plot into either training or testing dataset (Marconi et al., 2022). This ensured that the subplots within the same plot would not end up in both the train and test set. We then randomly created a split of 80:20% data based on the plot location. We used a train set (80%) for training our models and a test set (20%) to evaluate the performance of different models.

3.4.2 Model development

We developed a custom deep learning (CNN) model using the PyTorch (Paszke et al., 2019) framework in Python for the classification of forest type. Our custom CNN model uses two convolutional layers with 3x3 kernels, followed by two linear layers. Each convolutional layer was followed by batch normalization, rectified linear units (ReLu) as the activation function, and max pooling. Batch normalization reduces training time and overfitting (Ioffe and Szegedy, 2015). These features were then converted to one-dimensional vectors before passing to the linear layer. Finally, we get the probability values of classes using the softmax in the last layer.

We compared the performance of the convolutional neural network model with eXtreme gradient boosting (XGBoost), which is known to outperform other machine learning models for supervised classification. Image crop of canopy height, elevation, slope, aspect, and vegetation indices were the input for the CNN model. For the machine learning models, we used the summary statistics of each predictor variable. A total of 343 predictor variables were used for machine learning models.

3.4.3 Model training

For both models, we normalized the data with a z-score using the mean and the standard deviation of the training set. For training deep learning models, we used cross-entropy loss, and an Adam optimizer. We used augmentation techniques to avoid overfitting and improve the generalization of the model on unseen data. During training, we applied different augmentation techniques, such as random horizontal and vertical flipping, and Gaussian blur using the torchvision package (Marcel & Rodriguez, 2010). We trained deep learning models using NVIDIA 2080 Ti GPUs on the Hyak supercomputer of the University of Washington, Seattle, United States. Our models were trained for 100 epochs with a batch size of 16 and a learning rate of 1e-3, of which we saved the last epoch model for the evaluation model.

We implemented our machine learning models using scikit-learn (Pedregosa et al., 2011). Instead of using default hyperparameter values, we tuned hyperparameters during the training phase to improve the classification accuracy. We tuned the hyperparameter separately for each model, using a randomized search. We used a randomized search on five five-parameter combinations with five-fold random cross-validation on training data and the best cross-validation score model was fit to the complete training set.

3.4.4 Model evaluation

To quantify model performance, we used overall accuracy (OA), precision (also known as user's accuracy (UA)), recall (also known as producer's accuracy (PA)), and F1 score. We also used a macro averages of precision, recall, and F1 score, which take the average across classes for multi-class classification to determine the best data modality and model (Mäyrä et al., 2021). These metrics were derived using the following formulas with true positives (TP), true negatives (TN), false positives (FP), false negatives (FN), and total numbers of items (N).

$$(1)\mathrm{OA} = \frac{\mathrm{TP} + \mathrm{TN}}{\mathrm{N}} \qquad (2)Recall = \frac{TP}{TP+FN} \qquad (3)Precision = \frac{TP}{TP+FP}$$

$$(4)F1 = 2 * \frac{Precision * Recall}{Precision + Recall}$$

3.4.5 Model interpretation and variable importance

Machine learning models are considered a black box because the process leading to model outputs is difficult to understand and interpret. However, there are methods like Shapley Additive exPlanations (SHAP) (Lundberg et al., 2018; Lundberg & Lee, 2017), that are model-agnostic and provides detailed and individualized explanations and attributes for individual variables, as opposed to providing only general interpretations across the entire dataset (Li, 2022). The SHAP method is a powerful tool for interpreting models confidently (Lundberg et al., 2018). For the local interpretation of predictors, we used the SHAP method with only the XGBoost model for simplicity and efficiency. We implemented SHAP by using the package called shapviz (Mayer & Stando, 2024) in R (version 4.3.1).

We used a beeswarm plot to interpret individual predictor's contribution to the model output. The SHAP value on the x-axis is the measure of the impact of each feature on the model's prediction. A SHAP value of zero means the feature has no impact. A positive SHAP value indicates that the feature is pushing the prediction towards one class and a negative SHAP value is pushing the prediction towards another class. Each row represents a feature used in the model ordered based on its importance. The x position of the dot shows the impact on the model's output and the color of the dot represents the value of the feature from low to high.

In addition, to understand which topographical variables were more associated with paper birch, black spruce, white spruce, and nonforest, we used a dependence plot with the XGBoost

model using SHAP. The dependence plots help to understand the relationship between individual predictors and forest type. In the dependence plots, the y-axis represents SHAP values, indicating the impact of each feature on the model's prediction for a particular forest type. Positive SHAP values indicate that the feature contributes towards classifying the area as that forest type, while negative values indicate prediction away from that forest type.

3.5 RESULTS

3.5.1 Classification results

We compared the performance of CNNs with XGBoost model for the classification of forest type using high resolution remote sensing data and FIA subplot for three different forest type classifications. All CNN models outperformed the XGBoost models with the highest macro average F1 score and overall accuracy for all classification levels (Figure 3.4).

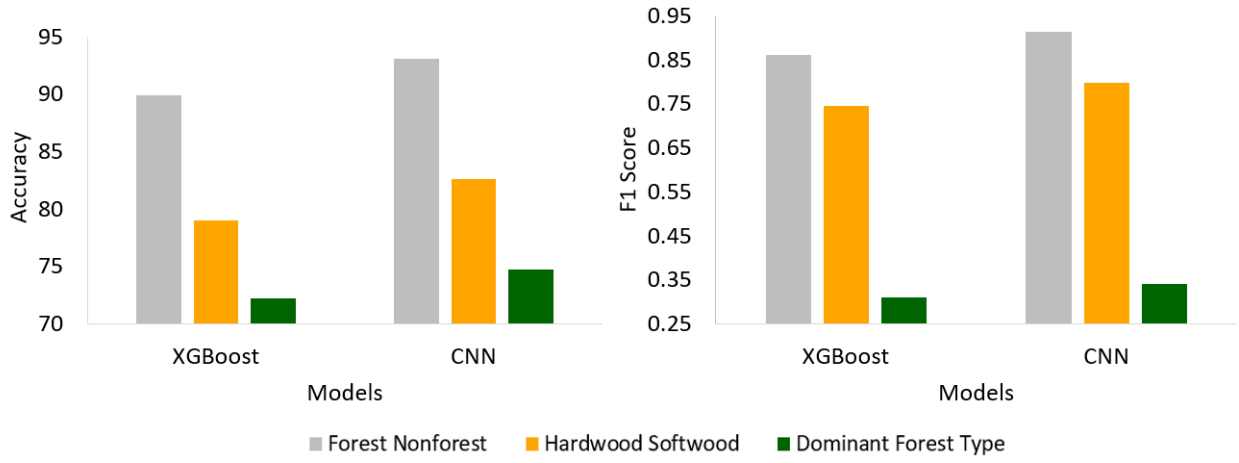

Figure 3.4: Summary of the results showing CNN model performs better than XGBoost in terms of the overall accuracy and F1 score for each classification level. Dominant forest type includes paper birch, black spruce, white spruce and nonforest.

Table 3.4: Test set results of XGBoost and CNN model for different forest type classifications.

Forest and nonforest						
	XGBoost			CNN		
	Precision	**Recall**	**F1**	**Precision**	**Recall**	**F1**
Forest	0.90	0.98	0.93	0.92	0.99	0.95
Nonforest	0.91	0.69	0.79	0.96	0.80	0.87
Macro Avg	0.91	0.83	0.86	0.94	0.89	0.91
OA			89.94 %			93.06 %
Hardwood, softwood and nonforest						
	XGBoost			CNN		
	Precision	Recall	F1	Precision	Recall	F1
Hardwood	0.71	0.50	0.59	0.72	0.64	0.68
Nonforest	0.92	0.73	0.81	0.92	0.81	0.86
Softwood	0.77	0.92	0.84	0.81	0.90	0.85
Macro avg	0.80	0.72	0.75	0.82	0.78	0.80
OA			79.01 %			82.59 %
Dominant forest type: Paper birch, black spruce, white spruce and nonforest						
	XGBoost			CNN		
	Precision	Recall	F1	Precision	Recall	F1
Paper Birch	0.62	0.44	0.52	0.62	0.67	0.64
Black spruce	0.10	0.88	0.18	0.11	0.83	0.20
Nonforest	0.04	0.78	0.07	0.04	0.83	0.07
White spruce	0.54	0.41	0.47	0.53	0.37	0.44
Macro avg	0.33	0.63	0.31	0.32	0.67	0.34
OA			72.22 %			74.74 %

3.5.1.1 Classification of forest and nonforest

The forest and nonforest classification had the highest accuracy for both models compared to other classifications. The CNN model had an overall accuracy of 93.06% with a macro average F1 score of 0.91. Whereas the overall accuracy of XGBoost was 89.94% with a macro average F1 score of 0.86. The CNN model had the higher F1 score, precision, and recall for both forest and nonforest classes compared to XGBoost (Table 3.4). Generally, forest was classified with higher accuracies and nonforest was confused with forest over 20% of the time (Figure B1).

3.5.1.2 Classification of hardwood, softwood, and nonforest

The CNN model had over all accuracy of 82.59% with a macro average F1 score of 0.80. Whereas the overall accuracy of XGBoost was 79.01% with a macro average F1 score of 0.75. The F1 score for all classes was higher with the CNN model (Table 3.4). The hardwood and nonforest classes were mostly confused with softwood (Figure B2). The performance of the CNN model for all classes was more balanced and better than XGBoost.

3.5.1.3 Classification of paper birch, black spruce, white spruce and nonforest

Along with nonforest, we selected three dominant forest types including paper birch, black spruce, and white spruce as they comprise over 80% of the forested land in Interior Alaska for classification (Cahoon & Baer, 2022). The CNN model had an overall accuracy of 74.74% with 0.34 macro average F1 score. Whereas XGBoost model had an overall accuracy of 72.22% with 0.31 macro average F1 score (Table 3.4). Typically, black spruce and nonforest were classified with higher accuracy, and white spruce was the most difficult species to classify correctly and was confused mostly with black spruce and some with birch (Figure B3).

3.5.2 Model interpretation

3.5.2.1 Global feature contribution

To better interpret the optimal importance of different predictors with XGBoost, we used SHAP. In Figure 3.5, the x-axis is the mean SHAP values, which represents the average impact on the model output. The canopy height model and elevation were consistently the top predictors across different classifications. Otherwise, feature contributions varied across different classifications (Figure 3.5). For forest and nonforest classification, solar radiation, aspect, Derivative Chlorophyll Index (DCI), Vogelmann (VOG), Anthocyanin Reflectance Index

(ARI1), and Renormalized Difference Vegetation Index (RDVI) had the largest impact. For hardwood, softwood and nonforest classification, slope, Pigment Specific Normalized Difference (PSND), Photochemical Reflectance Index (PRI), Normalized Phaeophytinization Index (NPQI), solar radiation, and aspect had the largest impact. For paper birch, black spruce, white spruce and nonforest classification, slope, solar radiation, aspect, PSND, PRI, and NPQI had the largest impact on the model output. The variation in the canopy height and elevation for different forest types is shown in Figure 3.6. The paper birch displayed the largest canopy height on average.

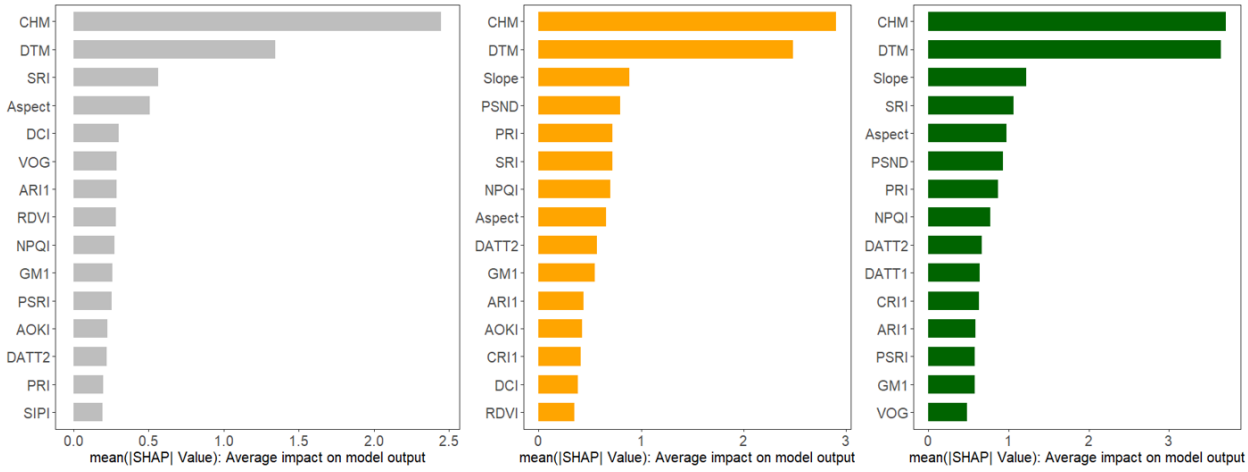

Figure 3.5: The top 15 predictors for different level forest type classifications where (left) forest or nonforest, (middle) hardwood, softwood or nonforest, and (right) birch, black spruce, nonforest and white spruce. All acronyms in the above graphs are found in Table 3.2 & 3.3.

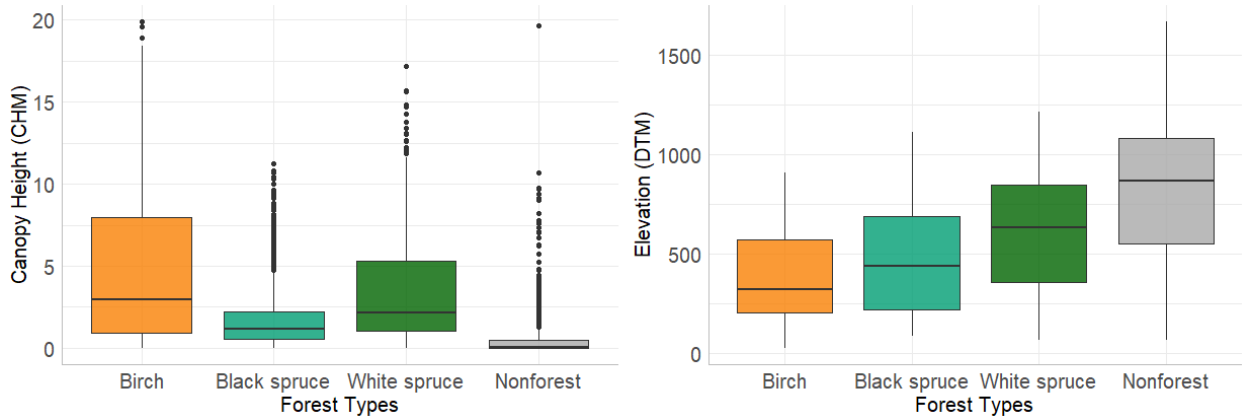

Figure 3.6: Demonstrating box plot for the canopy height (CHM) and elevation (DTM) for three dominating forest types and nonforest classification.

3.5.2.2. Individual feature contribution

3.5.2.2.1. Forest and nonforest

For forest and nonforest classification, the widest spread of SHAP values and those further from zero are the most important features, including canopy height, elevation, and SRI (Figure 3.7). The lower canopy height exhibits a positive SHAP value, indicating that lower canopy height values are important for predicting nonforest class. Conversely, the higher canopy height values spread towards negative SHAP values pushes the prediction towards the forest class. In contrast, higher elevation is spread towards positive SHAP values, indicating higher elevation lean towards nonforest and vice versa. The lower ARI1 values tend to lean towards nonforest. Features whose high and low values are spread in both positive and negative directions of graph suggest that their impact on the model's output depends on the combination with other features.

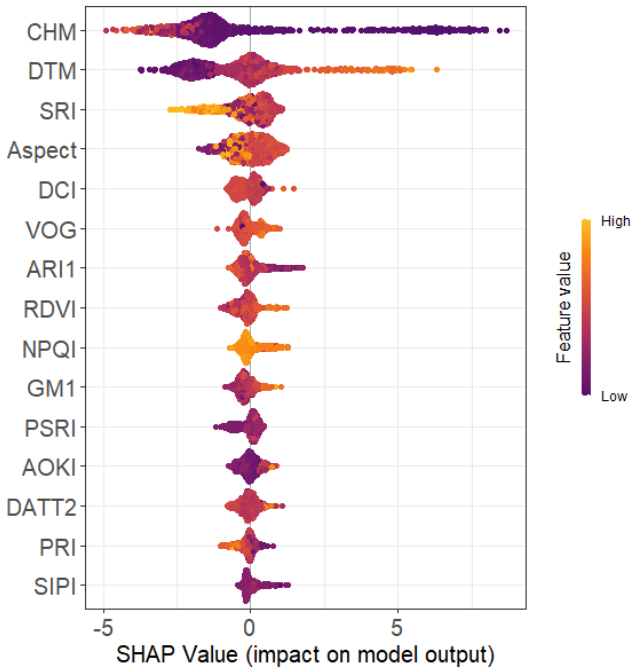

Figure 3.7: Comparison of individual feature contributions (top 15) for forest and nonforest classification. Where each dot represents SHAP value of specific data point and its position on x-axis show impact on the model's output. Positive SHAP value indicates features pushing prediction towards nonforest and negative towards forest class.

3.5.2.2.2 Hardwood and softwood and nonforest

We found that elevation was the most important feature for hardwood classification, while canopy height was the most important feature for nonforest and softwood classification (Figure 3.8). For hardwood classification, lower elevation had positive SHAP values indicating that lower elevation pushes the model towards predicting the hardwood. Similarly, medium slope, higher canopy height and PRI values tend to lean towards hardwood. Interestingly, PSND with lower values tend to lean towards hardwood. Further, those features with high and low values spread in both directions suggested that their impact on model depends on the combination of other features.

For softwood, medium to low canopy height values tend to have a higher probability of being softwood. In contrast to hardwood, higher PSND and DATT2 values tend to predict softwood. Lower slope (less steep) and GM1 tends to lean towards softwood. Other presented features showed an interactive effect, which means their effect on the model depends on a combination of other features. For nonforest class, most of the interpretation was similar to section 4.2.2.1.

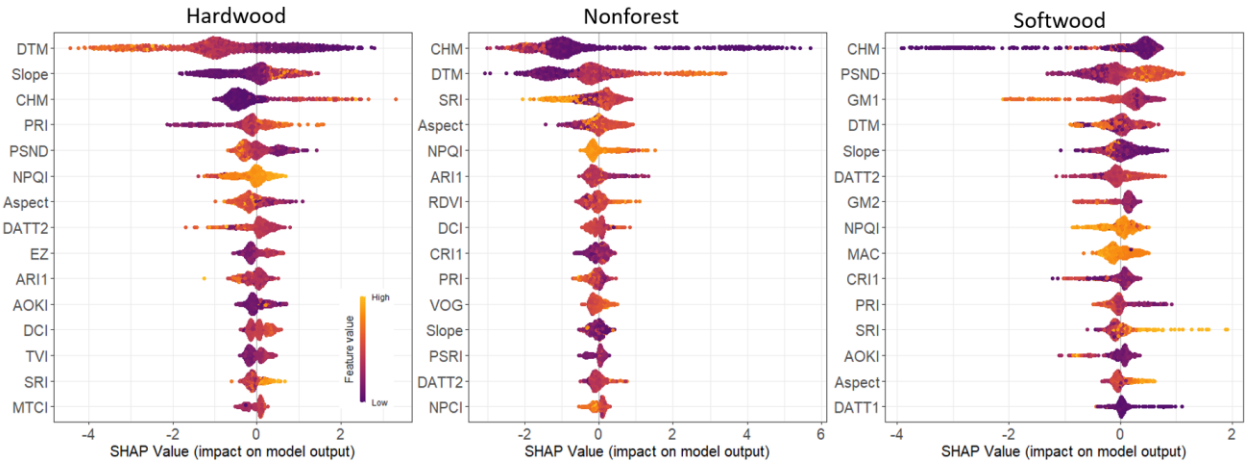

Figure 3.8: Comparison of individual feature contributions (top 15) for hardwood, nonforest and softwood classification where class 1: hardwood, class 2: nonforest and class 3: softwood.

3.5.2.2.3. Paper birch, black spruce, white spruce and nonforest

We found that canopy height was the most important feature for classifying black spruce, white spruce and nonforest while elevation was most important for paper birch (Figure 3.9). Lower elevations had positive SHAP values, indicating that lower elevation favors both paper birch and black spruce. While higher elevation values lean towards nonforest and white spruce. Medium slope tends towards predicting paper birch. A higher canopy height favors paper birch, lower canopy height favors black spruce and nonforest, and medium canopy height favors white spruce.

Among the vegetation indices, NPQI, PRI and DATT2 had interactive effects on paper birch classification. Whereas lower PSND and higher GM2 tend towards predicting paper birch. Similarly, higher PSND tend to predict black spruce and white spruce. PSND was not an important feature for a nonforest class. In addition, other vegetation indices, such as PRI, DATT1 had an interactive effect for both black spruce and white spruce prediction.

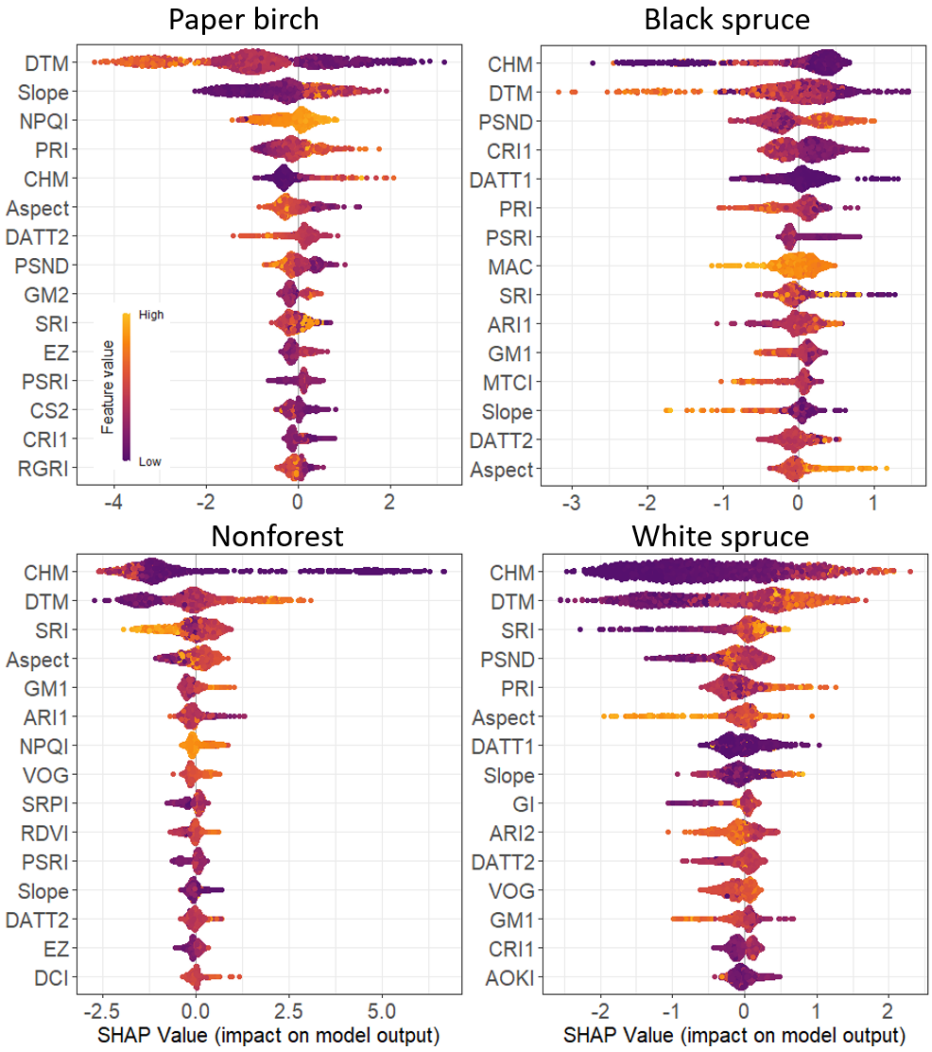

Figure 3.9: Comparison of individual feature contributions (top 15) for forests and nonforest classification where class 1: paper birch, class 2: black spruce, class 3: nonforest and class 4: white spruce..

3.5.3 Topographical variables associated with forest types

We used the dependence plots to understand the importance of each topographical variable (Figure 3.10). The elevation was consistently important for all forests and nonforest classes. For paper birch and black spruce, lower elevations were favorable, while for nonforest higher elevations were more favorable. For white spruce, there was no clear trend, but there were clusters of high and low values at various elevations. This indicated that elevation has a more complex relationship with the presence of white spruce.

Slope was generally more influential for forest types but in a different way. For paper birch, the SHAP value tends to decrease as the slope increases, indicating that moderately steep areas were more likely to be associated with paper birch. For black spruce, with the increase in slope, the SHAP value decreases, indicating that less steep areas are more likely associated with black spruce. For white spruce, the SHAP values are concentrated around zero, with a slight trend where both low and high slopes have negative SHAP values. This suggested that moderate slopes may be favorable for white spruce. There is a wide distribution of SHAP values across the slope for nonforest with slight concentration of positive values at higher slope indicating that steeper slope may have higher likelihood of nonforest. Both solar radiation and aspect had less clear direct effects on forests and nonforest classification, suggesting their impact might depend on interaction with other features.

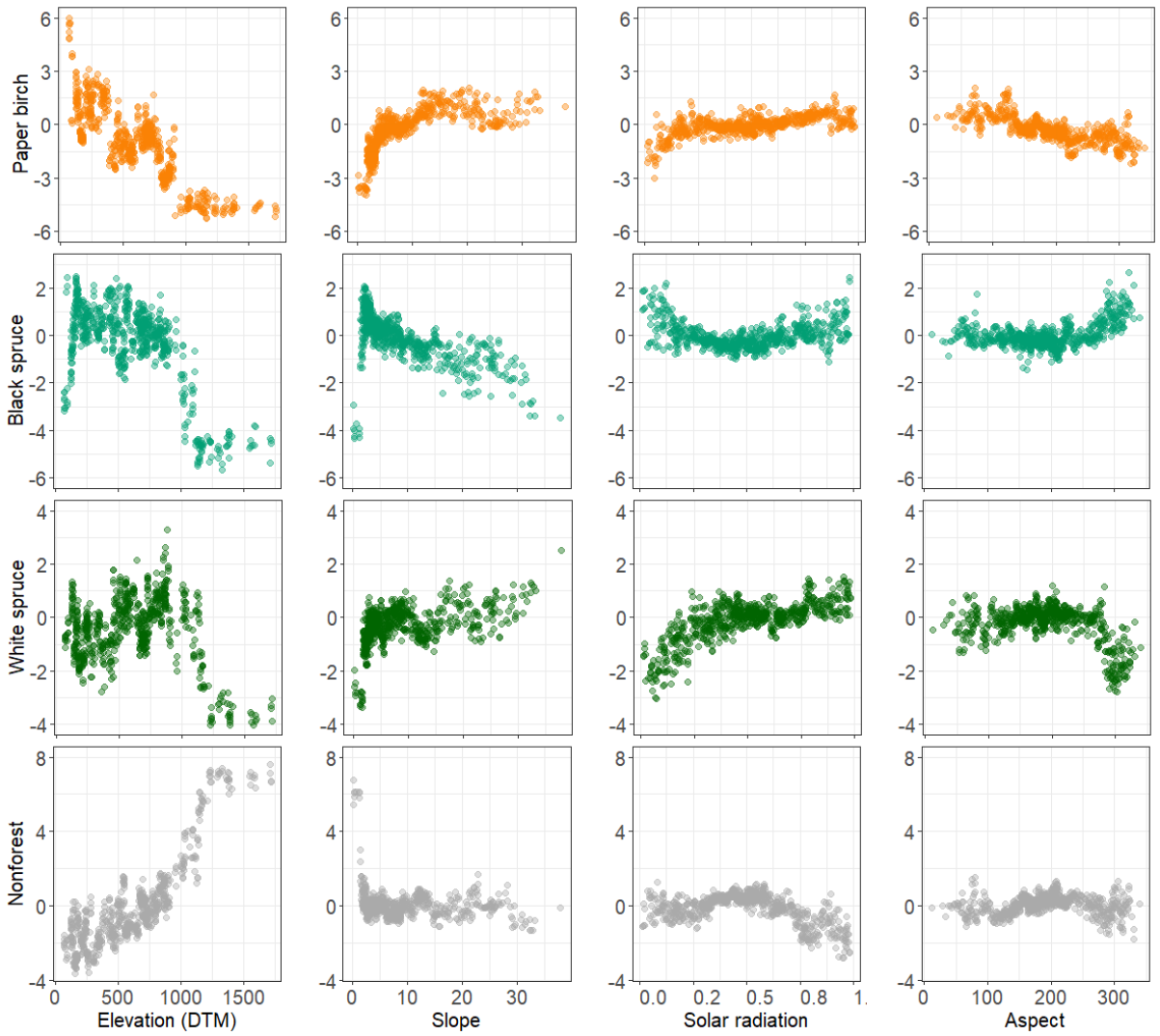

Figure 3.10: Dependence plots demonstrate the association of topographic variables with different forest types.

3.6 DISCUSSION

In this study, we compared the performance of the convolutional neural network with XGBoost model for identifying forest type using the combination of FIA field plot and high-resolution G-LiHT remote sensing data in the boreal forest of Interior Alaska. For the forest type classification, we conducted classification at three different levels including 1) forest and nonforest, 2) hardwood and softwood and nonforest, and 3) dominant forest type including paper

birch, black spruce, white spruce and nonforest. In addition, we used the SHAP method to understand the global and local feature importance.

Our results showed that forest and nonforest classification was conducted with the higher accuracy (96.06%). Whereas we achieved an overall accuracy of 82.59% for hardwood, softwood, and nonforest and 74.74% for four class classification including paper birch, black spruce, white spruce, and nonforest. The CNN model outperformed the XGBoost model in terms of overall accuracy and macro average F1 score for all three different level classifications (Figure 3.4). This results aligns with Mäyrä et al., (2021) who found CNN to outperform various commonly used machine learning models. The CNN models performed especially better in separating forest and nonforest, which can provide important information to forest managers. The CNN model also performed better in separating hardwood, softwood and nonforest, which can provide a beneficial method for industry, since commercial interest focuses on softwood. Further, among various features used, we found that canopy height and elevation were the topmost important predictors across all classifications.

We also found that the commonly used Normalized Difference Vegetation Index (NDVI) was not useful for the boreal forest type classification. Instead, vegetation indices such as Anthocyanin Reflectance Index (ARI) to be useful for forest nonforest classification and Pigment Specific Normalized Difference (PSND), Photochemical Reflectance Index (PRI), and Gitelson and Merzlyak (GM1) to be most useful for differentiating between hardwood and softwood.

Accurate, high-resolution forest type maps are useful in a variety of contexts including estimation of aboveground biomass and carbon, supporting forest management plans, managing timber production, and harvesting (Triviño et al., 2015) and aid information to rural communities that depend on nearby forest resources (Shoot et al., 2021). The high-resolution forest type map

can further our understanding of fine scale ecological processes and provide a strong basis for ecological studies.

3.6.1 Most important features

Our results showed that canopy height and elevation were the most important variable across all classifications. Lower canopy height, higher elevation, lower solar radiation was related to nonforest this could be due to nonforest includes grasses and shrubs whose canopy heights are generally lower than tree and are found above tree line at higher elevations with low temperatures.

Similarly, our study showed that lower elevation, medium slope, and higher canopies were associated with hardwood. The hardwood stands include aspen, paper birch and balsam poplar that are mostly found in less steep slope (Chapin et al., 2006). Further, we found medium to low canopy height was more associated with softwood stands. The softwood stands include black spruce, white spruce, and tamarack.

Further, vegetation indices that measure important plant features and characteristics like greenness, leaf pigmentation, and light use efficiency, proved highly valuable in differentiating among forest types in Interior Alaska. We will discuss specific vegetation indices later in our discussion.

3.6.2. Ecological interpretation

3.6.2.1 Potential sources of misclassification

In this section, we present potential ecological reasons to explain misclassification observed among forest types. Our classification was based identifying the dominant forest type within in subplots, each covering an area with 24 ft radius (around 7 meters). Each subplot may have a

mix of forest types, with one dominant species assigned to it. Some of the nonforest subplots were confused with the forest class which could be due to nonforest class also includes shrubs, grasslands and the areas that do not pass FIA's the minimum canopy threshold of 10% (USDA, 2018).

Among hardwood, softwood, and nonforest classification, softwood was classified most accurately (90%). While hardwood was confused with softwood class, this could be because hardwood forest stands such as aspen have a mixture of white spruce (Chapin et al., 2006). Similarly, birch dominated stands could have sporadically spread of white spruce and black spruce (Chapin et al., 2006; Douglas et al., 2014).

Similarly, among the three dominant forest type along with nonforest classification, black spruce and nonforest had the higher accuracy. The birch class was mostly misclassified as black spruce, this could be because birch stands could have scattered black spruce that replace the birch in later succession (Chapin et al., 2006). While white spruce was misclassified as both birch and black spruce. This could be because mixed white spruce stands could have birch (Douglas et al., 2014). In addition, both black spruce and late-successional white spruce are mostly available in cooler and moist areas (Chapin et al., 2006).

3.6.2.2 Importance of remote sensing variables

Among various remote sensing variables canopy height was the most important variable across all classifications. In addition, key plant traits allowed discrimination of forest types using vegetation indices. We found that Anthocyanin Reflectance Index (ARI1) with lower values, were more related to nonforest. This is because ARI1 is used for describing anthocyanin content in plants, which are higher in deciduous trees (Gould, 2004).

Similarly, our study showed that higher Photochemical Reflectance Index (PRI) and lower Pigment Specific Normalized Difference (PSND) were associated with hardwood. The PRI index is used as the indicator of photosynthetic radiation found in both hardwood and softwood forests (Gamon et al., 1997). However, softwood forest has low photosynthetic rate during mid-day relative to the hardwood forest because of which higher PRI is more related to hardwood (Gamon et al., 1997). Further, the PSND index is highly correlated with chlorophylls (Blackburn, 1999) and hardwood forests during fall change color and have lower chlorophylls. That is why lower PSND values were more associated with hardwood forest.

Further, we found higher PSND and DAAT2 were associated with softwood. The PSND and DAAT2 is closed related to the higher chlorophyll content in the leaf (Blackburn, 1999; Datt, 1999). Consequently, higher values of these indices are associated with softwood forests, where foliage maintains its green color without significant changes like hardwood forest. While lower Gitelson and Merzlyak (GM1) index is related to softwood because this index is related to chlorophyll content of yellow-green leaf (Gitelson, Merzlyak, et al., 1996).

3.6.2.3 Importance of topographic and solar radiation variables

Among various topographical variables, including elevation, slope, aspect, and solar radiation, we found elevation was consistently important for all forest types and nonforest.

We found that lower elevation, moderately steep areas with east- and south-facing slopes had a higher probability of associating with paper birch. This aligns with previous studies that have found birch stands to be more common on upland and south-facing slopes (Douglas et al., 2014) while others have found on east- and west-facing slopes that are cool and moist (Chapin et al., 2006). Since birch can be found either in south-facing or west-, and east-facing, which has very

different solar radiation therefore we were not able to find a clear relationship between solar radiation and paper birch.

We found that lower elevations, less steep slopes, north facing areas with medium solar radiation have a higher likelihood to be associated with black spruce. Among all topographic variables, elevation was strongly associated with black spruce that aligns with the results of previous studies (Calef et al., 2005). In general, black spruce stands are found to dominate the north-facing upland slopes with permafrost because they prefer cool and moist places (Chapin et al., 2006; Douglas et al., 2014).

Similarly, we found that moderate slope with either very high or low solar radiation is likely to be associated with white spruce. The lower elevations were associated with white spruce but not as strong as black spruce. Previous studies have shown that mixed white spruce stands can be found in uplands and lowlands and north-facing slopes (Douglas et al., 2014) and late successional white spruce are found in lower elevations on south-, east-, and west-facing slopes (Chapin et al., 2006). Since white spruce can be found in slope with different directions due to which we were not able to find a clear relationship between aspect and white spruce. White spruces are generally found in cooler and moist areas (Chapin et al., 2006). which aligns with our finding of white spruce being associated with moderate solar radiation. And higher elevation and lower solar radiation were associated with nonforest.

3.7 CONCLUSION

In this study, we presented a framework for forest type classification combining FIA field plots and high-resolution remote sensing data in the boreal forest of Interior Alaska. We conducted forest type classification at three different levels, including 1. Forest and nonforest, 2.

Hardwood, softwood, and nonforest and 3. Three dominant forest types, including paper birch, black spruce, white spruce, and nonforest. In addition, we also identified the importance of topographic and remote sensing variables for each forest type classification. The study showed that forest type classification can be conducted with high accuracy using deep learning methods and high-resolution remote sensing data. The study also showed that elevation was the most important topographic factor associated with these forest types. In addition, we found that canopy height and vegetation indices including Photochemical Reflectance Index (PRI), Pigment Specific Normalized Difference (PSND), and Gitelson and Merzlyak (GM1) were important for differentiating between hardwood and softwood while Anthocyanin Reflectance Index (ARI1) was important for differentiating between forest and nonforest.

This is the first study to use a systematic sampling of field data with high-resolution airborne data collected over large areas under variable sky condition and evaluate a performance of deep learning and machine learning models to classify forest types in Interior Alaska. This research highlights the importance and uses of high-resolution remote sensing to complement field especially in cases where field locations are inaccessible by humans. In future, we aim to use these models to produce forest type classifications over the entire G-LiHT footprint. The development and evaluation of models using field and high-resolution remote sensing for mapping forest type will be crucial for long-term monitoring for forest ecosystem to detect changes and estimating above ground biomass, carbon, and supporting forest management plans.

APPENDIX B

Table B1. Additional vegetation indices that were used in the analysis.

Vegetation Index	Formula	Ref
Carter Stress (CS1)	R_695 / R_760	(Carter, 1994)
Carotenoid Reflectance Index (CRI2)	(1/R_510) - (1/R_700)	(Gitelson et al., 2007)
Curvature Index (CI)	(R_683 * 2)/(R_675 * R_691)	(Zarco-Tejada et al., 2002)
Difference Vegetation Index (DVI)	R_800 – R_680	(Tucker, 1979)
Filella and Penuelas (FP)	R_(680-780)	(Filella & Penuelas, 1994)
Modified Chlorophyll Absorption Ration Index Improved (MCARI2)	1.5*((2.5*(R_800-R_670))-(1.3*(R_800-R_550)))/(sqrt(((((2*R_800+1)*(2*R_800+1))))-(6*R_800-(5*(sqrt(R_670)))-0.5)))	(Haboudane, 2004)
Modified Red Edge Normalized Difference Vegetation Index (MRENDVI)	(R_750-R_705)/(R_750+R_705+(2*R_445))	(Datt, 1999)
Modified Red Edge Simple Ratio (MRESR)	(R_750-R_445)/(R_705-R_445)	(Sims & Gamon, 2002)
Modified Simple Ration (MSR)	((R_800/(R_678-1))/sqrt((R_800/R_760)+1))	(Chen, 1996)
Modified Triangular Vegetation Index (MTVI)	1.2*((1.2*(R_800-R_550))-(2.5*(R_670-R_550)))	(Haboudane, 2004)
Modified Triangular Vegetation Index Improved (MTVI2)	(1.5*((1.2*(R_800-R_550))-(2.5*(R_670-R_550))))/(sqrt(((2*R_800+1)*(2*R_800+1))-(6*R_800-(5*(sqrt(R_670))))-0.5))	(Haboudane, 2004)
Modified Chlorophyll Abosrption Ratio Index (MCARI)	1.2*((2.5*(R_800 – R_670)) -(1.3*(R_800 – R_550)))	(Haboudane, 2004)
Normalize Difference Vegetation Index (NDVI)	(R_800 – R_680) / (R_800+R_680)	(Rouse et al., 1974)
Optimized Soil Adjusted Vegetation Index (OSAVI)	(R_800-R_680)/(R_800+R_680+0.16)	(Peñuelas et al., 1994)
Pigment Specific Simple Ration (PSSR)	R_600/R_680	(Blackburn, 1998)
Ratio Vegetation Index (RVI)	R_800/R_680	(Royle & Lathrop, 2002)
Red Edge Inflection Point (REIP)	R_750/R_700	(Vogelmann et al., 1993)

Red Edge Normalized Difference Vegetation Index (RENDVI)	(R_750 – R_705) / (R_750 + R_705)	(Gitelson et al., 1996)
Vogelmann Red Edge Index (VOGREI)	R_740 / R_720	(Vogelmann et al., 1993)

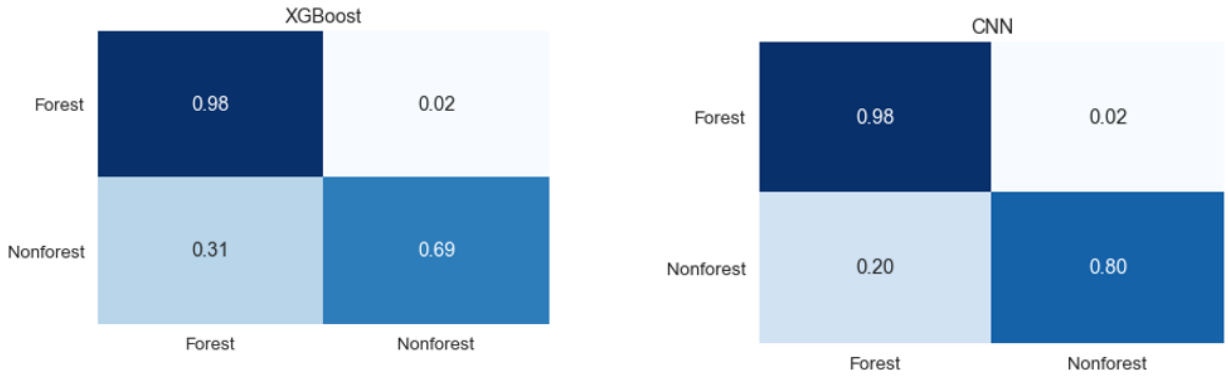

Fig. B1. Confusion matrix of forest and nonforest classification using XGBoost and CNN models. Rows indicate correct labels and columns indicate predicted labels.

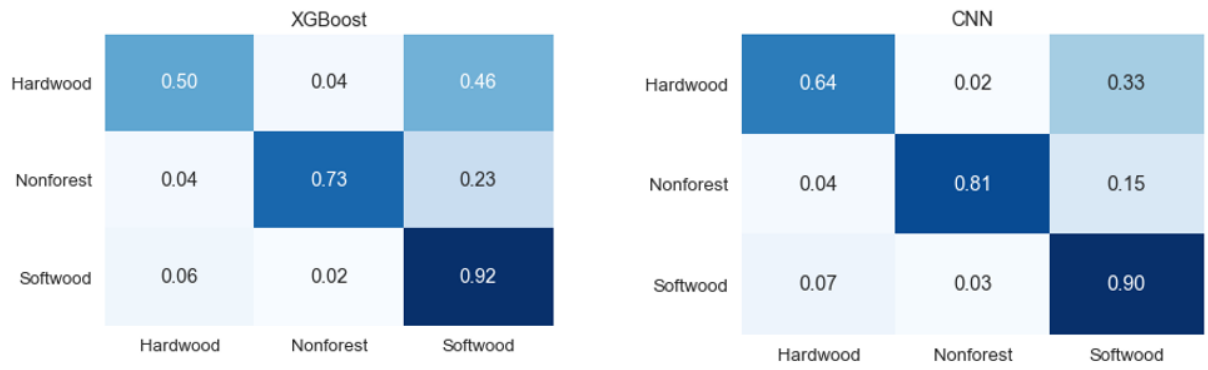

Fig. B2. Confusion matrix of hardwood, nonforest and softwood classification using XGBoost and CNN models. Rows indicate correct labels and columns indicate predicted labels.

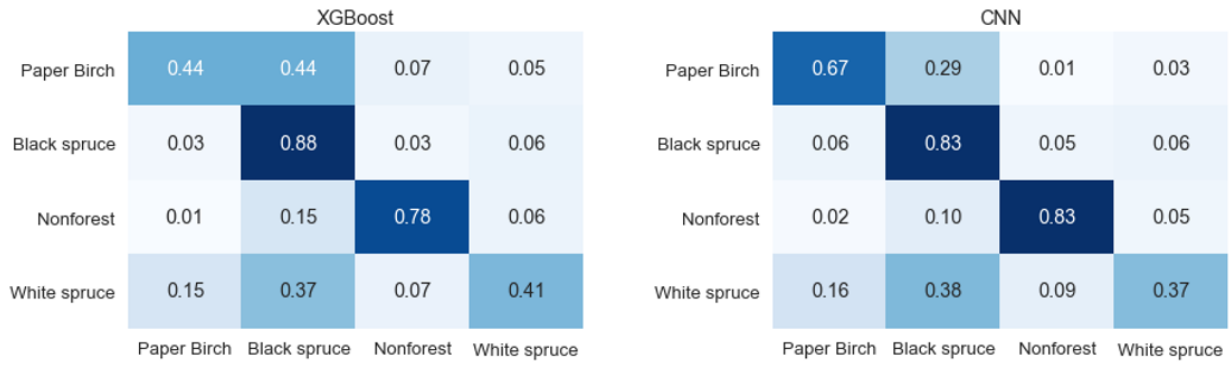

Fig. B3. Confusion matrix of paper birch, black spruce, nonforest and white spruce classification using XGBoost and CNN models. Rows indicate correct labels and columns indicate predicted labels.

3.8 REFERENCES

Akao, M., Aoki, H., & Kato, K. (1981). Mechanical properties of sintered hydroxyapatite for prosthetic applications. *Journal of Materials Science*, *16*(3), 809–812. https://doi.org/10.1007/BF02402799

Alonzo, M., Andersen, H.-E., Morton, D., & Cook, B. (2018). Quantifying Boreal Forest Structure and Composition Using UAV Structure from Motion. *Forests*, *9*(3), 119. https://doi.org/10.3390/f9030119

Andersen, H., Babcock, C., Pattison, R., Cook, B., Morton, D., & Finley, A. (2015). The 2014 tanana inventory pilot: A USFS-NASA partnership to leverage advanced remote sensing technologies for forest inventory. *In: Stanton, Sharon M.; Christensen, Glenn A., Comps. 2015. Pushing Boundaries: New Directions in Inventory Techniques and Applications: Forest Inventory and Analysis (FIA) Symposium 2015. 2015 December 8--10; Portland, Oregon. Gen. Tech. Rep. PNW-GTR-931*, *931*, 40–41.

Barber, V. A., Juday, G. P., & Finney, B. P. (2000). Reduced growth of Alaskan white spruce in the twentieth century from temperature-induced drought stress. *Nature*, *405*(6787), 668–673. https://doi.org/10.1038/35015049

Barnes, J. D., Balaguer, L., Manrique, E., Elvira, S., & Davison, A. W. (1992). A reappraisal of the use of DMSO for the extraction and determination of chlorophylls a and b in lichens

and higher plants. *Environmental and Experimental Botany*, *32*(2), 85–100. https://doi.org/10.1016/0098-8472(92)90034-Y

Bechtold, W. A., & Patterson, P. L. (2005). The enhanced forest inventory and analysis program—National sampling design and estimation procedures. *USDA Forest Service, Southern Reserach Station*, *80*.

Beck, P. S. A., Horning, N., Goetz, S. J., Loranty, M. M., & Tape, K. D. (2011). Shrub Cover on the North Slope of Alaska: A circa 2000 Baseline Map. *Arctic, Antarctic, and Alpine Research*, *43*(3), 355–363. https://doi.org/10.1657/1938-4246-43.3.355

Blackburn, G. A. (1998). Spectral indices for estimating photosynthetic pigment concentrations: A test using senescent tree leaves. *International Journal of Remote Sensing*, *19*(4), 657–675. https://doi.org/10.1080/014311698215919

Blackburn, G. A. (1999). Relationships between Spectral Reflectance and Pigment Concentrations in Stacks of Deciduous Broadleaves. *Remote Sensing of Environment*, *70*(2), 224–237. https://doi.org/10.1016/S0034-4257(99)00048-6

Broge, N. H., & Leblanc, E. (2001). Comparing prediction power and stability of broadband and hyperspectral vegetation indices for estimation of green leaf area index and canopy chlorophyll density. *Remote Sensing of Environment*, *76*(2), 156–172. https://doi.org/10.1016/S0034-4257(00)00197-8

Cahoon, S. M. P., & Baer, K. C. (2022). *Forest resources of the Tanana unit, Alaska: 2018* (PNW-GTR-1005; p. PNW-GTR-1005). U.S. Department of Agriculture, Forest Service, Pacific Northwest Research Station. https://doi.org/10.2737/PNW-GTR-1005

Calef, M. P., David McGuire, A., Epstein, H. E., Scott Rupp, T., & Shugart, H. H. (2005). Analysis of vegetation distribution in Interior Alaska and sensitivity to climate change using a logistic regression approach. *Journal of Biogeography*, *32*(5), 863–878. https://doi.org/10.1111/j.1365-2699.2004.01185.x

Carter, G. A. (1994). Ratios of leaf reflectances in narrow wavebands as indicators of plant stress. *International Journal of Remote Sensing*, *15*(3), 697–703. https://doi.org/10.1080/01431169408954109

Chapin, F. S., McGuire, A. D., Ruess, R. W., Hollingsworth, T. N., Mack, M. C., Johnstone, J. F., Kasischke, E. S., Euskirchen, E. S., Jones, J. B., Jorgenson, M. T., Kielland, K., Kofinas, G. P., Turetsky, M. R., Yarie, J., Lloyd, A. H., & Taylor, D. L. (2010). Resilience of

Alaska's boreal forest to climatic changeThis article is one of a selection of papers from The Dynamics of Change in Alaska's Boreal Forests: Resilience and Vulnerability in Response to Climate Warming. *Canadian Journal of Forest Research*, *40*(7), 1360–1370. https://doi.org/10.1139/X10-074

Chapin, F. S., Oswood, M. W., Van Cleve, K., Viereck, L. A., & Verbyla, D. L. (2006). *Alaska's Changing boreal forest*. Oxford University Press.

Chen, J. M. (1996). Evaluation of Vegetation Indices and a Modified Simple Ratio for Boreal Applications. *Canadian Journal of Remote Sensing*, *22*(3), 229–242. https://doi.org/10.1080/07038992.1996.10855178

Cook, B., Corp, L., Nelson, R., Middleton, E., Morton, D., McCorkel, J., Masek, J., Ranson, K., Ly, V., & Montesano, P. (2013). NASA Goddard's LiDAR, Hyperspectral and Thermal (G-LiHT) Airborne Imager. *Remote Sensing*, *5*(8), 4045–4066. https://doi.org/10.3390/rs5084045

Cook, B. D., Corp, L. A., Nelson, R. F., Middleton, E. M., Morton, D. C., Mccorkel, J. T., Masek, J. G., Ranson, K. J., Ly, V., & Montesano, P. M. (2013). NASA Goddard's LiDAR, Hyperspectral and Thermal (G-LiHT) Airborne Imager. *Remote Sensing*, *5*(8), 4045–4066. https://doi.org/10.3390/rs5084045

Dalponte, M., Ørka, H. O., Ene, L. T., Gobakken, T., & Næsset, E. (2014). Tree crown delineation and tree species classification in boreal forests using hyperspectral and ALS data. *Remote Sensing of Environment*, *140*, 306–317. https://doi.org/10.1016/J.RSE.2013.09.006

Dash, J., & Curran, P. J. (2007). Evaluation of the MERIS terrestrial chlorophyll index (MTCI). *Advances in Space Research*, *39*(1), 100–104. https://doi.org/10.1016/j.asr.2006.02.034

Datt, B. (1998). Remote Sensing of Chlorophyll a, Chlorophyll b, Chlorophyll a+b, and Total Carotenoid Content in Eucalyptus Leaves. *Remote Sensing of Environment*, *66*(2), 111–121. https://doi.org/10.1016/S0034-4257(98)00046-7

Datt, B. (1999). Visible/near infrared reflectance and chlorophyll content in Eucalyptus leaves. *International Journal of Remote Sensing*, *20*(14), 2741–2759. https://doi.org/10.1080/014311699211778

Douglas, T. A., Jones, M. C., Hiemstra, C. A., & Arnold, J. R. (2014). Sources and sinks of carbon in boreal ecosystems of interior Alaska: A review. *Elementa: Science of the Anthropocene*, *2*, 000032. https://doi.org/10.12952/journal.elementa.000032

Douglas, T. A., Jones, M. C., Hiemstra, C. A., Arnold, J. R., & Blum, J. D. (2014). Sources and sinks of carbon in boreal ecosystems of interior Alaska: A review. *Elementa: Science of the Anthropocene*, *2*, 1–39. https://doi.org/10.12952/journal.elementa.000032

Elvidge, C. D., & Chen, Z. (1995). Comparison of broad-band and narrow-band red and near-infrared vegetation indices. *Remote Sensing of Environment*, *54*(1), 38–48. https://doi.org/10.1016/0034-4257(95)00132-K

Euskirchen, E. S., McGuire, A. D., Chapin, F. S., & Rupp, T. S. (2010). The changing effects of Alaska's boreal forests on the climate systemThis article is one of a selection of papers from The Dynamics of Change in Alaska's Boreal Forests: Resilience and Vulnerability in Response to Climate Warming. *Canadian Journal of Forest Research*, *40*(7), 1336–1346. https://doi.org/10.1139/X09-209

Evans, E., & Murphy, M. (2021). *"spatialEco." R package version 1.3-6* [Computer software]. https://github.com/jeffreyevans/spatialEco

Filella, I., & Penuelas, J. (1994). The red edge position and shape as indicators of plant chlorophyll content, biomass and hydric status. *International Journal of Remote Sensing*, *15*(7), 1459–1470. https://doi.org/10.1080/01431169408954177

Fricker, G. A., Ventura, J. D., Wolf, J. A., North, M. P., Davis, F. W., & Franklin, J. (2019). A Convolutional Neural Network Classifier Identifies Tree Species in Mixed-Conifer Forest from Hyperspectral Imagery. *Remote Sensing*, *11*(19), 2326. https://doi.org/10.3390/rs11192326

Gallant, A. L. (1995). *Ecoregions of Alaska*. US Government Printing Office.

Gamon, J. A., Serrano, L., & Surfus, J. S. (1997). The photochemical reflectance index: An optical indicator of photosynthetic radiation use efficiency across species, functional types, and nutrient levels. *Oecologia*, *112*(4), 492–501. https://doi.org/10.1007/s004420050337

Gamon, J. A., & Surfus, J. S. (1999). Assessing leaf pigment content and activity with a reflectometer. *New Phytologist*, *143*(1), 105–117. https://doi.org/10.1046/j.1469-8137.1999.00424.x

Gitelson, A. A., Kaufman, Y. J., & Merzlyak, M. N. (1996). Use of a green channel in remote sensing of global vegetation from EOS-MODIS. *Remote Sensing of Environment*, *58*(3), 289–298. https://doi.org/10.1016/S0034-4257(96)00072-7

Gitelson, A. A., Merzlyak, M. N., & Chivkunova, O. B. (2007). Optical Properties and Nondestructive Estimation of Anthocyanin Content in Plant Leaves¶. *Photochemistry and Photobiology*, *74*(1), 38–45. https://doi.org/10.1562/0031-8655(2001)0740038OPANEO2.0.CO2

Gitelson, A. A., Merzlyak, M. N., & Lichtenthaler, H. K. (1996). Detection of Red Edge Position and Chlorophyll Content by Reflectance Measurements Near 700 nm. *Journal of Plant Physiology*, *148*(3–4), 501–508. https://doi.org/10.1016/S0176-1617(96)80285-9

Gitelson, A., & Merzlyak, M. N. (1994a). Quantitative estimation of chlorophyll-a using reflectance spectra: Experiments with autumn chestnut and maple leaves. *Journal of Photochemistry and Photobiology B: Biology*, *22*(3), 247–252. https://doi.org/10.1016/1011-1344(93)06963-4

Gitelson, A., & Merzlyak, M. N. (1994b). Spectral Reflectance Changes Associated with Autumn Senescence of Aesculus hippocastanum L. and Acer platanoides L. Leaves. Spectral Features and Relation to Chlorophyll Estimation. *Journal of Plant Physiology*, *143*(3), 286–292. https://doi.org/10.1016/S0176-1617(11)81633-0

Gould, K. S. (2004). Nature's Swiss Army Knife: The Diverse Protective Roles of Anthocyanins in Leaves. *Journal of Biomedicine and Biotechnology*, *2004*(5), 314–320. https://doi.org/10.1155/S1110724304406147

Haboudane, D. (2004). Hyperspectral vegetation indices and novel algorithms for predicting green LAI of crop canopies: Modeling and validation in the context of precision agriculture. *Remote Sensing of Environment*, *90*(3), 337–352. https://doi.org/10.1016/j.rse.2003.12.013

Hinzman, L. D., Viereck, L. A., Adams, P. C., Romanovsky, V. E., & Yoshikawa, K. (2006). Climate and permafrost dynamics of the Alaskan boreal forest. In *Alaska's changing boreal forest* (pp. 39–61).

Johnstone, J. F., Celis, G., Chapin, F. S., Hollingsworth, T. N., Jean, M., & Mack, M. C. (2020). Factors shaping alternate successional trajectories in burned black spruce forests of Alaska. *Ecosphere*, *11*(5), e03129. https://doi.org/10.1002/ecs2.3129

Johnstone, J. F., Hollingsworth, T. N., Chapin, F. S., & Mack, M. C. (2010). Changes in fire regime break the legacy lock on successional trajectories in Alaskan boreal forest. *Global Change Biology*, *16*(4), 1281–1295. https://doi.org/10.1111/j.1365-2486.2009.02051.x

Jorgenson, M., Racine, C. H., Walters, J. C., & Osterkamp, T. E. (2001). Permafrost degradation and ecological changes associated with a warming climate in central Alaska. *Climate Change*, *48*(4), 551–579.

Kasischke, E. S., Verbyla, D. L., Rupp, T. S., McGuire, A. D., Murphy, K. A., Jandt, R., Barnes, J. L., Hoy, E. E., Duffy, P. A., Calef, M., & Turetsky, M. R. (2010). Alaska's changing fire regime — implications for the vulnerability of its boreal forestsThis article is one of a selection of papers from The Dynamics of Change in Alaska's Boreal Forests: Resilience and Vulnerability in Response to Climate Warming. *Canadian Journal of Forest Research*, *40*(7), 1313–1324. https://doi.org/10.1139/X10-098

Lundberg, S. M., Erion, G. G., & Lee, S.-I. (2018). *Consistent Individualized Feature Attribution for Tree Ensembles*. https://doi.org/10.48550/ARXIV.1802.03888

Maccioni, A., Agati, G., & Mazzinghi, P. (2001). New vegetation indices for remote measurement of chlorophylls based on leaf directional reflectance spectra. *Journal of Photochemistry and Photobiology B: Biology*, *61*(1–2), 52–61. https://doi.org/10.1016/S1011-1344(01)00145-2

Marcel, S., & Rodriguez, Y. (2010). Torchvision the machine-vision package of torch. *Proceedings of the 18th ACM International Conference on Multimedia*, 1485–1488. https://doi.org/10.1145/1873951.1874254

Marconi, S., Weinstein, B. G., Zou, S., Bohlman, S. A., Zare, A., Singh, A., Stewart, D., Harmon, I., Steinkraus, A., & White, E. P. (2022). Continental-scale hyperspectral tree species classification in the United States National Ecological Observatory Network. *Remote Sensing of Environment*, *282*, 113264. https://doi.org/10.1016/j.rse.2022.113264

Mayer, M., & Stando, A. (2024). *shapvis: SHAP Visualizations* [Computer software]. https://cran.r-project.org/web/packages/shapviz/index.html

Mäyrä, J., Keski-Saari, S., Kivinen, S., Tanhuanpää, T., Hurskainen, P., Kullberg, P., Poikolainen, L., Viinikka, A., Tuominen, S., Kumpula, T., & Vihervaara, P. (2021). Tree species classification from airborne hyperspectral and LiDAR data using 3D convolutional neural

networks. *Remote Sensing of Environment*, *256*, 112322. https://doi.org/10.1016/j.rse.2021.112322

Mcguire, A. D., & Chapin III, F. S. (2006). Climate feedbacks in the Alaskan boreal forest. In *Alaska's changing boreal forest* (pp. 309–322). Oxford University Press.

Merzlyak, M. N., Gitelson, A. A., Chivkunova, O. B., & Rakitin, V. Yu. (1999). Non-destructive optical detection of pigment changes during leaf senescence and fruit ripening. *Physiologia Plantarum*, *106*(1), 135–141. https://doi.org/10.1034/j.1399-3054.1999.106119.x

Ohse, B., Huettmann, F., Ickert-Bond, S. M., & Juday, G. P. (2009). Modeling the distribution of white spruce (Picea glauca) for Alaska with high accuracy: An open access role-model for predicting tree species in last remaining wilderness areas. *Polar Biology*, *32*(12), 1717–1729. https://doi.org/10.1007/s00300-009-0671-9

Paszke, A., Gross, S., Massa, F., Lerer, A., Bradbury, J., Chanan, G., Killeen, T., Lin, Z., Gimelshein, N., Antiga, L., Desmaison, A., Köpf, A., Yang, E., DeVito, Z., Raison, M., Tejani, A., Chilamkurthy, S., Steiner, B., Fang, L., … Chintala, S. (2019). PyTorch: An Imperative Style, High-Performance Deep Learning Library. *arXiv:1912.01703 [Cs, Stat]*. http://arxiv.org/abs/1912.01703

Pedregosa, F., Varoquaux, G., Gramfort, A., Michel, V., Thirion, B., Grisel, O., Blondel, M., Prettenhofer, P., Weiss, R., Dubourg, V., Vanderplas, J., Passos, A., Cournapeau, D., Brucher, M., Perrot, M., & Duchesnay, E. (2011). *Scikit-learn: Machine Learning in Python*. *12*, 2825–2830.

Peñuelas, J., Frederic, B., & Fiella, I. (1995). Semi-empirical indices to assess carotenoids/chlorophyll a ratio from leaf spectral reflectance. *Photosynthetica*, *31*(2), 221–230.

Peñuelas, J., Gamon, J. A., Fredeen, A. L., Merino, J., & Field, C. B. (1994). Reflectance indices associated with physiological changes in nitrogen- and water-limited sunflower leaves. *Remote Sensing of Environment*, *48*(2), 135–146. https://doi.org/10.1016/0034-4257(94)90136-8

Peñuelas, J., Gamon, J. A., Griffin, K. L., & Field, C. B. (1993). Assessing community type, plant biomass, pigment composition, and photosynthetic efficiency of aquatic vegetation

from spectral reflectance. *Remote Sensing of Environment*, *46*(2), 110–118. https://doi.org/10.1016/0034-4257(93)90088-F

Rondeaux, G., Steven, M., & Baret, F. (1996). Optimization of soil-adjusted vegetation indices. *Remote Sensing of Environment*, *55*(2), 95–107. https://doi.org/10.1016/0034-4257(95)00186-7

Roujean, J.-L., & Breon, F.-M. (1995). Estimating PAR absorbed by vegetation from bidirectional reflectance measurements. *Remote Sensing of Environment*, *51*(3), 375–384. https://doi.org/10.1016/0034-4257(94)00114-3

Rouse, J. W., Haas, H. R., Deering, D. W., Schell, J. A., & Harlan, J. C. (1974). Monitoring the vernal advancement and retrogradation (green wave effect) of natural vegetation. *No. E75-10354.*

Royle, D. D., & Lathrop, R. G. (2002). Discriminating Tsuga canadensis hemlock forest defoliation using remotely sensed change detection. *Journal of Nematology*, *34*(3), 213.

Ruefenacht, B., Finco, M. V., Nelson, M. D., Czaplewski, R., Helmer, E. H., Blackard, J. A., Holden, G. R., Lister, A. J., Salajanu, D., Weyermann, D., & Winterberger, K. (2008). Conterminous U.S. and Alaska Forest Type Mapping Using Forest Inventory and Analysis Data. *Photogrammetric Engineering & Remote Sensing*, *74*(11), 1379–1388. https://doi.org/10.14358/PERS.74.11.1379

Schiefer, F., Kattenborn, T., Frick, A., Frey, J., Schall, P., Koch, B., & Schmidtlein, S. (2020). Mapping forest tree species in high resolution UAV-based RGB-imagery by means of convolutional neural networks. *ISPRS Journal of Photogrammetry and Remote Sensing*, *170*, 205–215. https://doi.org/10.1016/j.isprsjprs.2020.10.015

Shoot, C., Andersen, H.-E., Moskal, L. M., Babcock, C., Cook, B. D., & Morton, D. C. (2021). Classifying Forest Type in the National Forest Inventory Context with Airborne Hyperspectral and Lidar Data. *Remote Sensing*, *13*(10), 1863. https://doi.org/10.3390/rs13101863

Shoot, C., Andersen, H.-E., Moskal, M., Babcock, C., & Cook, B. (2021). Classifying Forest Type in the National Forest Inventory Context with Airborne Hyperspectral and Lidar Data. *Remote Sensing*.

Shulski, M., & Wendler, G. (2007). *The climate of Alaska*. University of Alaska Press.

Sims, D. A., & Gamon, J. A. (2002). Relationships between leaf pigment content and spectral reflectance across a wide range of species, leaf structures and developmental stages. *Remote Sensing of Environment*, *81*(2–3), 337–354. https://doi.org/10.1016/S0034-4257(02)00010-X

Smith, R., Adams, J., Stephens, D., & Hick, P. (1995). Forecasting wheat yield in a Mediterranean-type environment from the NOAA satellite. *Australian Journal of Agricultural Research*, *46*(1), 113. https://doi.org/10.1071/AR9950113

Triviño, M., Juutinen, A., Mazziotta, A., Miettinen, K., Podkopaev, D., Reunanen, P., & Mönkkönen, M. (2015). Managing a boreal forest landscape for providing timber, storing and sequestering carbon. *Ecosystem Services*, *14*, 179–189. https://doi.org/10.1016/j.ecoser.2015.02.003

Tucker, C. J. (1979). Red and photographic infrared linear combinations for monitoring vegetation. *Remote Sensing of Environment*, *8*(2), 127–150. https://doi.org/10.1016/0034-4257(79)90013-0

USDA. (2018). Field Instructions for the Annual Inventory of Alaska 2018 Supplement for Interior Alaska. *Department of Agriculture, Forest Service, Pacific Northwest Reserach Station: Portland, OR, USA*.

Vogelmann, J. E., Rock, B. N., & Moss, D. M. (1993). Red edge spectral measurements from sugar maple leaves. *International Journal of Remote Sensing*, *14*(8), 1563–1575. https://doi.org/10.1080/01431169308953986

Walker, X. J., Okano, K., Berner, L. T., Massey, R., Goetz, S. J., Johnstone, J. F., & Mack, M. C. (2023). Shifts in Ecological Legacies Support Hysteresis of Stand Type Conversions in Boreal Forests. *Ecosystems*, *26*(8), 1796–1805. https://doi.org/10.1007/s10021-023-00866-w

Zarco-Tejada, P. J., Miller, J. R., Mohammed, G. H., Noland, T. L., & Sampson, P. H. (2002). Vegetation Stress Detection through Chlorophyll *a* + *b* Estimation and Fluorescence Effects on Hyperspectral Imagery. *Journal of Environmental Quality*, *31*(5), 1433–1441. https://doi.org/10.2134/jeq2002.1433

Chapter 4. DEVELOPING A NEW MORTALITY METRIC TO ASSESS THE IMPACTS OF COMPOUND DISTURBANCES: INSIGHTS FROM THE 2020 CREEK FIRE, CALIFORNAI

4.1 ABSTRACT

Tree mortality due to drought, wildfires, and the interplay between drought and fire is increasing in frequency and extent. For example, the 2020 Creek Fire burned 153,738 ha of woodlands and the fire excluded forests. Pre-fire, the region was exposed to its prolonged warm drought-induced massive tree mortality event. A collection of high-resolution (<1m) remote sensing data was acquired pre- and post-fire (Creek Fire), which provides a novel opportunity to examine multi-temporal individual overstory tree mortality related to drought followed by fire. We present our methods for applying a multi-class classification framework to discriminate drought and fire related mortality of individual overstory trees using lidar, high-resolution imagery and deep learning. We derived mortality metrics using the individual overstory tree mortality maps to help address key ecological questions such as variations and patterns of pre- and post-fire mortality and produce management products. Specifically, we developed a new neighborhood canopy mortality metric to help managers identify the areas with regeneration failure due to compound disturbances. Further we compared the neighborhood canopy mortality with satellite derived relativized burn ratio (RBR) in representing areas with high preexisting mortality due to compound disturbances. To achieve this objective, we selected three different study sites within the Creek Fire region that cover over 1 million lidar derived trees. The overall accuracy of the model was 84% for detecting drought-induced tree mortality (pre-fire) and 87% for detecting fire-induced tree mortality (post-fire). Post-fire we found that there was a substantial increase (over 35%) in dead trees and a substantial decrease in live trees (over 25%). We found model

performance decreased in areas that had different vegetation types than training area. Further, the neighborhood canopy mortality, a new metric better captures the tree mortality post-fire in areas with or without preexisting tree mortality than RBR. A high-resolution neighborhood canopy mortality map can be used to estimate pre-fire mortality and post-fire survival trees that can potentially serve as seed source. The mortality map can be used by researchers and managers to understand mortality distribution and how fire impacted the forest ecosystem.

4.2 INTRODUCTION

Tree mortality events are growing in extent, severity, and frequency in association with multiple stressors and events, such as climate change, fire exclusion, drought, and wildfires (Hartmann et al., 2022; Stephens et al., 2018; Young et al., 2017). Unfortunately, the occurrence of these stressors and events are also increasing in frequency, resulting in coupled and compound disturbances (Paine et al., 1998), which can push temperate forests and woodlands beyond the thresholds of sustainability (Millar & Stephenson, 2015). For example, a century of fire exclusion in forests of the southern Sierra Nevada, California, resulted in structural changes that include increasing canopy bulk density and ladder fuel development (Collins et al., 2017; Stephens et al., 2018). This region has also suffered from prolonged drought (2012-2016) and multiple fires during and following drought events, causing extensive tree mortality. The resulting tree die-off events due to such compound disturbances have a deleterious impact on forest structure, ecological services, and forest recovery with potential type conversion (Allen et al., 2010; Stephens et al., 2018, 2022; Coop et al., 2020).

Fire effects can be exacerbated by these pre-fire large-scale tree mortality patterns across the landscape (Stephens et al., 2022). For example, in the southern Sierra Nevada, widespread drought-induced (2012- 20216) tree mortality had created extraordinary levels of surface and

ladder fuels (Stephens et al., 2018). The 2020 Creek Fire is the region exemplifies the consequences of this fuel buildup, burning approximately 154,000 hectares through the footprint of Aspen (2013) and French (2014) fire and ranking as one of the largest fire in history of California (Cova et al., 2023). This fire generated one of the tallest pyrocumulonimbus clouds ever observed in North America (Lee et al., 2023) and caused extensive damage to vegetation, with high levels of burn severity reported (Stephens et al., 2022).

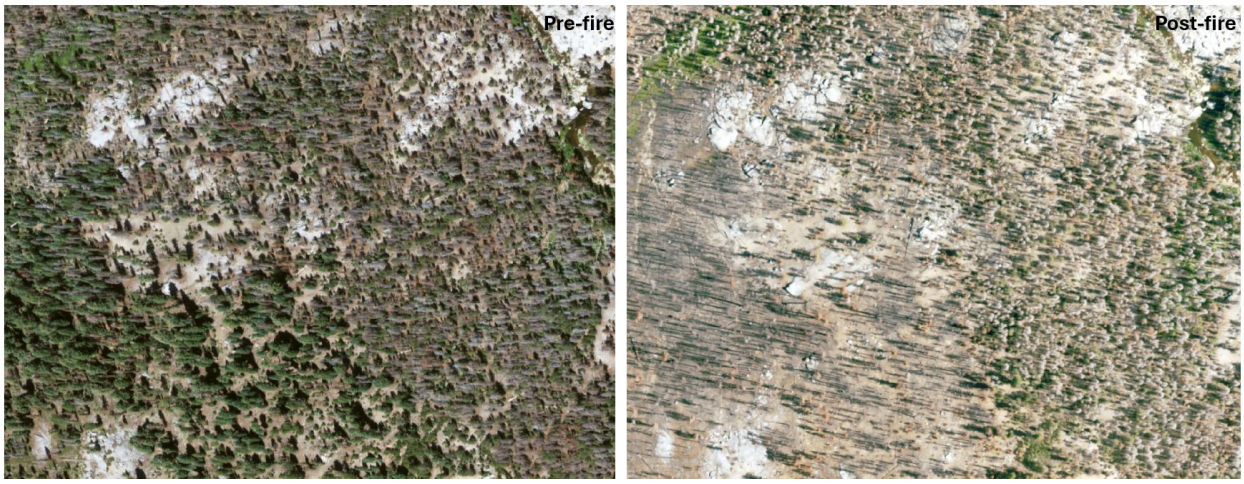

Figure 4.1: The pre-fire drought induced tree mortality and post-fire forest condition.

Remote sensing has been providing tools and measures to enhance our ability to track global forest changes due to disturbances (Figure 4.1). One such metric is satellite driven burn severity metric for guiding managers to identify where the largest amount of canopy loss and mortality has occurred (Miller & Thode, 2007). Historically, these indices were a provided managers with an adequate estimates of post-fire mortality because overwhelmingly the pre-fire tree mortality was low and most of the trees were alive (Miller & Thode, 2007). However, in the 21st century there are more frequent occurrences of fires in post drought-induced tree mortality events and prior fires. In the current global warming scenarios with compound disturbances, it is uncertain how well satellite driven burn severity performs to inform managers regarding fire impact and canopy loss.

Since the onset of the large-scale tree mortality events in the Sierra Nevada, the importance of mapping tree mortality has increased and there has been multiple efforts to map mortality at scale of individual tree (<1 m) (Cheng et al., 2024; Hemming-Schroeder et al., 2023; Khatri-Chhetri et al., 2024; Stovall et al., 2019) and at crown-scale (3 m) (Dixon et al., 2023). Using these methods, we can estimate overstory tree mortality patterns across large areas both pre- and post-fire. These methods have the potential for repeat measures of individual tree mortality through time.

The pre- and post- fire mortality information can be used to answer key ecological questions and produce management relevant products. For that we need to develop methods to derive mortality metrics and quantify their effectiveness. However, there are not enough studies that have focused on investigating how extensive individual overstory tree mortality maps can be used to derive useful metrics to address above questions. Therefore, in this study, we derived robust mortality metrics from overstory tree mortality maps that measure local and broader variation in the pattern of tree mortality and its variation. The mortality metrics can be derived for both pre- and post-fire forest conditions. The use case of both pre- and post-fire mortality metrics derived from this study is provided in the following paragraphs.

The pre-fire mortality metrics developed in this study enhance the investigation of drivers of burn severity and relationship between pre-fire mortality and burn severity and post-fire mortality. Even though many climatic factors and treatment effects have been studied for predicting fire severity (Holden et al., 2018; Littell et al., 2009; Parks & Abatzoglou, 2020), the influence of pre-fire tree mortality in relation to fire severity and post-fire tree mortality had remain limited particularly in xeric forest type (Stephens et al., 2018). Incorporating the pre-fire

mortality metric will provide a valuable addition to the future research of fire behaviour and drivers of mortality and burn severity.

Similarly, post-fire tree mortality metrics developed in this study can be used to understand the long-term impact of fire. For example, it can help identify locations where regeneration failure may be of concern due to compound disturbances, which thereby influences post-fire forest recovery over time (Hu et al., 2019). Post-fire mortality mapping can be a crucial tool for managers to predict fire effects through time, estimate delayed mortality, and develop management strategies (Furniss et al., 2019). Further, post-fire mortality metric can be utilized to identify the location of varying density of live trees that could potentially serve as seed sources.

Following the widespread tree mortality events in the Sierra Nevada, there has been a rapid increase in the availability of multi-temporal, open-source high-resolution aerial imagery and lidar data products across California and the United States. For instance, the Geological Survey's 3D Elevation Program (Arundel et al., 2018) has significantly expanded its collection of high-resolution airborne lidar data throughout the country. Similarly, the National Agricultural Imagery Program (NAIP) regularly collects 60 cm, high-resolution 4-band orthoimagery in each state biennially (USDA, 2023). These data provide an important opportunity to study tree mortality due to drought and fire over time.

Furthermore, the availability of immediate pre-fire lidar and pre- and post-fire high-resolution imagery from the 2020 Creek Fire provides an unmatched opportunity to examine tree mortality following drought and fire events. We were fortunate to have 2020 lidar data collected just a month before the fire. We used the NAIP 60 cm imagery along with 2020 lidar data to track the fate of over 1 M individual overstory trees before and after fire. Since the Creek Fire resulted from compound disturbances rather than burning in isolation, our goal is to derive a

mortality metric from overstory tree mortality that aids in addressing key ecological question and produce management relevant products.

The primary goal of this study is to investigate and establish methods to analyze the pattern of pre- and post-fire overstory tree mortality on different dominant forest types in one of the largest fires in Sierra Nevada. Further develop mortality metrics that can be useful for managers to identify impact of compound disturbances. In addition, we compared the developed mortality metric with a traditional satellite driven burn severity index.

To achieve these objectives, we selected three different study sites in the fire footprint of the 2020 Creek Fire with different dominant vegetation covers and applied Convolutional Neural Network (CNN) model (Khatri-Chhetri et al., 2024), to examine whether this method perform equally well across vegetation types. We assessed and reported the results independently for each study site. The information derived from both pre- and post-fire tree mortality maps can support research to examine compound disturbance events such as those that impacted the Creek Fire region (San Joaquin Watershed). The main objectives are as follows:

1. How well does the convolutional neural network (CNN) model perform in different vegetation types such as mixed conifer and Oak woodlands?
2. How can large-scale individual tree mortality be used to derive mortality metrics to investigate the impact of compound disturbances?
    a. Identify the pre- and post-fire patterns and variation in mortality.
    b. Identify locations post-fire that are at risk of regeneration because of distance from potential seed source.

3. How well do these high-resolution mortality maps correspond to traditional satellite burn severity maps?

4.3 MATERIALS

4.3.1 Study area

Our study area in the southern Sierra Nevada, California (Figure 4.2) has experienced compound disturbance: fire exclusion, a drought-induced tree mortality event, followed by a mass fire. More than 100 million trees were estimated to be dead due to drought in region (Byer & Jin, 2017) before 2020 Creek Fire. The Creek fire started on 4 September 2020 and was driven by up-canyon diurnal winds along with the availability of dried and dead trees due to the drought event (Lee et al., 2023). It burned 36% of the upper San Joaquin watershed destroying 853 and damaging 64 human structures (Lee et al., 2023). It also destroyed critical habitat, and snowpack storage (Lee et al., 2023). A total of around 154,000 hectares of land burned; and this fire was recorded as one of the largest fires of this decade in California (Cova et al., 2023).

The Creek Fire burned across a diversity of vegetation types including mixed conifer forests composed of ponderosa pine (*Pinus ponderosa*), sugar pine (*Pinus lambertiana*), white fir (*Abies concolor*), incense-cedar (*Calocedrus decurrens*), and California black oak (*Quercus kelloggii*), oak woodlands, montane hardwood, mixed chaparral (Stephens et al., 2022).

We selected three sites each ~1500 hectares with different vegetation cover that predominately represented low, moderate and high resultant vegetation burn severity by the RBR index (Parks et al., 2014) in areas with both pre- and post-fire NAIP imagery and lidar data. One of the study sites falls within the footprint of the 2013 Aspen fire (Figure 4.2). Study site 1 was dominated by oak woodlands, montane hardwood, mixed chaparral, and ponderosa pine (*P. ponderosa*). Study

sites 2 was mostly dominated with Sierran mixed conifer. And study site 3 was dominated by Sierran mixed conifer, red fir, and subalpine conifer forests red fir (*A. magnifica*), Sierran lodgepole pine (*P. contorta var. murrayana*) and white fir (*A. concolor*). Approximately 460K, 260K and 300K TAOs occupied study site 1, 2, and 3 respectively. In total, more than 1 million tree segments were derived from 2020 lidar that were used for the analysis.

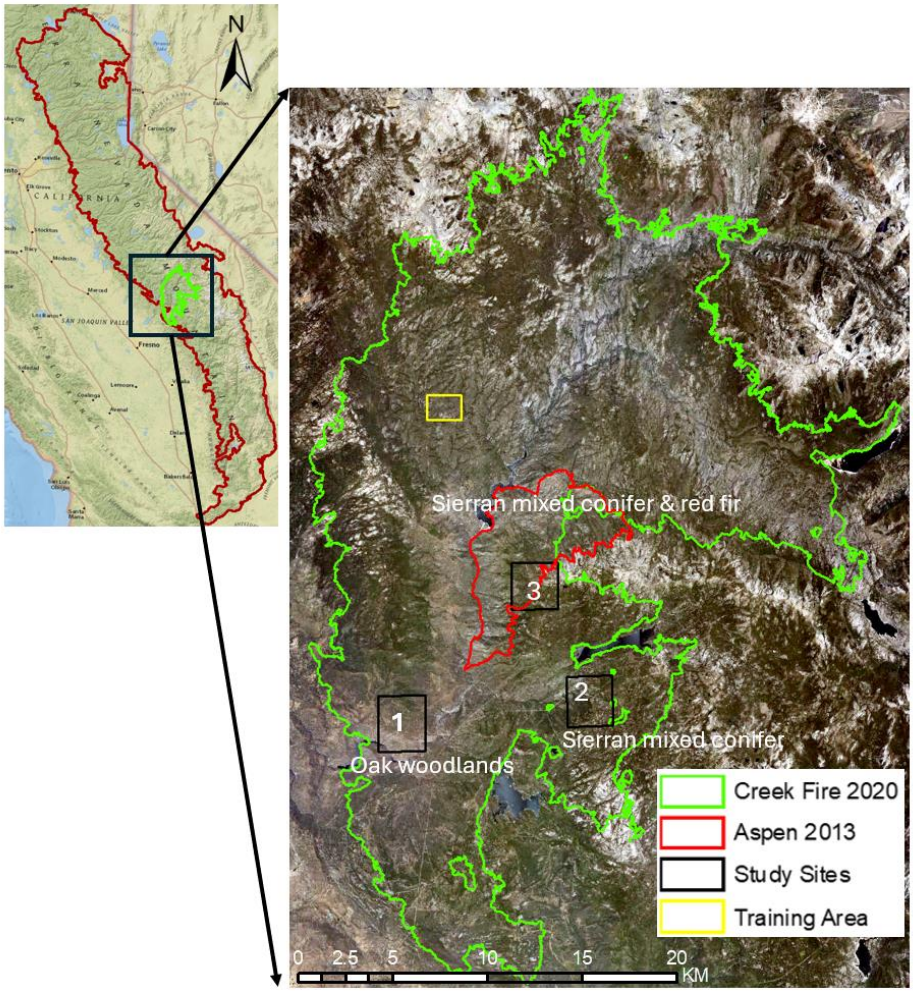

Figure 4.2: The Creek Fire boundary in green and the three study sites in black, Aspen 2013 fire in red and training area in yellow.

4.3.2 Airborne lidar, ortho-imagery and satellite data

Multi-temporal, high spatial remote sensing aerial imaging data along with high pulse density airborne lidar data were available for the study area. We used high fidelity aerial lidar data

collected during June 2020. We used high spatial resolution (60 cm) four-band (RGBNIR) imagery. In addition, we used Sentinel-II 10 m resolution RGBNIR data. Detailed information of data used for analysis is provided on Table 4.1.

Table 4.1: Data source, spectral and spatial resolution, and year of data used for the research.

Data Type	Imagery Year	Spectral Resolution (Bands)	Spatial Resolution (m)/ pulse density
Lidar (SSARR)	2020	NIR	≥8
NAIP RGBNIR	2020 & 2020	Blue, Green, Red, and NIR	60 cm
Sentinel-II (RBR)	2020 & 2021	Blue, Green, Red, and NIR	10 m

4.3.2.1 Airborne lidar data

The lidar data collected by USGS 3DEP program captured pre-fire forest conditions for more than half of the area within the Creek Fire perimeter (Figure 4.2). The lidar data is ≥ 8 pulses per square meter with over 50% flight line overlap.

4.3.2.2 National Agriculture Imagery Program (NAIP)

The NAIP program is administered by the USDA Farm Service Agency and collects biennial imagery during the leaf on phenology during the agricultural growing season. The NAIP imagery consists of four bands, including Blue (420–492 nm), Green (533–587 nm), Red (604–664 nm), and Near-Infrared (683–920 nm) (USDA, 2021) that were acquired 4877 m above ground using a Leica ADS 100 airborne digital sensor (Bhatt & Maclean, 2023). Across California including the study area, the data were collected in 2020 and 2022 at 0.6 m resolution during summer (June to August).

4.3.3 Relativized Burn Ratio (RBR)

The relativized burn ratio is used to quantify burn severity (Parks et al., 2014). The relativized burn ratio was derived using Sentinel-II data from the years 2020 (pre-fire) and 2021 (post-fire) at 10 m resolution. The relativized burn ratio was calculated using the following formula following Parks et al., (2014) method.

$$RBR = \frac{dNBR}{(NBR_{prefire} + 1.001)}$$

$$NBR = \frac{(NIR - SWIR)}{(NIR + SWIR)}$$

$$dNBR = \left(\left(NBR_{prefire} - NBR_{postfire}\right) * 1000\right) - dNBR_{offset}$$

Where, RBR = relativized burned ratio; dNBR = difference Normalized Burn Ratio; NBR= normalized burn ration, NIR = near infrared band, SWIR = shortwave infrared bands.

4.4 METHODS

To achieve our objectives, we divided tasks into four sections, i) lidar data were processed to produce the overstory tree segments, ii) a tree mortality map was generated using the CNN model and benchmark dataset developed by Khatri-Chhetri et al., (2024) for 2020 (pre fire) and 2022 (post fire), iii) a relative and neighborhood canopy mortality metrics was computed, and iv) patch analysis was conducted to assess how mortality metrics corresponds to traditional satellite driven burn severity index (RBR).

4.4.1 Lidar derived tree segments

We used the USDA Forest Service's FUSION software (McGaughey, 2018) to process the lidar and produce the tree segments. FUSION has a TreeSeg tool that implements the watershed

segmentation algorithm to generate tree segments. The watershed segmentation algorithm is well established and its accuracy has been well characterized for Sierra Nevada forests (Jeronimo et al., 2018; Van Wagtendonk, 2023). The tree segment polygon derived from the lidar data captures height above 2m and canopy area (Jeronimo et al., 2018). We refer to these tree segments as tree approximate objects (TAOs) because they can either represent one canopy dominant tree or an overstory tree with a number of unidentified subordinate trees. Throughout, we refer to tree segments as tree approximate objects (TAOs).

4.4.2 Generating training point and tree mortality

We used the convolutional neural network model and benchmark dataset developed in chapter 2 of this dissertation (Khatri-Chhetri et al., 2024). We retrained the model and assessed the model's performance using the test data specific to the 2020 Creek Fire. For training the model we combined benchmark dataset produced in chapter 2 with new training data specific to the Creek Fire produced for this study.

For creating training samples in the 2020 Creek Fire region, we randomly selected a training area separate from three of our study sites (Figure 4.2) based on forest type that included low, moderate, and high RBR-derived burn severity class to create labels. In addition, we also randomly selected the TAOs within the training area. The training area was predominantly covered with mixed conifer forest that is similar to forest type of two of our study sites. The training site had very little oak woodland vegetation type. Further, our CNN model (Khatri-Chhetri et al., 2024) was trained specifically for identifying drought-induced tree mortality in the mixed conifer forest. Therefore, the study site covered with Oak woodland was added as an exploration of the model performance in different vegetation cover in the same region.

We created labeled datasets for both pre- and post-fire forest condition as one of the following classes: live, dead, mixed (partially dead) and other (boulders, shadow, and non-tree object). We labeled 1,198 TAOs pre-fire and 4,142 TAOs for post-fire mortality status (Table 4.2). We increased the number of labeled TAO for post-fire to increase the representation of the tree mortality class due to fire because the benchmark data primarily included tree mortality due to drought.

We created a robust train-test split of 80-20, where 20% of the data was used to test the performance of the model. The 80% of the train set (Table 4.2) was merged with the 15K mortality benchmark dataset (Khatri-Chhetri et al., 2024) (Figure 4.3). The benchmark dataset is labeled based on mixed-conifer forest in Sierra Nevada that is located southeast of the Creek Fire. The merged dataset was used to train the convolutional neural network model (Khatri-Chhetri et al., 2024). Our model training and output workflow is displayed in figure 4.3.

We used overall accuracy, precision (user's accuracy), recall (producer's accuracy), and F1 score to evaluate the performance of the model. We also used macro averages of precision, recall, and F1 score which take the average across classes for multi-class classification for determining the best data modality and model (Mäyrä et al., 2021).

In addition to the test set, we wanted to assess predictive capabilities of the model for each study site, for that we randomly selected 200 TAOs on each study site. We manually created labels for these TAOs then calculated the overall accuracy of the predicted labels. Further, to estimate the accuracy of model in mixed chaparral pre-fire we randomly sampled 100 additional points below 4m height.

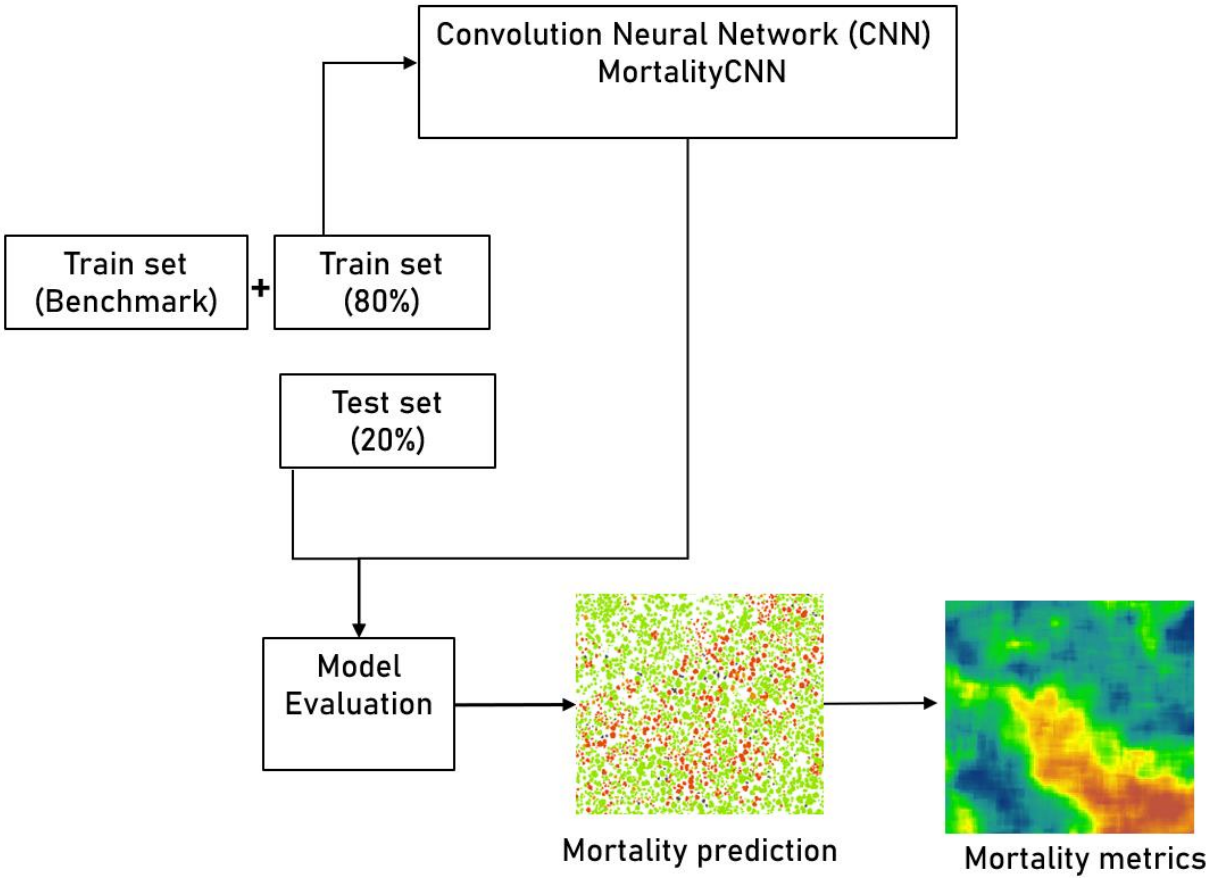

Figure 4.3: Demonstrating the workflow, we trained the Mortality CNN model with merged train set and benchmark data. We assessed the model performance on the test set of newly labeled TAO created within the Creek Fire area.

Table 4.2: Labeled TAOs specifically in the Creek Fire study area for pre- and post-fire TAO mortality in training sites. We labeled more post-fire TAOs to increase labels of fire-induced tree mortality.

Mortality Classes	NAIP (Pre-fire)	Percentage (%)	NAIP (post-fire)	Percentage (%)
Dead	564	47.08	2110	50.94
Live	388	32.39	1199	28.95
Mixed	112	9.35	398	9.61
Other	134	11.19	435	10.50
Total	1198	100	4142	100

4.4.3 Relative and Neighborhood Canopy Mortality Metrics

To improve ecological understanding and management response due to extensive mortality resulting from compound disturbances, we derived mortality metrics from individual overstory tree mortality. These mortality metrics can be useful for managers to identify impacts of compound disturbances and to answer key ecological questions such as identifying environmental drivers of mortality (Campbell et al., 2020) and fire severity (Stephens et al., 2018). We chose 10 m resolution for two reasons. First, we did so to match the high-resolution satellite driven burn severity indices such as RBR derived from Sentinel-II. Second, the 10 and 30 m resolutions of spatial data are units of measure familiar to forest managers and are often their unit of planning (North, 2012; North et al., 2021; Stephens et al., 2022).

The examination of individual overstory tree mortality can be very useful for research of mortality related to species, height, and basal area (Van Wagtendonk, 2023). However, a map of relative and neighborhood canopy mortality is more practical for managers to identify and prioritize interventions for locations with higher mortality rates and regeneration failure (North et al., 2019). Managers benefit from understanding the unit area impacted by tree mortality; the absolute value of tree mortality has more limited utility for managers who must plan forest management treatments.

We used the CNN model to generate modeled individual tree mortality maps across all study sites. The CNN model generated a tree status map with each TAO identified as one of the following classes: live, dead, mixed, or other. Using the polygon to raster tool in ArcMap (version 10.6.1), we converted the individual tree mortality map to a 1-meter resolution raster, *Y*, containing the predicted mortality class at each pixel. We used the rasterized overstory tree mortality map to derive relative and neighborhood canopy mortality metrics.

4.4.3.1. Calculating Relative Canopy Mortality (RCM)

The relative canopy mortality (RCM) metric measures the proportion of mortality within each 10 m grid cell (Figure 4.4). It is useful for understanding the local variation of mortality, which could be the result of drought, land conversion, or fire processes. We took a window size of 10 x 10 m that passes through the rasterized grid cell of overstory tree mortality to calculate the RCM. The RCM was calculated using the formula consistent to (Campbell et al., 2020):

$$Relative\ canopy\ mortality\ = \frac{\mathrm{A}_{dead} + 0.5 \times A_{mixed}}{\mathrm{Atotal}_{(live+dead+mixed)}}$$

Where, A_{dead} is the total number of pixels of dead TAO, A_{mixed} is half the number of pixels of TAO in the mixed class i.e. partially dead trees, and A$total$ is the sum of pixels of dead, mixed, and live TAO. Here, the other class was excluded from calculating percent mortality. While RCM can be calculated at larger window sizes, larger window sizes will make the output raster coarse in resolution, which could be more relevant for planning at regional scales.

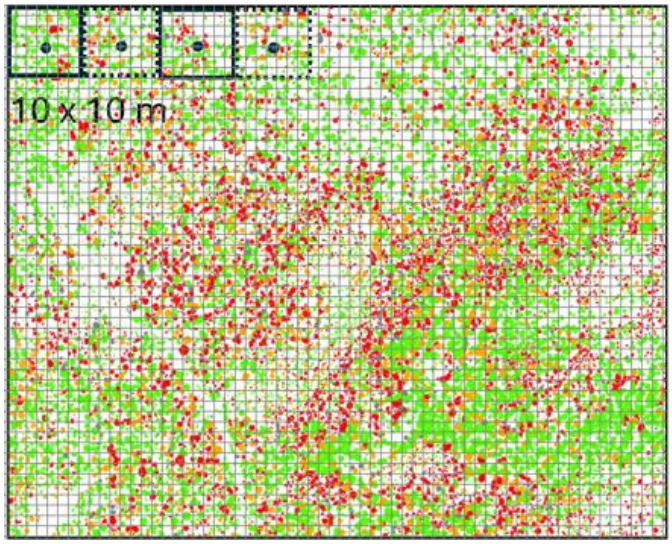

Figure 4.4: Demonstrating relative canopy mortality calculation, a window size of 10 x 10 passes through an overstory tree mortality, deriving RCM. The gride provided is representative of 1 m resolution with 10 x10 grid inside the moving window

4.4.3.2. Calculating Neighborhood Canopy Mortality (NCM)

Wildfires that result in large patches of high fire severity are associated with long distances from seed sources that limit post-fire recruitment, which can lead to regeneration failure over time (Davis et al., 2019; Tepley et al., 2017). Increase in high severity burned patch sizes will significantly increase tree regeneration failure (Davis et al., 2019). Managers would benefit from a spatially explicit metric that captures surviving trees around a moving window of locations that could serve as a potential seed source following wildfires. Potential seed source information is currently crudely estimated from fire severity data; however, fire severity data cannot explicitly identify overstory or seed producing tree mortality but it represent the structural change due to fire (McCarley et al., 2017; Miller & Thode, 2007). Fire severity at a specific location result from a complex function of fire dynamics at the time of the fire, weather, and the ecosystem conditions within the *neighborhood* around the location. To understand the potential for successful regeneration at fine resolution in the high severity burn patches, we recommend the development of a metric that captures surviving trees around the neighborhood of a pixel that could serve as a potential seed sources.

We propose a new index, neighborhood canopy mortality (NCM), which is derived by combining the concept of convolving kernel of neural network (O'Shea & Nash, 2015) and relative canopy mortality (Figure 4.5). The convolving kernel (window) moves across the rasterized overstory mortality map calculating RCM at a stride (i.e., the number of pixels by which the kernel move across the input). The kernel (window size) can vary based on the ecological and management requirement. NCM provides the ability to identify the relative canopy mortality across various distances yet maintains the fine-grained resolution of output

rasters. It does so by moving the kernel window with smaller stride (10 pixels) (Figure 4.5). In contrast, RCM calculated over larger window size will have coarser resolution output rasters.

There are multiple studies conducted at different distances to seed source such as 50 m, 80 m, 100 m in relation to regeneration failure (Kemp et al., 2016; Stevens-Rumann & Morgan, 2019; Tepley et al., 2017) across western US. In our analyses, we took a kernel (window size) of 100 x100 m with a stride of size 10 for demonstrating the NCM calculation. This setting provides the tree mortality/survival condition of a particular location in relation to 50 m distance on each side with output at 10 m resolution. We convolve the kernel (window size) over the tree mortality map to calculate relative canopy mortality for that window size and move to the next by moving the kernel by a stride of 10 (Figure 4.4). We added padding to neutralize the edge effect (O'Shea & Nash, 2015). The neighborhood canopy mortality was calculated using the following formula:

$$NCM_{(i,j)} = RCM(Y[i * s : i * s + h, j * s : j * s + w])$$

Where, Y is the rasterized individual overstory tree mortality at 1 m resolution as described above, s is stride (10), h is height (100), w is width (100), and (i, j) is output location.

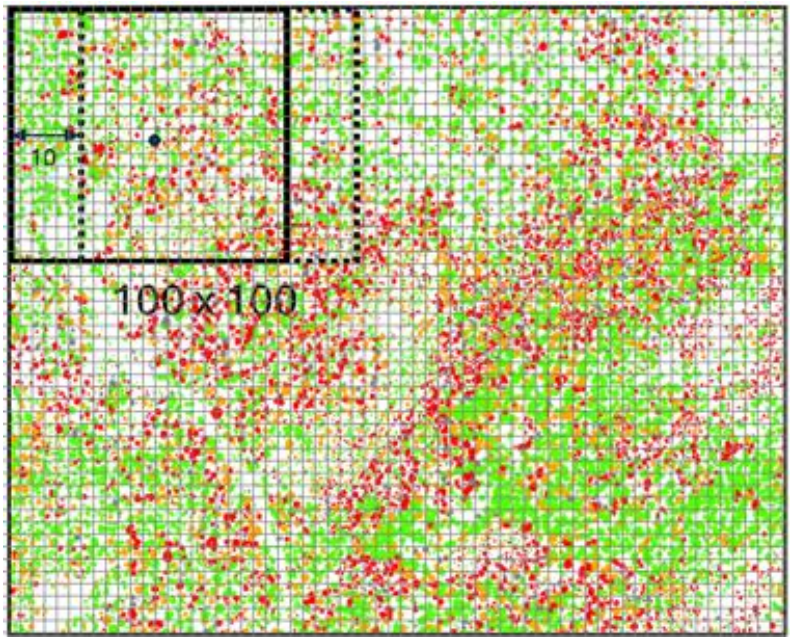

Figure 4.5: Demonstrating neighborhood canopy mortality calculation, a window size of 100 x 100 passes through an overstory tree mortality, deriving RCM and moving across stride of 10. The gride provided is representative of 1 m resolution with 100 x100 grid inside the moving window.

4.4.4 Comparison of RBR and NCM: Qualitative patch analysis

To compare the mortality metrics with satellite derived RBR, we conducted qualitative assessment of different patches ranging from 2 to 42 hectares within study sites. We used visual image interpretation analysis to estimate how well these metrics represent the status of mortality post-fire. We compared the representation of post-fire mortality by RCM, NCM and RBR and used NAIP imagery as a ground truth.

For this, we selected multiple locations within the study sites to assess the different scenarios such as high pre-fire mortality, no mortality for both pre- and post-fire, and areas with trees on high reflective surface. We selected three different areas with high pre-fire mortality due to prior fire and drought and two areas with live trees and one area with trees on reflective surface. Using

these selected areas we compared how mortality metrics (RCM & NCM) and burn severity (RBR) represent the mortality variations.

4.5 RESULTS

4.5.1 Classification results

We used CNN to generate the prediction of individual overstory tree mortality across the three study sites within the Creek Fire study area for the pre-fire (2020) and post-fire (2022) periods. Each TAO was predicted to be one of the four classes of live, dead, mixed and other. For the pre-fire mortality status, the CNN model had an overall accuracy of 82.57% and a macro average F1 score of 0.71 on test set (Table 4.3). Similarly, for post-fire, the CNN model had an overall accuracy of 87.08% with 0.77 macro average F1 score on test set (Table 4.3).

Table 4.3: Test set results of CNN models for pre- and post-fire forest conditions in training site.

Mortality Status	Pre-fire			Post-fire		
	Precision	Recall	F1	Precision	Recall	F1
Dead	0.84	0.89	0.87	0.87	0.96	0.91
Live	0.91	0.95	0.93	0.92	0.95	0.93
Mixed	0.45	0.39	0.42	0.80	0.75	0.77
Other	0.75	0.56	0.64	0.71	0.36	0.48
Macro avg	0.74	0.70	0.71	0.82	0.75	0.77
OA			82.57%			87.84%

Based on our assessment of mortality prediction, we found consistent performance above 80% accuracy in each study site pre- and post-fire with the exception of oak woodlands (Table 4.4). In oak woodlands, particularly for mixed chaparral below 4m height, we found accuracy of 55% in mortality prediction. There were an estimated 14.5% of mixed chaparral in the oak woodlands (as estimated from the proportion of trees below 4m height).

This showed that our model performed well in Sierra mixed conifer and Sierra mixed conifer & Red fir that were dominated with the similar forest types as training site. However, for oak woodland, we found that the model was confused between live and dead of mixed chaparral and in areas with meadows the model was confused by exposure of live grass cover underneath dead tree post-fire (Figure 4.6).

Table 4.4: Accuracy of model in each study sites using random samples.

Forest condition	Overall accuracy (%)		
	Oak woodlands	Sierran mixed conifer	Sierran mixed conifer & red fir
Pre-fire	81	83	85
Post-fire	75	83	87

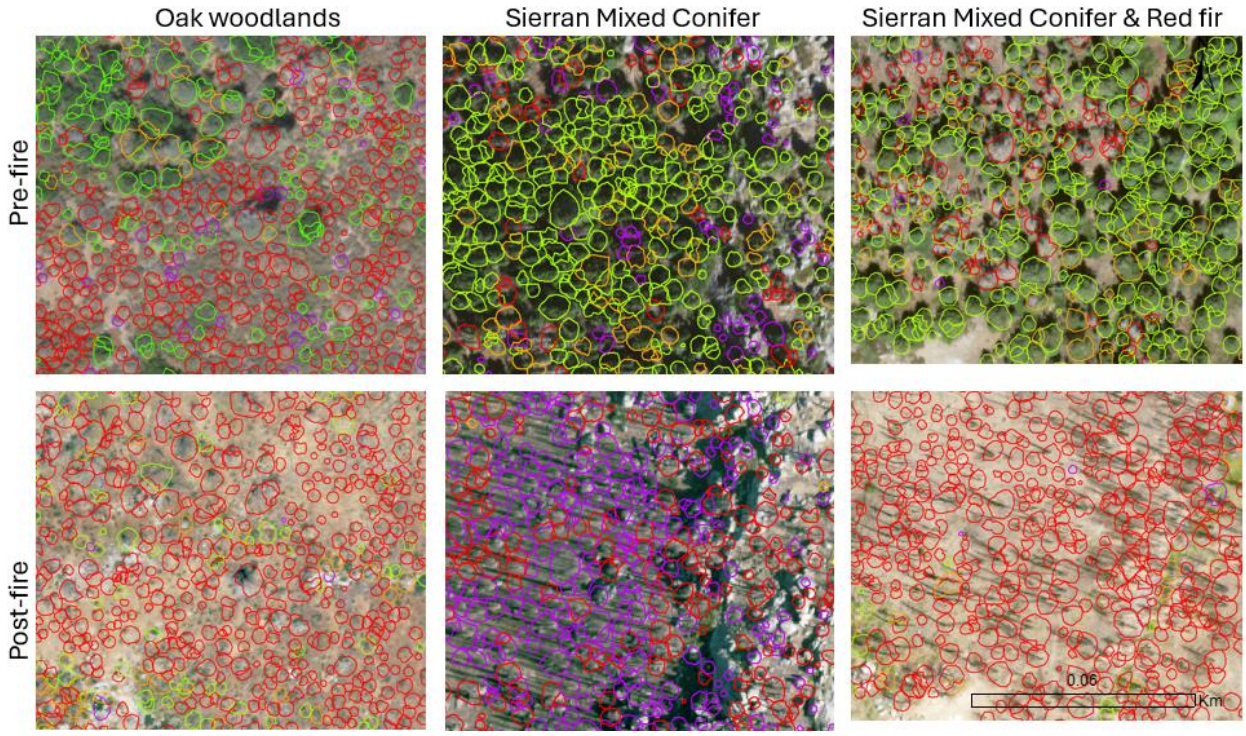

Figure 4.6: The overstory tree mortality status prediction over three study sites for both pre-fire (upper) and post-fire (lower). The oak woodlands covered with mixed chaparral has more dead predictions pre-fire while in Sierran Mixed conifer site post-fire prediction of other is increased due to exposure to boulder. In addition, Sierran Mixed conifer & red fir site post-fire has some live predictions of dead trees due to presence of meadows.

4.5.2 Patterns of pre-fire and post-fire mortality predictions

Both pre- and post-fire individual overstory tree mortality patterns showed that there was substantial increase in post-fire dead and substantial decrease in live trees for sierran mixed conifer and sierran mixed conifer & red-fire study sites. For oak woodlands there was substantial increase in other classes post-fire. We have presented some zoomed areas of all study sites to demonstrate the mortality prediction in Figure 4.5 while prediction for full study sites is presented in Figure C2 to C4.

For oak woodlands site, post-fire there was a substantial decrease in live trees (15.44%), and mixed trees (6.51%) (Table 4.5) with substantial increase in other class (20.70%). The change in percentage of dead trees was low. The prediction of dead class in pre-fire forest condition was high due to presence of mixed chapparal which appeared dead due to their drought tolerant traits.

For the sierran mixed conifer site, the comparison between pre- and post-fire mortality conditions shows that there was a substantial increase in dead trees (35.70%) with a corresponding decrease in live trees (37.37%). In addition, there was an increase in other class (7.98%) and decrease in mixed class (6.31%). The increase in other class post-fire was due to exposure of boulders (misclassified as trees) after severe burn from fire (Figure 4.5).

For the sierran mixed conifer & red fir site, the comparison between pre- and post-fire mortality conditions demonstrated a substantial increase in dead trees (37.16%) with a corresponding decrease in live trees (29.46%). In addition, there was a decrease in mixed class (7.48%) but other class did not change substantially.

Table 4.5: Percentage of pre- and post-fire mortality status and difference where negative values mean increase and positive values mean decrease.

	Oak woodlands			Sierran Mixed Conifer			Sierran Mixed Conifer & Red Fir		
Mortality	Pre	Post	Change	Pre	Post	Change	Pre	Post	Change
Dead	45.36	46.61	1.25	19.53	55.23	35.7	19.01	56.17	37.16
Live	36.38	20.94	15.44	59.49	22.12	37.37	57.68	28.22	29.46
Mixed	11.58	5.07	6.51	14.11	7.8	6.31	15.98	8.14	7.84
Other	6.68	27.38	20.7	6.87	14.85	7.98	7.33	7.47	0.14

4.5.3 Mortality metrics corresponds to burn severity

We classified RCM and NCM into three classes to represent low, moderate and high mortality. The low class represents mortality from 0 to 35%, moderate class represents mortality from 35 to 75% and high class represents mortality above 75%. The high mortality patches were mapped as >75% dead trees based on Stevens et al. (2017). Our results showed that both RCM and NCM captured the post-fire mortality well in areas with high pre-fire mortality (Figure 4.7). However, RBR showed low-moderate severity in areas with prior-fire and unburned to low-severity in areas with drought-induced mortality. This is because RBR measures the change in the vegetation and canopy cover.

In locations with more live trees both pre- and post-fire conditions, we found that all these metrics represent the overstory mortality status well based on the ground truth shown by NAIP imagery (Figure 4.8). The post-fire RCM showed fine local variation of low, moderate, and high mortality, while post-fire NCM is smoothed and showed the more generalized variations in mortality. Since both RCM and NCM are derived from high-resolution individual overstory tree mortality these metrics were more aligned with fine scale mortality pattern on ground than satellite driven RBR (Figure 4.7 A & B).

In an area where forest with some openings and clumps in boulder (high reflective surface), we found that both RCM and NCM identified the region as high mortality (Figure 4.8 C). Whereas this area was represented as low to moderate severity by RBR. This could be due to RCM and NCM metrics being derived from fine scale overstory tree mortality while RBR was satellite derived.

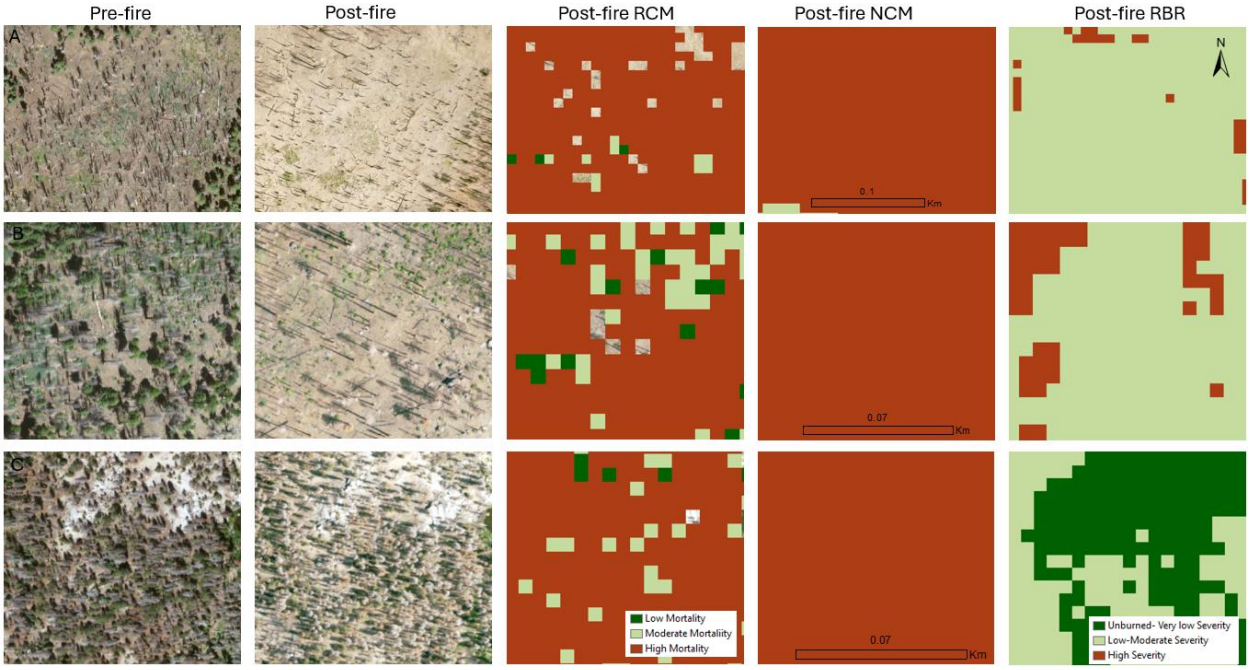

Figure 4.7: Demonstrating how areas with high pre-fire mortality due to prior fire (A & B) and drought (C) were captured by RCM, NCM and RBR.

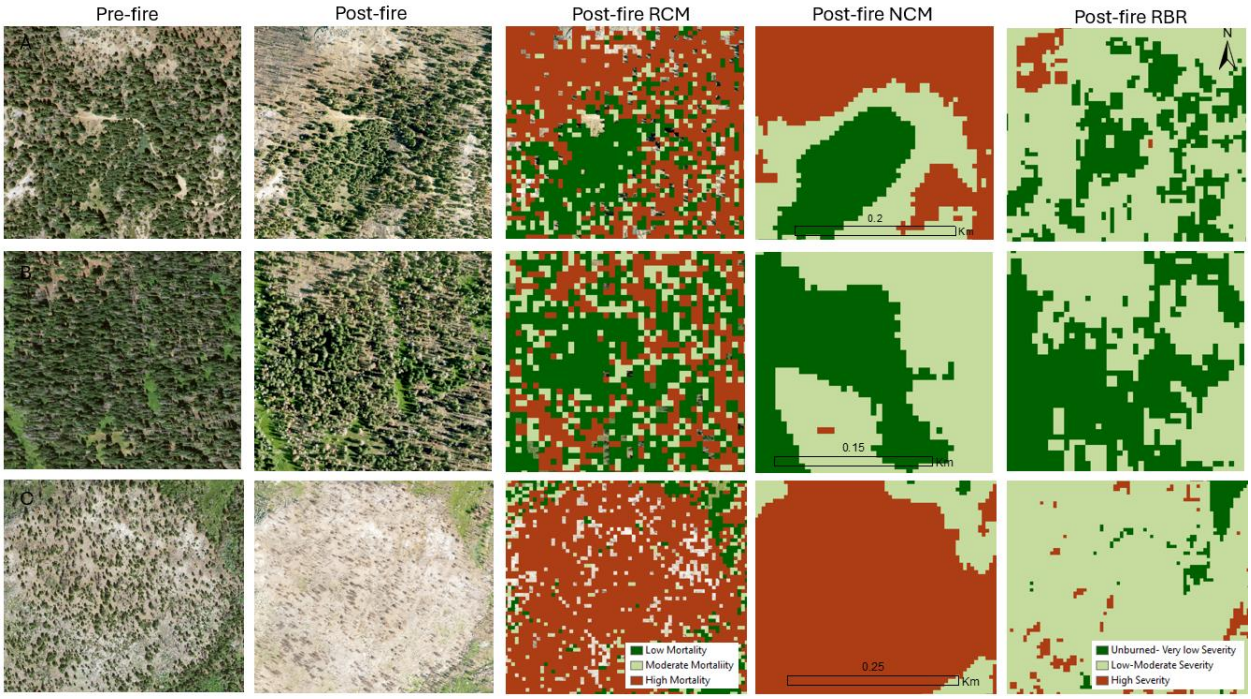

Figure 4.8: Demonstrating how areas with low mortality both pre- and post-fire forest conditions (A & B) and forest on high reflective surface (C) were captured by RCM, NCM and RBR.

4.6 DISCUSSION

In this study we used CNN model and trained to predict both drought-induced and fire-induced mortality. Our results showed that the CNN model performed well in sierran mixed conifer and sierran mixed conifer & red fir study sites. In these study sites, we found a substantial increase in tree mortality post-fire and a concomitant decrease in live trees. However, we found that the model performed poorly in differentiating between live and dead status for mixed chaparral found in oak woodlands area.

Further, our results indicated that RBR showed low to moderate severity in regions with high preexisting tree mortality due to both drought and prior fire (Figure 4.7). This shows that the RBR is not suitable to represent the post-fire mortality status in areas with compound disturbances or high preexisting mortality. This finding is in line with previous studies that have

found prior fire and prescribed burning decreased the satellite measured severity of subsequent burn (Cansler et al., 2022; Prichard & Kennedy, 2014). However, in areas with preexisting tree mortality due to drought or prior fire we found that the neighborhood canopy mortality (NCM) better captured the post-fire tree mortality state.

The post-fire neighborhood canopy mortality map can be used by researchers and managers to understand how fire impacted the landscape. In the face of climate change, where we are experiencing frequent mass fire, neighborhood canopy tree mortality mapping can serve as a critical resource to managers. Managers can use the post-fire NCM to identify locations with high neighborhood mortality at a given distance that helps identify areas in risk of regeneration. Similarly, NCM can be used to identify locations with high neighboring survival trees that can serve as potential seed source.

4.6.1 Model limitation and recommendations

In general, we found that the model performs well in a similar forest type to those in the training data. Significant ecological and vegetation type differences led to inaccuracies in model predictions (Oak woodlands). We also found that differences in atmospheric correction and data acquisition time of day of remote sensing data influence the tree mortality detection. Further, we found that meadows and riparian areas were creating problems in post-fire tree mortality detection (Figure 4.6).

In future, we recommend height cut off <4m to remove mixed chaparral (shrub) and add training labels specific to oak woodlands. We also suggest masking wetlands or creating training data for optimizing model performance. Overall, we recommend creating labels specific to the new region and vegetation type for applying CNN model. Then retrain CNN model combining

new labels with benchmark dataset. It will help improve model predictions and assess the model's performance in the specific region.

4.6.2 Neighborhood Canopy Mortality Corresponds to RBR

When comparing RBR with NCM we found that RBR is not suitable to represent the post-fire mortality status especially in areas with high preexisting mortality. As discussed in section (4.5.4), the RBR showed low to moderate severity in areas with high pre-existing tree mortality (13 hectare) and in the location with trees in granitic environments (42 hectare). Both these regions were covered with standing dead trees (Figure 4.7). We found there were conditions under which RBR does not accurately capture the post-fire tree mortality and suffered from the mixed pixel reflectance (Figure 4.7 & 4.8). Generally, RBR is used to assess the wildfire-caused structural changes such as a reduction in canopy cover (McCarley et al., 2017). In addition, certain impacts of wildfire such as carbon loss due to burning of pre-existing dead trees cannot be captured by RBR. Therefore, we propose a neighborhood canopy mortality, a new metric that captures post-fire tree mortality in all regions either with high or low pre-existing tree mortality, does not suffer from missing data problem and maintain fine-grain resolution even when derived for larger neighborhood.

4.6.3 Application of Mortality Metrics

We used individual overstory tree mortality maps to derive mortality metrics useful for managers to monitor the variation in local and broader mortality patterns. In this study we derived the RCM that represents the relative canopy mortality per unit area. Specifically in our study, we calculated RCM within an area of 100 sq. meters. We also derived the NCM for assessing post-fire seed dispersal. The NCM represents the neighborhood canopy mortality

within an area of 10,000 sq. meters (1 hectare) (Davis et al., 2019). Both of these metrics can be derived for both pre- and post-fire forest conditions.

The RCM can be useful to identify the locations with higher pre-fire mortality. This information can be useful for managers to plan and implement treatments to reduce dead canopies which could prevent the risk of high severity fire in future. Further, the pre-fire RCM map at 10 m resolution aids in the investigation of predictor and drivers of burn severity (Stephens et al., 2022) and mortality (Campbell et al., 2020).

The NCM is specifically derived for assisting managers in examining post-fire areas with high tree mortality or survival rates. The NCM can be derived for different sizes of neighborhood. The post-fire NCM provides the cumulative mortality that is important in current scenarios of more frequent repeat fire and drought-induced mortality. The post-fire NCM map captures surviving trees around the neighborhood of a pixel that could serve as a potential seed source. The NCM can be useful for managers to estimate fire impact, surviving mature trees (i.e., potential seed source for future), and to develop efficient management strategies (Furniss et al., 2019). Similarly, areas with high mortality can suffer from regeneration failure. This information can be used by managers to plan and develop strategies for planting seeds.

4.7 CONCLUSION AND FUTURE DIRECTION

We conducted comprehensive tree mortality mapping within multiple locations in the 2020 Creek Fire footprint. We set up the three study sites to assess the model performance for different vegetation types. We also examined the pattern of dead trees pre- and post-fire. We used overstory canopy mortality to derive aggregated relative and neighborhood mortality at pixel level. We found that the relativized burn ratio was classified as low to moderate severity in areas

with high preexisting tree mortality and in areas with no pre-fire mortality but forest in granitic environments. In contrast, we found that neighborhood canopy mortality was more effective for predicting tree mortality in these regions. Therefore, we propose neighborhood canopy mortality as a new metric to capture post-fire tree mortality in forest with or without preexisting tree mortality.

Further, we also found what needs to be addressed and improved before implementing this model to the entirety of the Creek Fire footprint. This footprint contains a variety of vegetation types and has experienced both drought and fire related mortality in the past. We recommend a height cut off >4 m for conducting tree mortality classification in mixed chaparral areas. We also recommend masking wetlands (meadows) or adding more training data for these regions while training the model to perform better. In the future, we will use neighborhood canopy mortality maps to produce potential seed source products that can be used by managers to address regeneration failure.

APPENDIX C

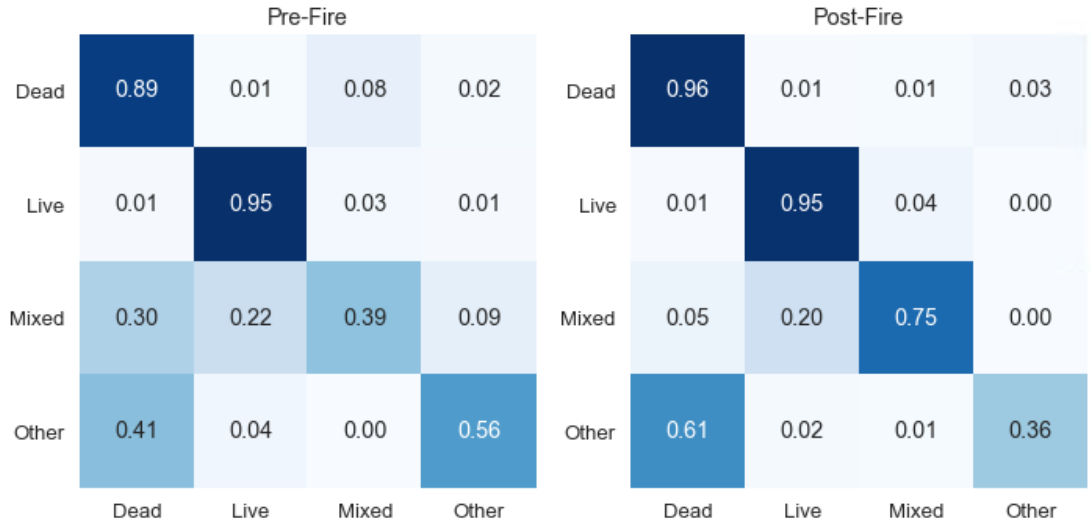

Figure C1: Confusion matrix of NAIP imagery for pre- and post-fire predictions. The rows indicate correct labels and columns indicate predicted labels.

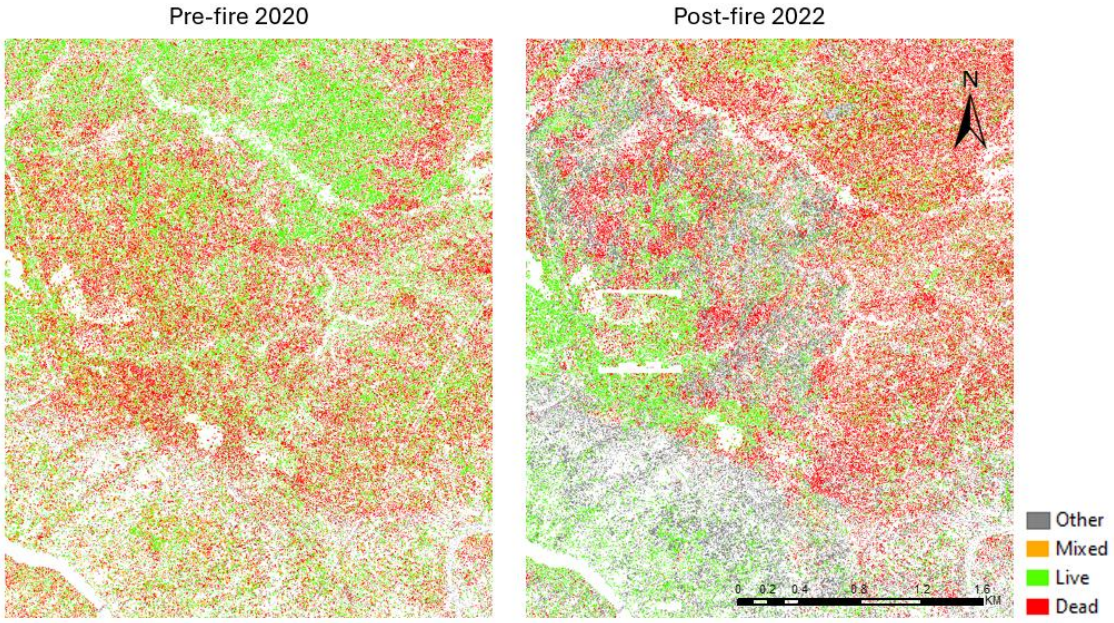

Figure C2: Overstory tree mortality of study site 1 that is dominated by oak woodland, montane hardwood, and mixed Chaparral for both pre-fire (2020) and post-fire (2022).

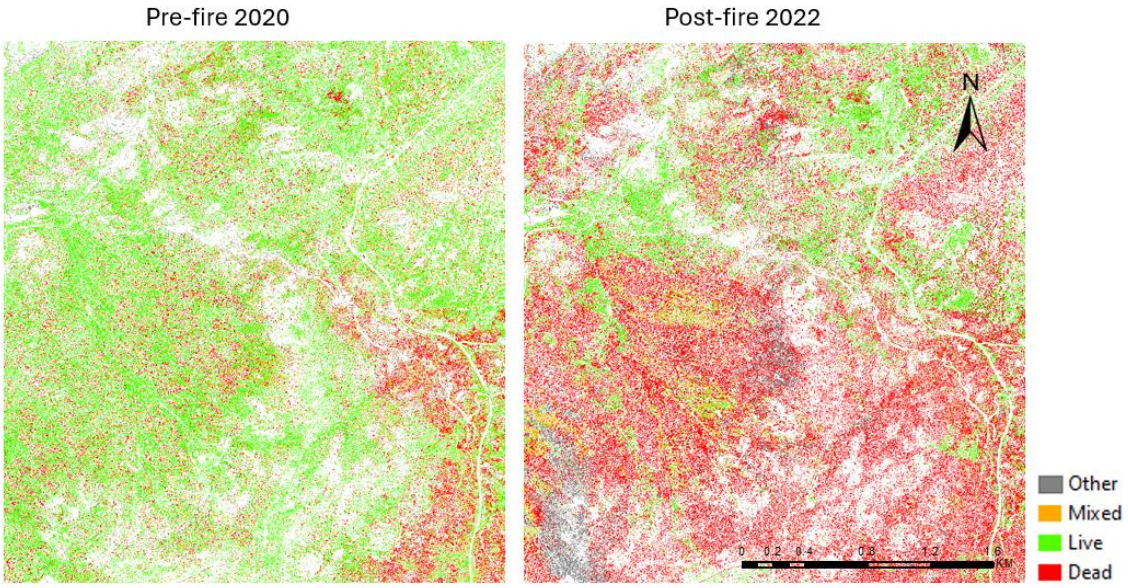

Figure C3: Overstory tree mortality of study site 2 that is dominated by Sierran mixed conifer and red fir for both pre-fire (2020) and post-fire (2022).

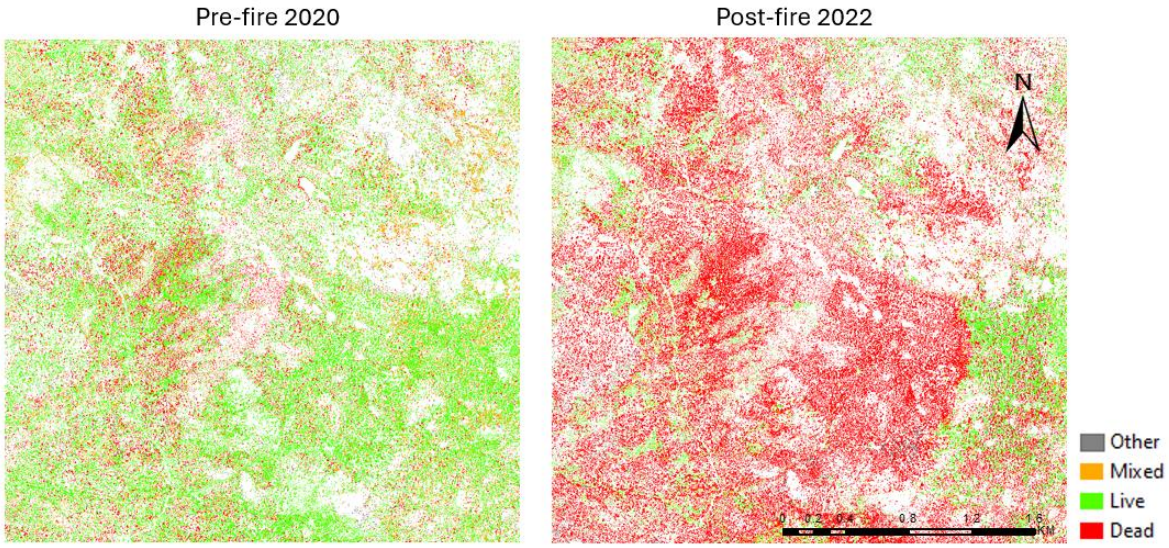

Figure C4: Overstory tree mortality of study site 3 that is dominated by Sierran mixed conifer and red fir for both pre-fire (2020) and post-fire (2022).

4.8 REFERENCES

Allen, C. D., Macalady, A. K., Chenchouni, H., Bachelet, D., McDowell, N., Vennetier, M., Kitzberger, T., Rigling, A., Breshears, D. D., Hogg, E. H. (Ted), Gonzalez, P., Fensham, R., Zhang, Z., Castro, J., Demidova, N., Lim, J.-H., Allard, G., Running, S. W., Semerci, A., & Cobb, N. (2010). A global overview of drought and heat-induced tree mortality reveals emerging climate change risks for forests. *Forest Ecology and Management*, *259*(4), 660–684. https://doi.org/10.1016/j.foreco.2009.09.001

Bhatt, P., & Maclean, A. L. (2023). Comparison of high-resolution NAIP and unmanned aerial vehicle (UAV) imagery for natural vegetation communities classification using machine learning approaches. *GIScience & Remote Sensing*, *60*(1), 2177448. https://doi.org/10.1080/15481603.2023.2177448

Byer, S., & Jin, Y. (2017). Detecting Drought-Induced Tree Mortality in Sierra Nevada Forests with Time Series of Satellite Data. *Remote Sensing*, *9*(9), 929. https://doi.org/10.3390/rs9090929

Campbell, M. J., Dennison, P. E., Tune, J. W., Kannenberg, S. A., Kerr, K. L., Codding, B. F., & Anderegg, W. R. L. (2020). A multi-sensor, multi-scale approach to mapping tree mortality in woodland ecosystems. *Remote Sensing of Environment*, *245*, 111853. https://doi.org/10.1016/j.rse.2020.111853

Cansler, C. A., Kane, V. R., Hessburg, P. F., Kane, J. T., Jeronimo, S. M. A., Lutz, J. A., Povak, N. A., Churchill, D. J., & Larson, A. J. (2022). Previous wildfires and management treatments moderate subsequent fire severity. *Forest Ecology and Management*, *504*, 119764. https://doi.org/10.1016/j.foreco.2021.119764

Cheng, Y., Oehmcke, S., Brandt, M., Rosenthal, L., Das, A., Vrieling, A., Saatchi, S., Wagner, F., Mugabowindekwe, M., Verbruggen, W., Beier, C., & Horion, S. (2024). Scattered tree death contributes to substantial forest loss in California. *Nature Communications*, *15*(1), 641. https://doi.org/10.1038/s41467-024-44991-z

Collins, B. M., Stevens, J. T., Miller, J. D., Stephens, S. L., Brown, P. M., & North, M. P. (2017). Alternative characterization of forest fire regimes: Incorporating spatial patterns. *Landscape Ecology*, *32*(8), 1543–1552. https://doi.org/10.1007/s10980-017-0528-5

Cova, G., Kane, V. R., Prichard, S., North, M., & Cansler, C. A. (2023). The outsized role of California's largest wildfires in changing forest burn patterns and coarsening ecosystem scale. *Forest Ecology and Management*, *528*, 120620. https://doi.org/10.1016/j.foreco.2022.120620

Davis, K. T., Dobrowski, S. Z., Higuera, P. E., Holden, Z. A., Veblen, T. T., Rother, M. T., Parks, S. A., Sala, A., & Maneta, M. P. (2019). *Wildfires and climate change push low-elevation forests across a critical climate threshold for tree regeneration* (Version 3, p. 1168759 bytes) [Dataset]. Dryad. https://doi.org/10.5061/DRYAD.PC3F9D8

Dixon, D. J., Zhu, Y., Brown, C. F., & Jin, Y. (2023). Satellite detection of canopy-scale tree mortality and survival from California wildfires with spatio-temporal deep learning. *Remote Sensing of Environment*, *298*, 113842. https://doi.org/10.1016/j.rse.2023.113842

Furniss, T. J., Larson, A. J., Kane, V. R., & Lutz, J. A. (2019). Multi-scale assessment of post-fire tree mortality models. *International Journal of Wildland Fire*, *28*(1), 46. https://doi.org/10.1071/WF18031

Hartmann, H., Bastos, A., Das, A. J., Esquivel-Muelbert, A., Hammond, W. M., Martínez-Vilalta, J., McDowell, N. G., Powers, J. S., Pugh, T. A. M., Ruthrof, K. X., & Allen, C. D. (2022).

Climate Change Risks to Global Forest Health: Emergence of Unexpected Events of Elevated Tree Mortality Worldwide. *Annual Review of Plant Biology*, *73*(1), 673–702. https://doi.org/10.1146/annurev-arplant-102820-012804

Hemming-Schroeder, N. M., Gutierrez, A. A., Allison, S. D., & Randerson, J. T. (2023). Estimating Individual Tree Mortality in the Sierra Nevada Using Lidar and Multispectral Reflectance Data. *Journal of Geophysical Research: Biogeosciences*, *128*(5), e2022JG007234. https://doi.org/10.1029/2022JG007234

Holden, Z. A., Swanson, A., Luce, C. H., Jolly, W. M., Maneta, M., Oyler, J. W., Warren, D. A., Parsons, R., & Affleck, D. (2018). Decreasing fire season precipitation increased recent western US forest wildfire activity. *Proceedings of the National Academy of Sciences*, *115*(36). https://doi.org/10.1073/pnas.1802316115

Hu, T., Ma, Q., Su, Y., Battles, J. J., Collins, B. M., Stephens, S. L., Kelly, M., & Guo, Q. (2019). A simple and integrated approach for fire severity assessment using bi-temporal airborne LiDAR data. *International Journal of Applied Earth Observation and Geoinformation*, *78*, 25–38. https://doi.org/10.1016/j.jag.2019.01.007

Jeronimo, S. M. A., Kane, V. R., Churchill, D. J., McGaughey, R. J., & Franklin, J. F. (2018). Applying LiDAR Individual Tree Detection to Management of Structurally Diverse Forest Landscapes. *Journal of Forestry*, *116*(4), 336–346. https://doi.org/10.1093/jofore/fvy023

Kemp, K. B., Higuera, P. E., & Morgan, P. (2016). Fire legacies impact conifer regeneration across environmental gradients in the U.S. northern Rockies. *Landscape Ecology*, *31*(3), 619–636. https://doi.org/10.1007/s10980-015-0268-3

Khatri-Chhetri, P., Van Wagtendonk, L., Hendryx, S. M., & Kane, V. R. (2024). Enhancing individual tree mortality mapping: The impact of models, data modalities, and classification taxonomy. *Remote Sensing of Environment*, *300*, 113914. https://doi.org/10.1016/j.rse.2023.113914

Lee, J. M., Mirocha, J. D., Lareau, N. P., Whitney, T., To, W., Kochanski, A., & Lassman, W. (2023). Sensitivity of Pyrocumulus Convection to Tree Mortality During the 2020 Creek Fire in California. *Geophysical Research Letters*, *50*(16), e2023GL104193. https://doi.org/10.1029/2023GL104193

Littell, J. S., McKenzie, D., Peterson, D. L., & Westerling, A. L. (2009). Climate and wildfire area burned in western U.S. ecoprovinces, 1916–2003. *Ecological Applications*, *19*(4), 1003–1021. https://doi.org/10.1890/07-1183.1

Mäyrä, J., Keski-Saari, S., Kivinen, S., Tanhuanpää, T., Hurskainen, P., Kullberg, P., Poikolainen, L., Viinikka, A., Tuominen, S., Kumpula, T., & Vihervaara, P. (2021). Tree species classification from airborne hyperspectral and LiDAR data using 3D convolutional neural networks. *Remote Sensing of Environment*, *256*, 112322. https://doi.org/10.1016/j.rse.2021.112322

McCarley, T. R., Kolden, C. A., Vaillant, N. M., Hudak, A. T., Smith, A. M. S., Wing, B. M., Kellogg, B. S., & Kreitler, J. (2017). Multi-temporal LiDAR and Landsat quantification of fire-induced changes to forest structure. *Remote Sensing of Environment*, *191*, 419–432. https://doi.org/10.1016/j.rse.2016.12.022

McGaughey, R. J. (2018). FUSION/LDV: Software for LIDAR Data Analysis and Visualization. *USDA Forest Service Pacific Northwest Research Station, Seattle, WA*. http://forsys.cfr.washington.edu/fusion/fusionlatest.html

Millar, C. I., & Stephenson, N. L. (2015). Temperate forest health in an era of emerging megadisturbance. *Science*, *349*(6250), 823–826. https://doi.org/10.1126/science.aaa9933

Miller, J. D., & Thode, A. E. (2007). Quantifying burn severity in a heterogeneous landscape with a relative version of the delta Normalized Burn Ratio (dNBR). *Remote Sensing of Environment*, *109*(1), 66–80. https://doi.org/10.1016/j.rse.2006.12.006

North, M. (2012). *Managing Sierra Nevada forests* (PSW-GTR-237; p. PSW-GTR-237). U.S. Department of Agriculture, Forest Service, Pacific Southwest Research Station. https://doi.org/10.2737/PSW-GTR-237

North, M. P., Stevens, J. T., Greene, D. F., Coppoletta, M., Knapp, E. E., Latimer, A. M., Restaino, C. M., Tompkins, R. E., Welch, K. R., York, R. A., Young, D. J. N., Axelson, J. N., Buckley, T. N., Estes, B. L., Hager, R. N., Long, J. W., Meyer, M. D., Ostoja, S. M., Safford, H. D., … Wyrsch, P. (2019). Tamm Review: Reforestation for resilience in dry western U.S. forests. *Forest Ecology and Management*, *432*, 209–224. https://doi.org/10.1016/j.foreco.2018.09.007

North, M. P., York, R. A., Collins, B. M., Hurteau, M. D., Jones, G. M., Knapp, E. E., Kobziar, L., McCann, H., Meyer, M. D., Stephens, S. L., Tompkins, R. E., & Tubbesing, C. L. (2021). Pyrosilviculture Needed for Landscape Resilience of Dry Western United States Forests. *Journal of Forestry*, *119*(5), 520–544. https://doi.org/10.1093/jofore/fvab026

O'Shea, K., & Nash, R. (2015). *An Introduction to Convolutional Neural Networks* (Version 2). arXiv. https://doi.org/10.48550/ARXIV.1511.08458

Paine, R. T., Tegner, M. J., & Johnson, E. A. (1998). Compounded Perturbations Yield Ecological Surprises. *Ecosystems*, *1*(6), 535–545. https://doi.org/10.1007/s100219900049

Parks, S. A., & Abatzoglou, J. T. (2020). Warmer and Drier Fire Seasons Contribute to Increases in Area Burned at High Severity in Western US Forests From 1985 to 2017. *Geophysical Research Letters*, *47*(22). https://doi.org/10.1029/2020GL089858

Parks, S., Dillon, G., & Miller, C. (2014). A New Metric for Quantifying Burn Severity: The Relativized Burn Ratio. *Remote Sensing*, *6*(3), 1827–1844. https://doi.org/10.3390/rs6031827

Prichard, S. J., & Kennedy, M. C. (2014). Fuel treatments and landform modify landscape patterns of burn severity in an extreme fire event. *Ecological Applications*, *24*(3), 571–590. https://doi.org/10.1890/13-0343.1

Stephens, S. L., Bernal, A. A., Collins, B. M., Finney, M. A., Lautenberger, C., & Saah, D. (2022). Mass fire behavior created by extensive tree mortality and high tree density not predicted by operational fire behavior models in the southern Sierra Nevada. *Forest Ecology and Management*, *518*, 120258. https://doi.org/10.1016/j.foreco.2022.120258

Stephens, S. L., Collins, B. M., Fettig, C. J., Finney, M. A., Hoffman, C. M., Knapp, E. E., North, M. P., Safford, H., & Wayman, R. B. (2018). Drought, Tree Mortality, and Wildfire in Forests Adapted to Frequent Fire. *BioScience*, *68*(2), 77–88. https://doi.org/10.1093/biosci/bix146

Stevens, J. T., Collins, B. M., Miller, J. D., North, M. P., & Stephens, S. L. (2017). Changing spatial patterns of stand-replacing fire in California conifer forests. *Forest Ecology and Management*, *406*, 28–36. https://doi.org/10.1016/j.foreco.2017.08.051

Stevens-Rumann, C. S., & Morgan, P. (2019). Tree regeneration following wildfires in the western US: A review. *Fire Ecology*, *15*(1), 15. https://doi.org/10.1186/s42408-019-0032-1

Stovall, A. E. L., Shugart, H., & Yang, X. (2019). Tree height explains mortality risk during an intense drought. *Nature Communications*, *10*(1), 4385. https://doi.org/10.1038/s41467-019-12380-6

Tepley, A. J., Thompson, J. R., Epstein, H. E., & Anderson-Teixeira, K. J. (2017). Vulnerability to forest loss through altered postfire recovery dynamics in a warming climate in the Klamath Mountains. *Global Change Biology*, *23*(10), 4117–4132. https://doi.org/10.1111/gcb.13704

USDA. (2021). *2020 California Image Dates* [Dataset]. https://naip-image-dates-usdaonline.hub.arcgis.com/datasets/3c550e2869cb40f1b12244666b0f7c5d_0/explore

Van Wagtendonk, L. (2023). Comparing, matching, detecting, and predicting drought-induced tree mortality in the Sierra Nevada, California. *Doctoral Dissertation, University of Washington*.

Young, D. J. N., Stevens, J. T., Earles, J. M., Moore, J., Ellis, A., Jirka, A. L., & Latimer, A. M. (2017). Long-term climate and competition explain forest mortality patterns under extreme drought. *Ecology Letters*, *20*(1), 78–86. https://doi.org/10.1111/ele.12711

Chapter 5: CONCLUSION

Forests are one of the largest and most important terrestrial ecosystems that cover approximately 30% of the Earth's landmass. Globally forests are important carbon pools and provide a variety of ecosystem services. However, they are undergoing rapid changes due to climate change induced disturbances. The forests in California's Sierra Nevada and Interior Alaska, for example, are under the threat of massive forest mortality, shift in species composition, and forest conversion to nonforest with corresponding changes in ecological processes. In this dissertation, I developed a robust framework (structured and systemic approach) (Figure 1) to identify and map forest conditions (mortality & forest types) by integrating high-resolution remote sensing data with cutting-edge artificial intelligence techniques. The framework can be used for monitoring of forest conditions over time to detect changes at the scale at which they occur and facilitate informed decision making in forest management and restoration efforts.

At the outset of this study, we identified a critical gap in availability of comprehensive frameworks and highly accurate predictive models for mapping forest conditions using remote sensing, validated with field data, which can be effectively deployed across larger areas to derive ecological insights. For example, the forests in Sierra Nevada, California, experienced a prolonged drought from 2012 to 2016 that resulted in extensive tree mortality (Millar & Stephenson, 2015; Swain, 2015). Subsequently, the region suffered from megafires in recent decades (Lee et al., 2023; Stephens et al., 2018). However, the study of mortality due to compound disturbance was limited (Stephens et al., 2018). Similarly, the boreal forest in the higher latitudes of Interior Alaska has been significantly affected by climate change, leading to shifts in dominant forest type and species range (Barber et al., 2000; Chapin et al., 2010;

Johnstone et al., 2010; Walker et al., 2015, 2023). These rapid ecological changes underscore the urgent need for fine-scale monitoring of the forest type combining remote sensing and field data to detect potential type conversion and inform management interventions.

Remote sensing has been used in detection and mapping forest conditions since the 20th centuries (Walsh, 1980; Xie et al., 2008). The availability of high-resolution remote sensing data enables us to identify and map forest conditions from individual tree scale, plot to regional scale. Simultaneously the development in cutting-edge technologies such as artificial intelligence are enabling us to produce accurate models. Artificial intelligence techniques have increased in forest ecology (Liu et al., 2018; Jain et al., 2020). However, there is still the need to research how artificial intelligence techniques can be useful to monitor and derive information from forest ecosystems to address ecological questions. In this research, I addressed this gap by developing a framework integrating remote sensing and artificial intelligence techniques to monitor mortality and forest types at scale appropriate to capture the ecological phenomena.

For instance, I focused on mapping of tree mortality status at the scale of overstory individual trees and dominant forest type at the forest stand level that can be predicted across larger extents. These components are key for estimating aboveground biomass and carbon, as well as supporting biodiversity monitoring efforts. Despite previous efforts to map tree mortality at the individual scale using remote sensing data (Hemming-Schroeder et al., 2023; Stovall et al., 2019), discrepancies between their findings and field studies (Stephenson & Das, 2020) have shown due to a lack of field validation. Additionally, there remains a notable gap in the production of spatially extensive, high-resolution (<1m) forest type maps, particularly in Interior Alaska where some locations are inaccessible to humans due to remoteness. Therefore, to

address these challenges, in this dissertation I present a comprehensive framework and models designed to generate high-resolution forest conditions maps including mortality and forest types.

5.1 SUMMARY OF KEY FINDING AND USE CASES

Collectively, the chapters of this dissertation serve as a comprehensive roadmap to demonstrate the development and application of the framework and models. These chapters showcase the process of leveraging advanced techniques to investigate the monitoring of rapid ecological resultant impact of climate change like drought and fire. For instance, in chapters 2 & 3, I developed models for identifying drought-induced mortality and fine scale forest type. In chapter 4, I used the mortality model from chapter 2 and trained it to capture fire driven mortality using additional training data reflecting the burn conditions. Further, using the prediction maps of mortality at individual tree level, I derived metrics that summarize the information to develop products useful for managers.

In chapter two, I found that the combination of high spatial resolution with convolutional neural network model produced highly accurate individual tree mortality maps in mixed conifer forest ecosystem (Figure 2.8). Among spatial resolution, spectral resolution, and orthorectification, I found orthorectification to be the most important factor in producing accurate models (Figure 2.9). Further, I developed and open-sourced a tree mortality benchmark dataset (Table 2.2) produced by combining lidar and high-resolution imagery, which will aid in improvement of mortality algorithms (Hartman et al., 2018). The mortality maps aid in ecological understanding of drivers of mortality (Byer & Jin, 2017; Campbell et al., 2020).

In chapter three, I found convolutional neural network model outperformed the XGBoost model for all forest type classifications (Figure 4.4). I found elevation and canopy height were

the most important factors for identifying the boreal forest types (Figure 4.6). I also identified important vegetation indices such as PSND, PRI, and GM1 (Table 3.3), for differentiating between hardwood and softwood (Figure 3.8 & 3.9) and ARI (Table 3.3) to be important for forest and nonforest (Figure 3.7). The forest type maps are important for quantifying aboveground biomass, assessing forest carbon, and conducting landscape modeling studies (Fassnacht et al., 2016; Mäyrä et al., 2021; Tian & Fu, 2020).

In chapter four, I applied the mortality model developed in the second chapter and trained to predict both drought-induced and fire driven mortality. I then applied this model to estimate both the pre- and post-fire individual tree mortality across three study sites within 2020 Creek Fire. I found the model performed well for areas with Sierra mixed conifer and red fir forests while the model was confused with mixed chaparral in Oak woodlands (Table 4.4). I also demonstrated the application of overstory tree mortality to produce mortality metrics (NCM) at 10 m resolution that summarize the mortality patterns. The NCM can be used to identify areas with potential seed sources and regeneration failure due to compound disturbance. NCM can be useful for managers to develop management strategies (Figure 4.6). These mortality metrics aid the investigation of the drivers of burn severity (Stephens et al., 2018, 2022).

Overall, the framework developed in this study can be applied in applications where both high-resolution remote sensing and field data are available. Among various models I found convolutional neural networks outperformed other models for forest condition prediction due to their ability to learn non-linear features automatically. The CNNs models can analyze and extract useful spatial and spectral information while machine learning requires manual feature engineering in extracting important features which required domain knowledge. For mortality detection, high spatial resolution with proper orthorectification imagery produces higher

accuracy, in contrast to previous work which has found hyperspectral to perform better for tree species (Fricker et al., 2019). Throughout the study, I found methods which maximize signal to noise ratio for the task at hand (including sufficiently representative training data, improved spatial resolution, and orthorectification) were important factors for achieving better results. Additionally, I found that more accurate high resolution overstory predictions leads to more accurate derived lower resolution metrics, such as our proposed NCM metric, by reducing noise and enabling the capture of ecologically important component such as distance to seed source. For forest type classification, integrating topographic variables with remote sensing data elevated the accuracy of the classification due to the strong influence of topography in dominant forest type, especially across the vast and varied expanses of Interior Alaska. Models developed in this research can be utilized to monitor and study long-term forest mortality, regeneration failure, and forest type with validation for specific regions. The maps can be used to derive insights on how forests are changing over time and assess the impact of climate change in forest ecosystems.

5.1.1. Model Insights and Generalizability

High-quality and large amounts of labeled data are required to effectively train both machine learning and deep learning models. The combination of high-resolution (<1m) remote sensing data with field validation yielded accurate model predictions. The implementation of data augmentation techniques also enhanced the model performance. Further, tuning hyperparameters to find the optimal setup for the given task is crucial. It is important to retrain the model with newly labeled data to maintain their performance, accuracy and relevance.

To apply these models in different regions, the new area should have similar forest ecosystem and vegetation types to those in the training data. The remote sensing data of the new area should match both spatial and spectral resolutions of the data used to train these models. The difference

in data will significantly affect the model's performance. Similarly, field validation is equally important to assess the model's predictions.

5.2 LIMITATION AND FUTURE WORK AND DIRECTIONS

This dissertation advances research of monitoring and mapping of forest conditions in mixed conifer forest and boreal forest ecosystems using remote sensing and artificial intelligence techniques at fine scale. However, many knowledge gaps remain. For example, building on chapter 2, we observed challenges with NAIP imagery alignment with lidar tree segments requires further experimentation with orthorectification procedures to address the problem. Building on Chapter 3, it will be important to continue producing fine-scale forest type maps to be able to identify climate change induced shift in dominant forest. A one-time period forest type map is not sufficient for this purpose and ongoing monitoring and mapping are necessary to capture and understand the changes over time. Building on Chapter 4, it will be important to continue investigating how mortality metrics can be used to model the future forest regeneration in the areas impacted by compound disturbances. Further, the field validation of our proposed neighborhood canopy mortality metric is required.

In future, we will continue to improve the performance of mortality algorithms by creating training points for oak woodlands. Further, labeling additional training and evaluation data capturing post-fire mortality and experimenting with splitting the mortality class into drought-induced versus fire-driven mortality would enable the development of more accurate post-fire mortality prediction and the detangling of fire versus drought impacts in compound disturbance environments. This will require creating more labeled dataset for fire-induced mortality and retraining the model with a new class such as dead due to fire. Additionally, scaling up the model predictions to cover the entire 2020 Creek Fire within Sierra Nevada for both pre- and post-fire

forest conditions will allow for a more comprehensive investigation of interaction between disturbance patterns. Future research should also explore different products that can be derived from overstory tree mortality, such as densities of dead tree per unit area (risk of fire) and densities of live tree above 4 m (which are likely to be future seed sources). These products can serve as useful tools for managers in building resilience forests. For future directions of our research in interior Alaska, it will be important to continue expanding forest type maps from G-LiHT footprint to produce wall-to-wall maps.

Overall, this research provides a robust framework for predicting forest conditions at a fine spatial resolution (<1m), which is appropriate for addressing complex ecological questions and facilitating informed decision-making in forest management and restoration efforts. It is my hope that the framework established in this study will pave the way for future analyses to effectively detect and respond to climate change impacts on forest ecosystems at fine scale.

5.3 REFERENCES

Barber, V. A., Juday, G. P., & Finney, B. P. (2000). Reduced growth of Alaskan white spruce in the twentieth century from temperature-induced drought stress. *Nature*, *405*(6787), 668–673. https://doi.org/10.1038/35015049

Byer, S., & Jin, Y. (2017). Detecting Drought-Induced Tree Mortality in Sierra Nevada Forests with Time Series of Satellite Data. *Remote Sensing*, *9*(9), 929. https://doi.org/10.3390/rs9090929

Campbell, M. J., Dennison, P. E., Tune, J. W., Kannenberg, S. A., Kerr, K. L., Codding, B. F., & Anderegg, W. R. L. (2020). A multi-sensor, multi-scale approach to mapping tree mortality in woodland ecosystems. *Remote Sensing of Environment*, *245*, 111853. https://doi.org/10.1016/j.rse.2020.111853

Chapin, F. S., McGuire, A. D., Ruess, R. W., Hollingsworth, T. N., Mack, M. C., Johnstone, J. F., Kasischke, E. S., Euskirchen, E. S., Jones, J. B., Jorgenson, M. T., Kielland, K., Kofinas, G. P., Turetsky, M. R., Yarie, J., Lloyd, A. H., & Taylor, D. L. (2010). Resilience of Alaska's boreal forest to climatic changeThis article is one of a selection of papers from The Dynamics of Change in Alaska's Boreal Forests: Resilience and Vulnerability in Response to Climate Warming. *Canadian Journal of Forest Research*, *40*(7), 1360–1370. https://doi.org/10.1139/X10-074

Fassnacht, F. E., Latifi, H., Sterenczak, K., Modzelewska, A., Lefsky, M., Waser, L. T., Straub, C., & Ghosh, A. (2016). Review of studies on tree species classification from remotely sensed data. *Remote Sensing of Environment*, *186*, 64–87. https://doi.org/10.1016/j.rse.2016.08.013

Fricker, G. A., Ventura, J. D., Wolf, J. A., North, M. P., Davis, F. W., & Franklin, J. (2019). A Convolutional Neural Network Classifier Identifies Tree Species in Mixed-Conifer Forest from Hyperspectral Imagery. *Remote Sensing*, *11*(19), 2326. https://doi.org/10.3390/rs11192326

Hemming-Schroeder, N. M., Gutierrez, A. A., Allison, S. D., & Randerson, J. T. (2023). Estimating Individual Tree Mortality in the Sierra Nevada Using Lidar and Multispectral Reflectance Data. *Journal of Geophysical Research: Biogeosciences*, *128*(5), e2022JG007234. https://doi.org/10.1029/2022JG007234

Johnstone, J. F., Hollingsworth, T. N., Chapin, F. S., & Mack, M. C. (2010). Changes in fire regime break the legacy lock on successional trajectories in Alaskan boreal forest. *Global Change Biology*, *16*(4), 1281–1295. https://doi.org/10.1111/j.1365-2486.2009.02051.x

Lee, J. M., Mirocha, J. D., Lareau, N. P., Whitney, T., To, W., Kochanski, A., & Lassman, W. (2023). Sensitivity of Pyrocumulus Convection to Tree Mortality During the 2020 Creek Fire in California. *Geophysical Research Letters*, *50*(16), e2023GL104193. https://doi.org/10.1029/2023GL104193

Mäyrä, J., Keski-Saari, S., Kivinen, S., Tanhuanpää, T., Hurskainen, P., Kullberg, P., Poikolainen, L., Viinikka, A., Tuominen, S., Kumpula, T., & Vihervaara, P. (2021). Tree species classification from airborne hyperspectral and LiDAR data using 3D convolutional neural networks. *Remote Sensing of Environment*, *256*, 112322. https://doi.org/10.1016/j.rse.2021.112322

Millar, C. I., & Stephenson, N. L. (2015). Temperate forest health in an era of emerging megadisturbance. *Science*, *349*(6250), 823–826. https://doi.org/10.1126/science.aaa9933

Stephens, S. L., Bernal, A. A., Collins, B. M., Finney, M. A., Lautenberger, C., & Saah, D. (2022). Mass fire behavior created by extensive tree mortality and high tree density not predicted by operational fire behavior models in the southern Sierra Nevada. *Forest Ecology and Management*, *518*, 120258. https://doi.org/10.1016/j.foreco.2022.120258

Stephens, S. L., Collins, B. M., Fettig, C. J., Finney, M. A., Hoffman, C. M., Knapp, E. E., North, M. P., Safford, H., & Wayman, R. B. (2018). Drought, Tree Mortality, and Wildfire in Forests Adapted to Frequent Fire. *BioScience*, *68*(2), 77–88. https://doi.org/10.1093/biosci/bix146

Stephenson, N. L., & Das, A. J. (2020). Height-related changes in forest composition explain increasing tree mortality with height during an extreme drought. *Nature Communications*, *11*(1), 3402. https://doi.org/10.1038/s41467-020-17213-5

Stovall, A. E. L., Shugart, H., & Yang, X. (2019). Tree height explains mortality risk during an intense drought. *Nature Communications*, *10*(1), 4385. https://doi.org/10.1038/s41467-019-12380-6

Swain, D. L. (2015). A tale of two California droughts: Lessons amidst record warmth and dryness in a region of complex physical and human geography: A TALE OF TWO CALIFORNIA DROUGHTS. *Geophysical Research Letters*, *42*(22), 9999-10,003. https://doi.org/10.1002/2015GL066628

Tian, L., & Fu, W. (2020). Bi-Temporal Analysis of Spatial Changes of Boreal Forest Cover and Species in Siberia for the Years 1985 and 2015. *Remote Sensing*.

Walker, X. J., Mack, M. C., & Johnstone, J. F. (2015). Stable carbon isotope analysis reveals widespread drought stress in boreal black spruce forests. *Global Change Biology*, *21*(8), 3102–3113. https://doi.org/10.1111/gcb.12893

Walker, X. J., Okano, K., Berner, L. T., Massey, R., Goetz, S. J., Johnstone, J. F., & Mack, M. C. (2023). Shifts in Ecological Legacies Support Hysteresis of Stand Type Conversions in Boreal Forests. *Ecosystems*, *26*(8), 1796–1805. https://doi.org/10.1007/s10021-023-00866-w

Walsh, S. J. (1980). Coniferous tree species mapping using Landsat data. *Remote Sensing of Environment*, *9*(1), 11–26.

Xie, Y., Sha, Z., & Yu, M. (2008). Remote sensing imagery in vegetation mapping: A review. *Journal of Plant Ecology*, *1*(1), 9–23. https://doi.org/10.1093/jpe/rtm005